Copernicus Europe's eyes on Earth

Copernicus Climate Change Service

Quality Evaluation Report for the Polar Multi-sensor Aerosol product (PMAp) Release 1

OD6.1

Issued by: EUMETSAT
Date: 01/07/2022
REF.: C3S_311b T6.1 M10 OD6.1

European Commission

Copernicus Europe's eyes on Earth

IMPLEMENTED BY ECMWF

Quality Evaluation Report for the Polar Multi-sensor Aerosol product (PMAp) Release 1

OD6.1

EUMETSAT
Marie Doutriaux-Boucher
Soheila Jafariserajehlou
Roger Huckle
Kristina Petraityte
Andriy Holdak
Bertrand Fougnie
Jörg Schulz

Date: 01/07/2022

REF.: C3S_311b T6.1 M10 D6.1

Contents

List of Figures

List of Tables

Acronyms

AERONET	AErosol RObotic NETwork
AOD	Aerosol Optical Depth
ATBD	Algorithm Theoretical Basis Document
AVHRR	Advanced Very High Resolution Radiometer
C3S	Copernicus Climate Change Service
COD	Cloud Optical Depth
CDR	Climate Data Record
CNES	Centre National d'Etudes Spatiales
CWL	Central WaveLength
ECMWF	European Center for Medium-Range Weather Forecasts
EUMETSAT	EUropean organisation for the exploitation of METeorological SATellites
ERA	European ReAnalysis
ERA-Interim	ECMWF interim reanalysis
FDR	Fundamental Data Record
FWHM	Full Width at Half Maximum
GOME-2	Global Ozone Monitoring Experiment-2
IASI	Infrared Atmospheric Sounding Interferometer
IR	InfraRed
L1b	Level 1b data
L1c	Level 1c data
L2	Level 2 data
Metop	Meteorological Operational Satellite
MODIS	Moderate Resolution Imaging Spectroradiometer
NASA	National Aeronautics and Space Administration
NH	Northern Hemishere
NOAA	National Oceanic and Atmospheric Administration
NRT	Near Real Time
NWP	Numerical Weather Prediction
OPE	Operational NRT product
PHOTONS	PHOtométrie pour le Traitement Opérationnel de Normalisation Satellitaire
PMAp	Polar Multi-sensor Aerosol product
PMD	Polarisation Measurement Device
R3	Release 3
RMSE	Root Mean Square Error
SDS-WAS	Sand and Dust Storm Warning Advisory and Assessment System
SH	South Hemisphere
SMAPE	Symmetric Mean Absolute Percentage Error
UTC	Universal Time Coordinated
VIS	Visible

1 Introduction

Aerosols are suspended particulate matter in the atmosphere carried by air masses. Aerosol particles can be solid or liquid and can cover a wide range of particle sizes, from 0.005 to 100 µm, depending on aerosol type. This wide range leads to a large variation in scattering and absorption characteristics of aerosols.

The **P**olar **M**ulti-sensor **A**erosol **p**roduct (PMAp) provides aerosol optical depth and type derived from data of several instruments on board of the Metop satellites. It is a synergistic product and it exploits the capabilities of the Global Ozone Monitoring Experiment–2 (GOME-2), the Infrared Atmospheric Sounding Interferometer (IASI) and the Advanced Very High Resolution Radiometer (AVHRR) sensors on board of all Metop platforms. PMAp provides global Aerosol Optical Depth (AOD) at 550 nm and aerosol classification at the GOME-2 Polarized Measurement devices (PMD) pixel level. It also provides related parameters available over all surface types under daylight condition. The Near Real Time (NRT) PMAp algorithm has been continuously developed and improved since its first implementation in 2014. The PMAp version 2.2.4 has been released in May 2021, and is currently used in operation for the Near Real Time generation and distribution of PMAp aerosol products. The performance of this aerosol product has been documented on the associated Product Validation Report (EUMETSAT, 2021c). The version 2.2.4 has shown significant improvements compared to previous PMAp versions, especially a clear improvement of the quality of the retrieval over land, and a better consistency between the results derived from the different Metop platforms.

The production of the PMAp Climate Data Record (CDR) aimed at the availability of a fully consistent long-term archive employing the most up-to-date available NRT version of the PMAp processor using as input the most up-to-date version of Level-1 products, especially with regard to the stability of the radiometry. For this, the Level-1 Fundamental Data Record (FDR) input data from GOME-2 (EUMETSAT, 2021d) and IASI (EUMETSAT, 2019), recently reprocessed and available at EUMETSAT, have been used, associated with the version 2.2.3 of the PMAp processor. The differences of the PMAp processor version 2.2.3 used for this CDR generation and the version 2.2.4 now deployed in NRT, is only on the handling of NRT/CDR related configurations, for more details see section 2.1.

The PMAp product contains various parameters produced by the retrieval. The most relevant parameter from this product is the AOD, other products being seen as by-products. As the CDR is intended focuses on AOD this is the only parameter that is extensively documented in terms of validation.

The CDR covers the 12-year period of Metop –A and –B measurements, since the launch of Metop-A in July-2007 until August 2019[1]. Metop-C, launched in November 2018 is not included in this first version of the CDR but will be considered for following releases.

The validation of the PMAp CDR presented in this document has two main objectives:

- Demonstrate that the PMAp performance from the CDR is consistent with the performance documented for the NRT processor, and potentially better, and;
- Demonstrate that this performance is valid for the entire CDR time series.

[1] The CDR stops in August 2019 as this is the end of ERA interim reanalysis data that is used as input for the retrieval

The evaluation of the CDR quality has been assessed using four types of analysis:

- Temporal analysis to verify if the reprocessed PMAp CDR is free of gaps, stable in time and exhibit well known geographical and seasonal features;
- Analysis of the consistency between AOD retrieved using instruments on-board Metop-A and Metop-B;
- Validation of the AOD using ground-based reference measurements from the AERONET network, and;
- Evaluation of the AOD using comparison against space-borne reference data from the Moderate Resolution Imaging Spectroradiometer (MODIS) AOD products.

In addition, to reinforce the understanding why AOD assimilation in global reanalyses or for climate studies should use the PMAp CDR rather than the archived PMAp NRT a comparison with EUMETSAT's NRT archived product is presented.

1.1 Purpose and scope

The purpose of this document is to provide a comprehensive report on the validation of the CDR generated for the PMAp. The document provides results of the validation of the PMAp AOD CDR generated using version 2.2.3 of the PMAp software (EUMETSAT, 2021a) and reprocessed input data from Metop-A and -B satellites. The validation presented is only addressing the AOD. Other parameters, being also part of the PMAp product, are provided together with the AOD but have not been analysed in this report.

1.2 Structure of the document

This document has the following sections:

Section 1	Introduction (this section)
Section 2	PMAp data record generation summary
Section 3	Validation and comparison data
Section 4	Evaluation overview
Section 5	Comparison to near real time PMAp
Section 6	Validation against independent data records (AERONET and MODIS)
Section 7	Known limitations
Section 8	Summary and conclusions

1.3 Reference Documents

Dee, D. P., Uppala, S. M., Simmons, A. J., Berrisford, P., Poli, P., Kobayashi, S., Andrae, U., Balmaseda, M. A., Balsamo, G., Bauer, P., Bechtold, P., Beljaars, A. C. M., Berg, L. van de, Bidlot, J., Bormann, N., Delsol, C., Dragani, R., Fuentes, M., Geer, A. J., Haimberger, L., Healy, S. B., Hersbach, H., Hólm, E. V., Isaksen, L., Kållberg, P., Köhler, M., Matricardi, M., McNally, A. P., Monge-Sanz, B. M., Morcrette, J.-J., Park, B.-K., Peubey, C., Rosnay, P. de, Tavolato, C., Thépaut, J.-N., and Vitart, F.: The ERA-Interim reanalysis: configuration and performance of the data assimilation system, Q. J. R. Meteorol. Soc., 137, 553–597, https://doi.org/10.1002/qj.828, 2011.

Eck, T. F., Holben, B. N., Giles, D. M., Slutsker, I., Sinyuk, A., Schafer, J. S., Smirnov, A., Sorokin, M., Reid, J. S., Sayer, A. M., Hsu, N. C., Shi, Y. R., Levy, R. C., Lyapustin, A., Rahman, M. A., Liew, S.-C., Cortijo, S. V. S., Li, T., Kalbermatter, D., Keong, K. L.,

Yuggotomo, M. E., Aditya, F., Mohamad, M., Mahmud, M., Chong, T. K., Lim, H.-S., Choon, Y. E., Deranadyan, G., Kusumaningtyas, S. D. A., and Aldrian, E.: AERONET Remotely Sensed Measurements and Retrievals of Biomass Burning Aerosol Optical Properties During the 2015 Indonesian Burning Season, J. Geophys. Res. Atmospheres, 124, 4722–4740, https://doi.org/10.1029/2018JD030182, 2019.

EUMETSAT: GOME-2 Factsheet, https://www.eumetsat.int/media/37899, 2017.

EUMETSAT: Validation Report – IASI-A Level 1c FCDR release 1, https://www.eumetsat.int/media/47452, 2019.

EUMETSAT: Polar Multi-Sensor Aerosol Product: ATBD, https://www.eumetsat.int/media/39255, 2021a.

EUMETSAT: Polar Multi-Sensor Aerosol Product: User Guide, https://www.eumetsat.int/media/39243, 2021b.

EUMETSAT: Polar Multi-Sensor Aerosol Product: Validation Report, https://www.eumetsat.int/media/40632, 2021c.

EUMETSAT: Validation Report GOME2 FCDR R3, https://doi.org/10.15770/EUM_SEC_CLM_0039, 2021d.

Hilton, F., Armante, R., August, T., Barnet, C., Bouchard, A., Camy-Peyret, C., Capelle, V., Clarisse, L., Clerbaux, C., Coheur, P.-F., Collard, A., Crevoisier, C., Dufour, G., Edwards, D., Faijan, F., Fourrié, N., Gambacorta, A., Goldberg, M., Guidard, V., Hurtmans, D., Illingworth, S., Jacquinet-Husson, N., Kerzenmacher, T., Klaes, D., Lavanant, L., Masiello, G., Matricardi, M., McNally, A., Newman, S., Pavelin, E., Payan, S., Péquignot, E., Peyridieu, S., Phulpin, T., Remedios, J., Schlüssel, P., Serio, C., Strow, L., Stubenrauch, C., Taylor, J., Tobin, D., Wolf, W., and Zhou, D.: Hyperspectral Earth Observation from IASI: Five Years of Accomplishments, Bull. Am. Meteorol. Soc., 93, 347–370, https://doi.org/10.1175/BAMS-D-11-00027.1, 2012.

Levy, R. C., Mattoo, S., Munchak, L. A., Remer, L. A., Sayer, A. M., Patadia, F., and Hsu, N. C.: The Collection 6 MODIS aerosol products over land and ocean, Atmospheric Meas. Tech., 6, 2989–3034, https://doi.org/10.5194/amt-6-2989-2013, 2013.

Munro, R., Lang, R., Klaes, D., Poli, G., Retscher, C., Lindstrot, R., Huckle, R., Lacan, A., Grzegorski, M., Holdak, A., Kokhanovsky, A., Livschitz, J., and Eisinger, M.: The GOME-2 instrument on the Metop series of satellites: instrument design, calibration, and level 1 data processing – an overview, Atmospheric Meas. Tech., 9, 1279–1301, https://doi.org/10.5194/amt-9-1279-2016, 2016.

Paul Hubanks, Steven Platnick, Micheal King, and Bill Ridgway: MODIS Atmosphere L3 Gridded Product Algorithm Theoretical Basis Document (ATBD) & Users Guide, https://atmosphere-imager.gsfc.nasa.gov/sites/default/files/ModAtmo/L3_ATBD_C6_C61_2019_02_20.pdf, 20 February 2019.

Sebastien Garrigues: Evaluation of PMAp version 2.2c, https://ceos.org/document_management/Virtual_Constellations/AC-VC/Meetings/AC-VC-16/Day4_Aerosol/4.02-GarriguesQuesada_v5.pdf, 20 December 2019.

Sudarchikova, N., Basart, S., Katragkou, E., Petersen, K., Akritidis, D., Kartsios, S., Zanis, P., Melas, D., Chabrillat, S., Christophe, Y., Ramonet, M., Bennouna, Y., Clark, H., Wagner, A., and Schulz, M.: Compendium of case studies for the period 2015-2018, 113, 2018.

2 PMAp Data Record generation summary

2.1 Definition of PMAp

For the generation of this Climate Data Record the version 2.2.3 of the PMAp software was used. The version currently running in the EUMETSAT ground segment in the near real time production is the version 2.2.4. The version 2.2.4 was updated over 2.2.3 to differently handle GOME-2 NRT input data (GOME-2 degradation correction in forecast mode and associated offset correction), as these differ from the CDR production. The underlying algorithm remains unchanged. Therefore, conclusions gained during the validation of the algorithm version 2.2.4 can be mapped to this data record. Additionally one as to bear in mind the general differences between an NRT and a CDR production scheme. These differences are mainly the usage of different input auxiliary Numerical Weather Prediction (NWP) data and the degradation correction approach for GOME-2 radiances.

2.1.1 The PMAp aerosol retrieval

PMAp is dedicated to retrieve AOD at 550nm and a series of associated aerosol and clouds parameters listed in 2.1.2. The algorithm uses a multi-sensor approach exploiting the synergy of GOME-2, AVHRR and IASI instruments. The product is delivered as a GOME-2 product with the (spatial) target resolution of the GOME-2 PMDs. The PMAp aerosol retrieval algorithm consists of three steps.

- Step 1: At the beginning, a pre-classification is applied based on AVHRR and IASI data, both co-located in this phase to the GOME-2 pixel used as a pivot. This includes the detection of clouds, calculation of cloud correction factors (for subpixel-cloud decontamination), the strong aerosol events (in particular volcanic ash and dust) and a pre-classification of possible aerosol types;
- Step 2: A set of AODs at 550nm are retrieved using one GOME-2 PMD band. The selected band depends on the condition (dark ocean, ocean with slight glint effects, dense vegetation, bright surfaces/deserts or continents with moderate albedo). Each of these AODs is retrieved with respect to different aerosol types and microphysical properties. At this point, it is not known which selection of aerosol type and microphysical properties is the best representation of the given scene. For clear sky pixels over ocean, the chlorophyll pigment concentration is fitted in addition;
- Step 3: The AOD from step 2 that best fits to the GOME-2 PMD measurements (reflectance and stokes fractions) is selected to be usable for the given scene. The included bands may depend, e.g., on the surface albedo, the predicted clear-sky top of atmosphere stokes fraction and the cloud coverage.

The full ATBD (EUMETSAT, 2021a) and a product user guide (EUMETSAT, 2021b) has been published by EUMETSAT.

2.1.2 Overview of the PMAp aerosol product

The PMAp aerosol product, fully described in the Product User Guide (EUMETSAT, 2021b), contains the following parameters:

- Aerosol Optical Depth: AOD is the core parameter provided at 550nm for the GOME-2 PMD pixel;
- aerosol-type parameters containing "aerosol_class" (7 possible classes), "flag_ash" (activated when ash detected);
- quality parameters containing "error_aerosol_optical_depth" (error associated to the AOD), "quality_flags_aerosol (series of flags informing about degraded cases)
- by-product parameters containing "pmap_geometric_cloud_fraction" (cloud fraction of the PMD pixel from AVHRR), "flag_cirrus_cloud" and "flag_snow_ice" (presence of cirrus cloud and ice within the pixel), "reflectance_inhomogeneity" (variance of the radiometry from AVHRR), "chlorophyll_pigment_concentration" (resulting of the surface estimation);
- information parameters containing "retrieval_algorithm" (used branch of the retrieval), "wind_speed" and "land_fraction" (for the PMD pixel);
- cloud parameters containing "cloud_optical_depth" (for the GOME-2 PMD pixel), "cloud_top_temperature" (from AVHRR), "quality_flag_cloud" (associated quality flag).

2.1.3 Summary of the PMAp NRT retrieval performance

The quality of the PMAp algorithm used to produce the CDR has already been documented in the context of the NRT operational processor for version 2.2.4 (EUMETSAT, 2021c). A summary of the conclusions from the validation of the algorithm is given below.

Over ocean:

- PMAp has no remaining issues over the ocean, except for the apparent overestimation of dust close to the west coast of the Sahara. It is not clear whether this is really an overestimate because the comparison was made with MODIS data served by the Copernicus Atmospheric Monitoring Service (CAMS), which reportedly underestimates dust in this area (Sudarchikova et al., 2018).
- According to reports from CAMS (Sebastien Garrigues, 2019), the improvements in version 2.2.4 over ocean brings PMAp more in line with the ECMWF model and MODIS estimates.
- The consistency between the two Metop -A and -B is well achieved (also valid for Metop-C).

Over land:

- The validation vs. Aeronet data indicates that over normal/dark land surfaces, PMAp from Metop-A and Metop-B are within the threshold range (error either below 0.3 or less than 40%). However, over bright land surfaces PMAp overestimates AOD in some cases. However, temporal and spatial dynamics are well captured even over bright land.
- The new improvements made in v2.2.4 addresses the "too much underestimation" issue reported by CAMS in many areas for all previous versions of PMAp.
- The comparison of Metop-A and -B based on 2 benchmarking periods shows a very good agreement and consistency between the satellites. Discrepancies are

observed in the Sahara belt and higher latitudes which can be due to the remaining issue over bright land surfaces, or simply the fact the two satellites do not sample exactly the same part of the Earth's surface.

More extensive results, statistics, and description are available in the NRT product validation report (EUMETSAT, 2021c).

Table 1: Summary of the PMAp 2.2.4 performance as estimated using Aeronet matchups for two 3 month reference periods. Performance for land surfaces is shown for filtered data (excluding bright surfaces). The gain and offset refer to the slope and offset of the line of best fit in the scatterplot of PMAp and Aeronet AOD. R and N stands for Pearson correlation coefficient and number of retrievals.

	PMAp v. 2.2.4 Ocean				PMAp v. 2.2.4 Land			
	June - Sept 2013		Feb – May 2015		June - Sept 2013		Feb – May 2015	
Metop	**A**	**B**	**A**	**B**	**A**	**B**	**A**	**B**
gain	0.94	0.51	1.3	0.96	1.0	0.64	0.53	0.63
offset	0.03	0.09	-0.02	-0.005	-0.03	0.03	0.08	0.07
R	0.71	0.55	0.87	0.68	0.71	0.72	0.75	0.67
N	99	117	62	105	165	142	412	371

2.2 Input data

GOME-2 radiances are the main input data to the retrieval scheme. In addition, data from IASI and AVHRR are also used for the AOD retrieval. Because the GOME-2 pixels are spatially large, AVHRR is used to improve the sub-pixel cloud detection and aerosol pre-classification. A correction of GOME-2 reflectance is done based on the heterogeneity of AVHRR reflectance within the GOME-2 pixels and a pre-classification of the PMD pixel. IASI is currently used to flag dust and ash events using indexes based on a composite of 100 channels. Additional auxiliary input data are taken from NWP models, for the CDR ERA-Interim reanalyses data from ECMWF were used.

The three instruments and the ERA-Interim data are briefly described in the following sections.

2.2.1 GOME-2 data

GOME-2 is a medium-resolution UV-VIS spectrometer (Munro et al., 2016), fed by a scan mirror which enables across-track scanning in nadir, as well as sideways viewing for polar coverage and instrument characterisation measurements using the moon. The scan mirror directs light into a telescope, designed to match the field of view of the instrument to the dimensions of the entrance slit. This scan mirror can also be directed towards internal calibration sources or towards a diffuser plate for calibration measurements using the sun.

GOME-2 comprises four main optical channels which focus the spectrum onto linear silicon photodiode detector arrays of 1024 pixels each, and two Polarisation Measurement Devices (PMDs) containing the same type of arrays for measurement of linearly polarised intensity in two perpendicular directions. The spatial resolution of the PMD observations is 10x40 km^2 (Metop-B and -C, Metop-A until July 2013) and 5x40 km^2 (Metop-A from July 2013 onwards).

The PMDs are required because GOME-2 is a polarisation-sensitive instrument and therefore the intensity calibration must take the polarisation state of the incoming light into account. This is achieved using Stokes-fraction information from the PMDs.

Aerosol optical properties are retrieved using the reflectances and stokes fractions measured by the PMD. PMDs are available in 14 wavelength ranges (Table 2).

Table 2: Spectral Characteristics of GOME-2 PMD bands used for PMAp retrieval

Number	5	6	7	8	9	10	11	12	13	14
CWL (nm)	369.46	382.12	414.33	463.37	522.01	554.62	590.81	640.37	756.83	799.22
FWHM (nm)	17.16	3.56	29.16	57.89	53.97	3.79	44.93	44.15	24.17	8.99

For this CDR, radiances from the GOME-2 FCDR release 3 (doi:10.15770/EUM_SEC_CLM_0039) have been used (EUMETSAT, 2021d). PMAp uses GOME-2 PMDs at three selected wavelengths: 414 nm, 463 nm and 640 nm. The pixel sizes and swath width are described in Table 3.

Table 3: GOME-2 PMD footprint (across track x along track)

Satellite Platform	**Spatial resolution (GOME-2 PMD spatial resolution)**	**Swath**
Metop-A (before 15. July 2013)	10 km × 40 km	1920 km
Metop-A (since 15. July 2013)	5 km × 40 km	960 km
Metop-B	10 km × 40 km	1920 km

Since its launch, the GOME-2 instrument is degrading. The instrument degradation has been observed in GOME-2 causing a differential spectral degradation in the recorded signals, which is affecting the retrieval of several products. Being spectrally non-homogeneous, this degradation affects significantly the aerosol optical properties retrieval. In order to retrieve a homogeneous AOD over the entire reprocessed period, the GOME-2 level1b data therefore needs to be corrected.

A list of contributors to the observed signal degradation of GOME-2 has been identified as thermal instability of the optical bench, internal contamination of the optical path, degradation of the scan mirror with viewing angle dependent response and solar optical path degradation. A model of this degradation has been developed taking into account these issues and a platform dependent matrix of spectral coefficients has been computed to correct the PMD channel signals before the aerosol processing into PMAp.

Degradation coefficients (Munro et al., 2016) where computed and applied to the release 3 level 1b GOME-2 data generating the GOME-2 level 1c that is used as input to the retrieval.

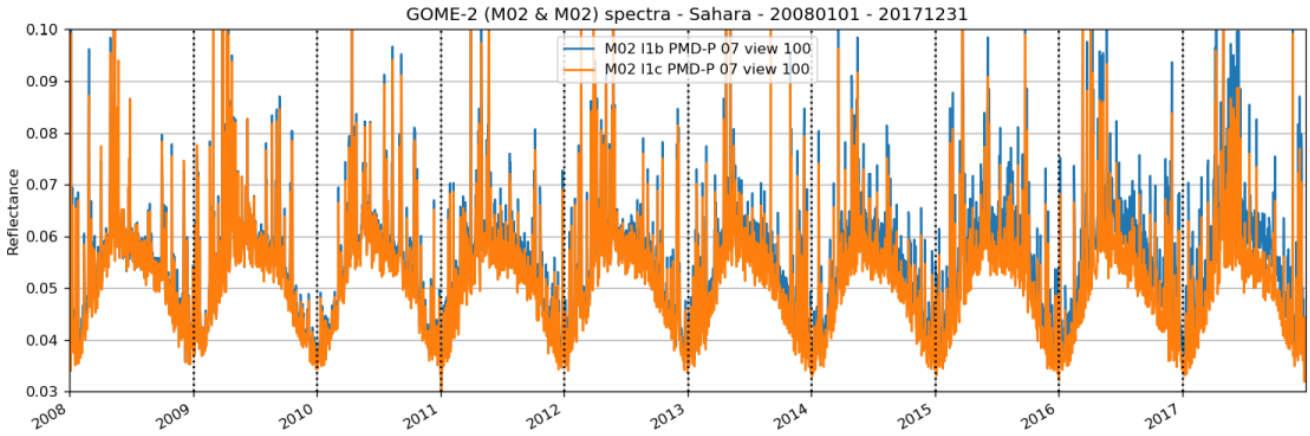

Figure 1: GOME-2 Metop-A (M02) reflectance, level 1b (blue) and degradation corrected (level 1c) (orange), for nadir PMD pixel. The degradation corrected time series is very stable, compared to the original level 1b data, which shows a clear trend.

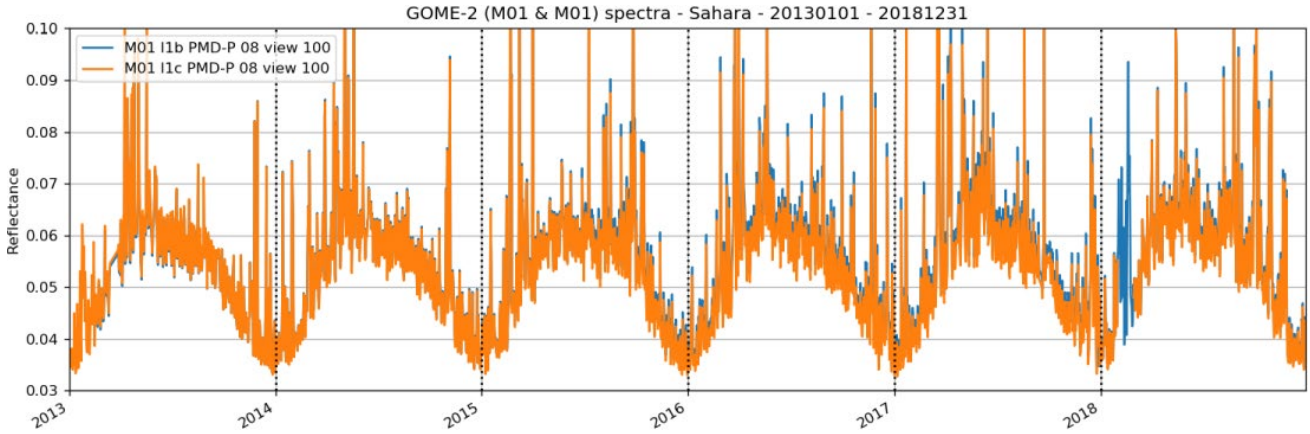

Figure 2: same as Figure 1 but for Metop-B (M01).

The reflectance used as input to PMAp are stable and consistent over the entire period, see Figure 1 and Figure 2. Assuming that the reflectance for a desert target is not changing over time the shown time series demonstrate that the L1b data show a false trend that is eliminated by the correction leading to L1c data, while preserving essential features such as the annual cycle.

As the Metop-A satellite is drifting and the instrument continues to degrade, the PMAp CDR stops at the end of January 2018 for Metop-A, with the first loss of solar visibility. Once a correction for the time of the loss of solar visibility and thereafter is available, this period could potentially be included in a future release of the PMAp CDR.

2.2.2 IASI data

The Infrared Atmospheric Sounding Interferometer (Hilton et al., 2012) is a Fourier transform spectrometer providing infrared spectra with a high resolution between 645 and 2760cm^{-1} (3.6 µm to 15.5 µm). IASI has 8461 spectral samples with a spectral resolution of 0.5 cm^{-1} after apodisation (L1c spectra). The spectral sampling interval is 0.25 cm^{-1}.

The main goal of the IASI mission is to provide atmospheric emission spectra to derive temperature, humidity and trace gas profiles with high vertical resolution and accuracy.

For this CDR, IASI data from Metop-A and -B were used. The IASI L1c used for PMAp processing are homogeneous throughout the period as they are derived using the same algorithm version: the release 1 of the fundamental climate data record (FCDR) reprocessed IASI L1c (EUMETSAT, 2019) was used as input up to December 2016. After that date for IASI-A, and for the entire period for IASI-B, the L1c products from the operational near real time processing were used.

In the PMAp retrieval, IASI L1c data are used to flag dust events using a desert dust index, which is calculated making use of one hundred channels selected in the infrared thermal spectra provided by IASI, a previously collected mean clear sky and polluted spectra. For more details on the IASI dust index calculation, see the section 3.1.1.2 of the PMAp ATBD (EUMETSAT 2021a).

2.2.3 AVHRR data

The AVHRR/3 is a six-channel scanning radiometer providing three solar channels in the visible/near-infrared region and three thermal infrared channels. The AVHRR/3 has two one-micrometre wide channels between 10.3 and 12.5 micrometres.

In the PMAp retrieval, AVHRR data are used to improve the cloud screening as well as for a pre-classification of aerosols. A correction of GOME-2 reflectance based on the heterogeneity of AVHRR radiances within the GOME-2 pixels is performed (EUMETSAT, 2021a).

2.2.4 ERA-Interim data

The ECMWF ERA-Interim reanalysis (Dee et al., 2011) is used as input for the reprocessing as an auxiliary information and background checks. We use the 6 and 12 hour forecast from the 0 and 12 UTC base times, leading to 4 forecast files per day (0, 6, 12 and 18 UTC). The forecast grid is 0.5°x0.5° with 60 vertical levels. The three parameters used for the processing are listed in Table 4. More details on the ERA-Interim re-analysis data can be found on the ECMWF web site[2]. ERA-interim has stopped in August 2019, therefore the PMAp CDR ends with the 31 August 2019.

Table 4: ERA-Interim data fields used for PMAp processing.

Parameter name	Parameter number	Type of variable	Description
u-component	165	Model layer (1-60)	Wind zonal component
v-component	166	Model layer (1-60)	Wind meridional component
lnsp	152	Surface	Log of the surface pressure

[2] Link valid 23/03/2021 https://www.ecmwf.int/en/forecasts/datasets/archive-datasets/reanalysis-datasets/era-interim

3 Validation and Comparison Data

To validate the AOD CDR we used two independent AOD datasets, the ground-based AERONET data and the satellite MODIS AOD estimates. Furthermore we compare the CDR data to the NRT data, to reinforce the understanding why using this CDR rather than PMAp NRT for assimilation in reanalysis or for climate studies.

3.1 Ground-based data: AERONET

AERONET (AErosol RObotic NETwork) is a globally distributed network of approximately 700 ground-based sun photometers established by National Aeronautics and Space Administration (NASA) and PHOTONS (PHOtométrie pour le Traitement Opérationnel de Normalisation Satellitaire). AERONET provides long-term (>25 years) and continuous measurements of AOD at different wavelengths (340, 380, 440, 500, 550, 670, 870, 940 and 1020 nm), inversion products and precipitable water (Holben et al., 1998). The high temporal resolution of 15 minutes for these data and expected high accuracy of ~0.01 to 0.021 (Eck et al., 2019), as well as readily accessible public domain database, provide a suitable data set for aerosol validation.

AERONET data are categorised and available at three levels: level 1.0 (unscreened), level 1.5 (cloud screened and quality controlled) and level 2.0 (quality assured). Most of the comparisons to AERONET data use the operational monitoring tool that is set up for level 1.5 AOD data. However, the comparison to all stations over the whole time series in section 6.4.4 has been performed with a new tool that is capable using L2 data from version 3 (https://amt.copernicus.org/articles/13/3375/2020/)[3].

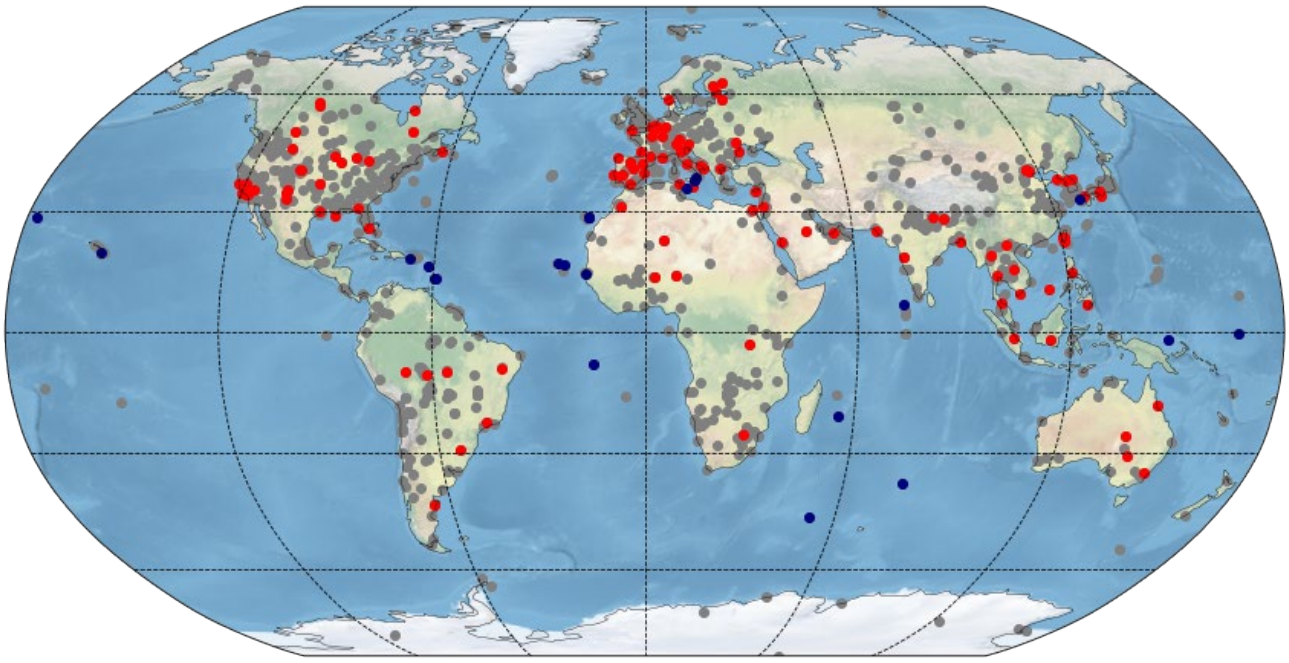

Figure 3: Available AERONET stations (grey) and those used for the analysis in red (land) and blue (ocean).

[3] https://aeronet.gsfc.nasa.gov/new_web/download_all_v3_aod.html

3.2 Space-based data: MODIS

We use an independent set of aerosol retrievals from satellite for comparison with the PMAp CDR. MODIS AOD is produced using a mature algorithm and covers the entire period of the PMAp CDR. MODIS Terra was used because its equator crossing time is close to that of Metop. The collection 6.1 of aerosol optical depth data (Levy et al., 2013) record monthly[4] and daily[5] was used for the comparison (Paul Hubanks et al., 2019). Daily Level-2 data are available at the spatial resolution of a 10x10 km^2 (at nadir). All MODIS Atmosphere L3 are stored on an equal-angle latitude-longitude grid at 1°x1° resolution. Several AOD at 550nm are available. For this validation, we use the "Combined" Deep Blue (DB) + Dark Target (DT) Aerosol Optical Depth (AOD) at 550 nm microns for the monthly geographical comparison. For the overall comparison over land and ocean, the respective land Deep Blue AOD and oceanic product are used (see Table 5). More information about MODIS products can be found on the NASA website[6].

Table 5: MODIS MOD08 M3 used for the monthly comparison

Variable	Variable Name
Land	Deep_Blue_Aerosol_Optical_Depth_550_Land_Mean_Mean
Ocean	Aerosol_Optical_Depth_Average_Ocean_Mean_Mean
Globe	AOD_550_Dark_Target_Deep_Blue_Combined_Mean_Mean

3.3 Operational near real time PMAp data

PMAp was proposed as a day-2 product for the near real time processing to be introduced only at a later stage at EUMETSAT. The Metop-A and -B PMAp operation therefore started only on the 16 January 2014. Several changes and improvements took place since then, e.g., upgrade of the algorithm including correction of errors and improvements and upgrade of radiometric corrections (EUMETSAT, 2021c). In 2016, the PMAp retrieval, initially limited to ocean, started production also over land.

The near real time forecasts from ECMWF are used in the NRT production as auxiliary input data.

4 Evaluation overview

In this section, the temporal and spatial coherency of the AOD CDR is evaluated based on qualitative analysis. Note that no filtering on AOD was made for this analysis, all available AOD where used. The daily average has been obtained averaging all available strictly positive AOD values for each day at the original PMAp resolution (10/5x40 km^2).

4.1 Temporal analysis

4.1.1 Metop-A

The AOD time series from PMAp/Metop-A is shown in Figure 4. The AOD is displayed as a global daily average (small dots) together with a 30-day running mean (solid lines). The global average is presented in grey, the AOD over land in green and over ocean in blue. The time series appears generally smooth without outliers and with a characteristic

[4] https://ladsweb.modaps.eosdis.nasa.gov/archive/allData/61/MOD08_M3/
[5] https://ladsweb.modaps.eosdis.nasa.gov/archive/allData/61/MOD08_D3/
[6] https://darktarget.gsfc.nasa.gov/content/what-dark-targetdeep-blue-merged-product

annual cycle. Over land, high values of AOD occur during the March to July period. These are linked to massive dust events, e.g., occurring over the Sahara and the Arabian peninsula as well as biomass burning, e.g., occurring in South Africa, South America, and Siberia.

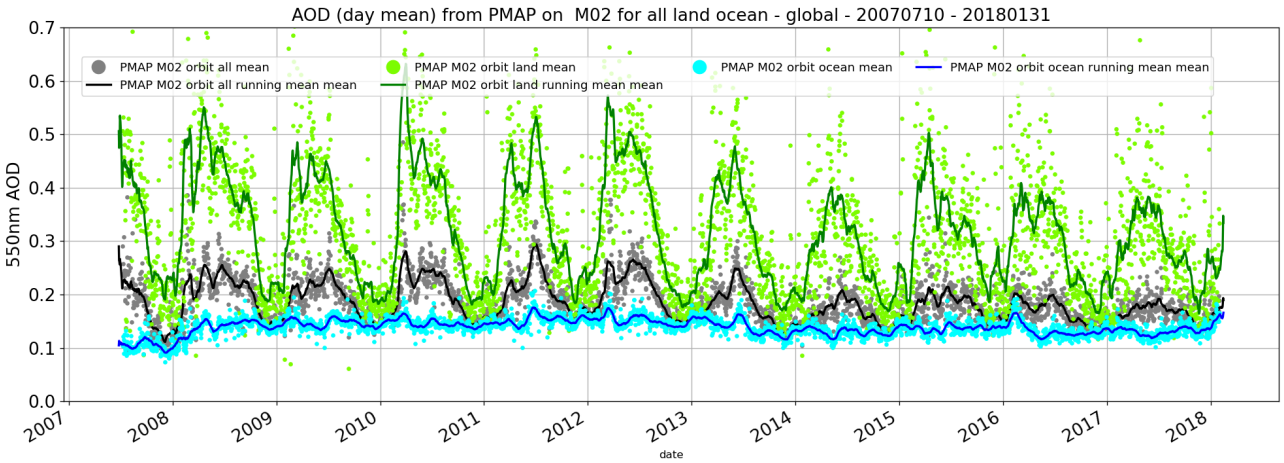

Figure 4: Daily average of the Metop-A (M02) PMAp AOD at 550 nm over the entire globe (black), land (green) and ocean (blue). Plain dark lines are the running mean over 30 days.

Two steps however are noticeable: the first in the beginning of 2008, less than a year after operational GOME-2 L1 data was available. This is mostly observed over ocean for which AOD increases from values around 0.1 to above 0.15, but also a smaller decrease over land. The change is explained by the change in the GOME-2 PMD band definitions[7] that occurs on the 11th of March 2008 (EUMETSAT, 2017). Mid 2013, a slight decrease is also detected. This can be associated with the swath width change of GOME-2 instrument on Metop-A, to a narrower swath (Table 3). In the previous years, while Metop-A swath was wider, unusual high values of AOD towards the edges of the swath have sometimes been detected (see Figure 5).

The impact of the swath on AOD is shown in Figure 6 where the daily AOD values are shown before 2013 as retrieved (dark colours) and after limitation to the narrow (light colours). As can be seen, after the swath reduction, the step in mid-2013 mostly disappears over ocean, strongly suggesting a slight decrease of performance at the swath edges. One possible reason for this could be the correction for the radiometric degradation applied to the GOME-2 input data, which may require a new adjustment for the wide swath edges on Metop-A.

[7] https://www-cdn.eumetsat.int/files/2020-04/pdf_gome_factsheet.pdf see band definitions table 13 and 14 page 17.

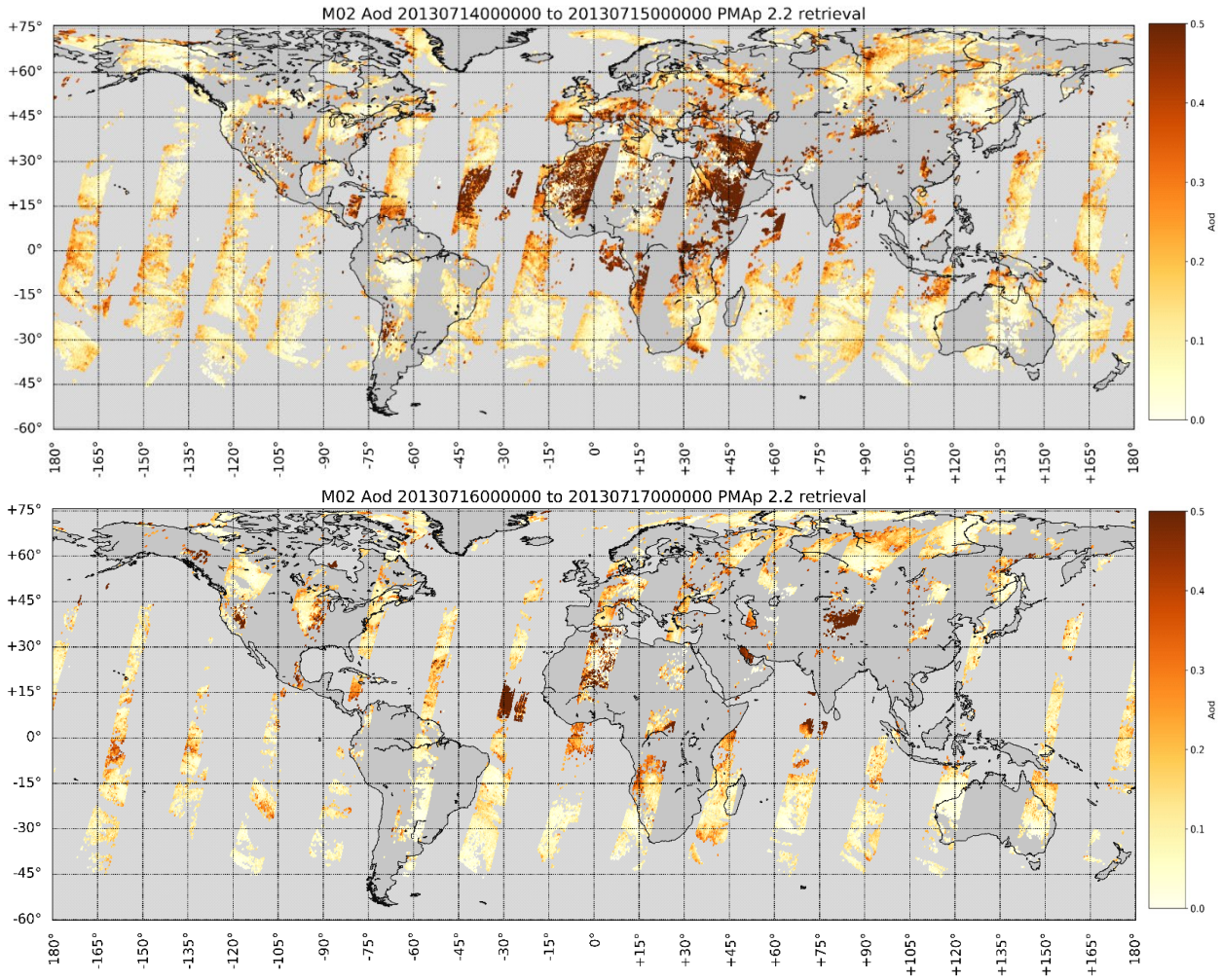

Figure 5: Daily AOD map from Metop-A, the top panel shows the data before swath width reduction (swath = 1920 km) and the bottom panel after the swath width reduction (swath = 960 km) on 14 and 16 of July 2013, respectively.

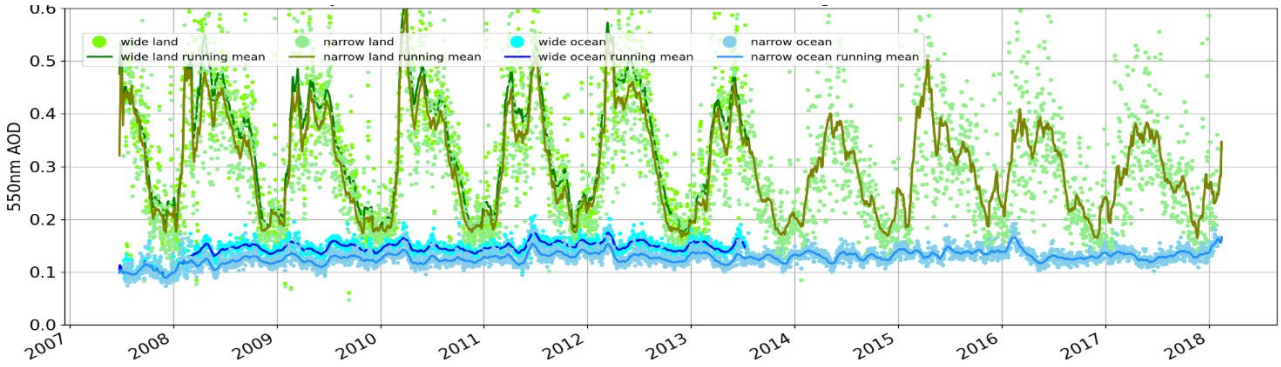

Figure 6: Daily AOD for Metop-A (M02) in the original setup (wide swath until July 2013 and narrow swath after) (dark colours) and only using data with a reduced viewing angle (960 km), to mimic a narrow swath measurement (light colours).

4.1.2 Metop-B

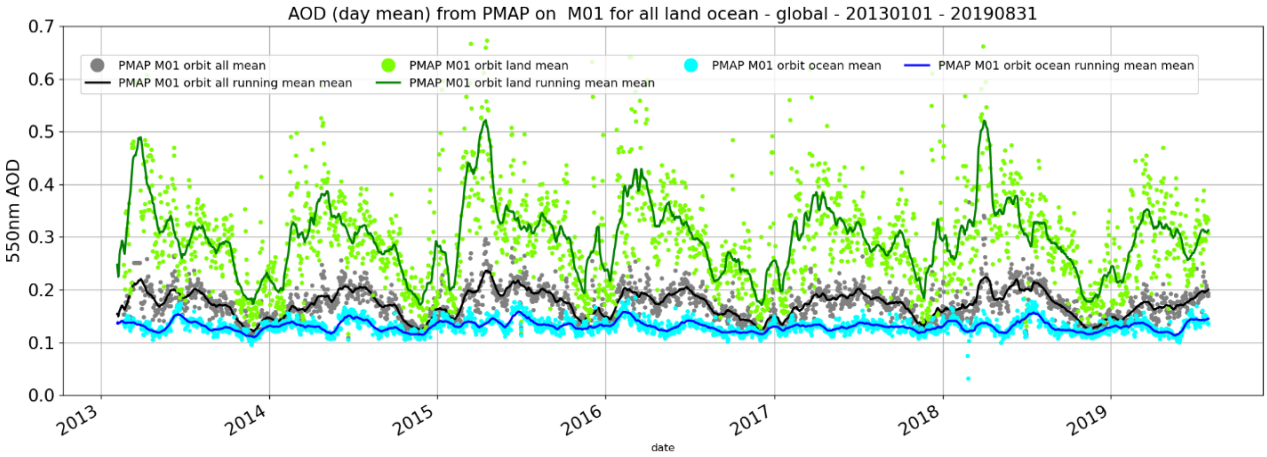

Figure 7: Daily average of the Metop-B (M01) PMAp AOD at 550 nm over the entire globe (black), land (green) and ocean (blue). Plain dark lines are the running mean over 30 days.

The daily averaged PMAp AOD for Metop-B is shown in Figure 7, with the same setup as in Figure 4. Overall, the AOD time series is homogeneous throughout the period. The daily global averaged AOD at 550nm is 0.16 varying between 0.1 and 0.25. Over land and ocean, the daily AOD is 0.12 and 0.25, respectively. There is a small seasonal cycle over land with larger AOD values in March and April.

4.2 Temporal consistency of Metop-A and –B

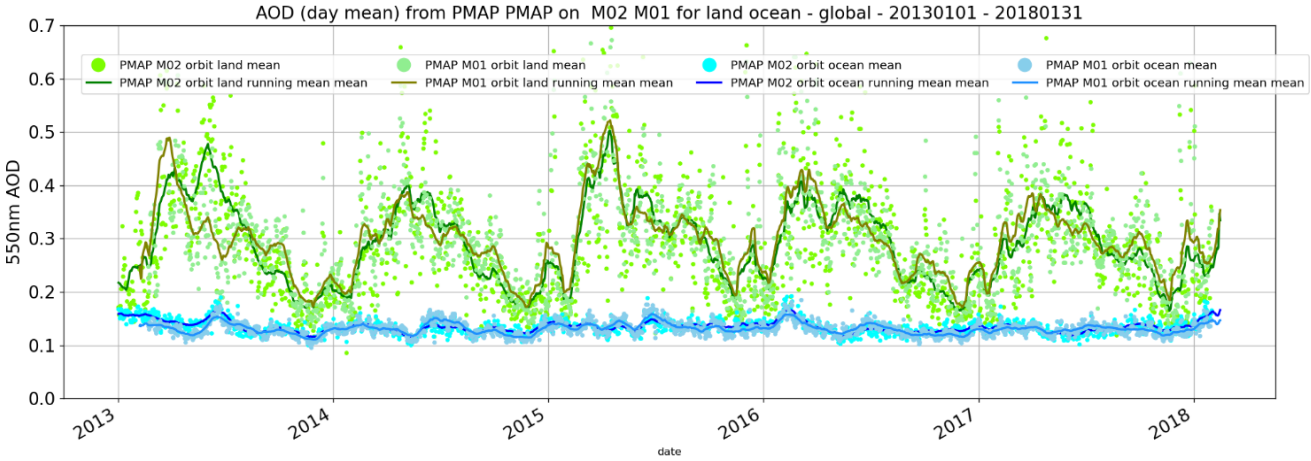

Figure 8: Time series of daily mean AOD of Metop-A and B for the overlap period from January 2013 to January 2018, AOD over land in green and ocean in blue.

The comparison of the land and ocean AOD values between Metop-A and -B is shown in Figure 8. The overall agreement between Metop-A and Metop-B AOD retrieval is good keeping in mind that from 2013 Metop-A swath is 960 km while Metop-B swath is 1920 km. Over ocean, the agreement is very good and AOD from both Metop satellites exhibits similar temporal variability (intra- and inter-annual) for the whole time series. Over land, larger differences are found for 2013, which is mostly due to the explained change in

swath width as already explained. However, for the remaining period, the differences are small and the temporal variability is similar.

4.3 Temporal and regional homogeneity

In this section, we present the temporal homogeneity of the AOD time series for three regions depending on the latitude. Figure 9 shows the daily averaged AOD for Metop-A over three different geographical areas, the Northern Hemisphere (0-90° N, *a*), the tropics (23°S-23°N, *b*) and the Southern Hemisphere (90°S-0, *c*). For both hemispheres, a peak in AOD is observed for their respective spring season with values around 0.5 for the Northern Hemisphere (NH) and 0.2 in the Southern Hemisphere (SH).

a) Northern hemisphere

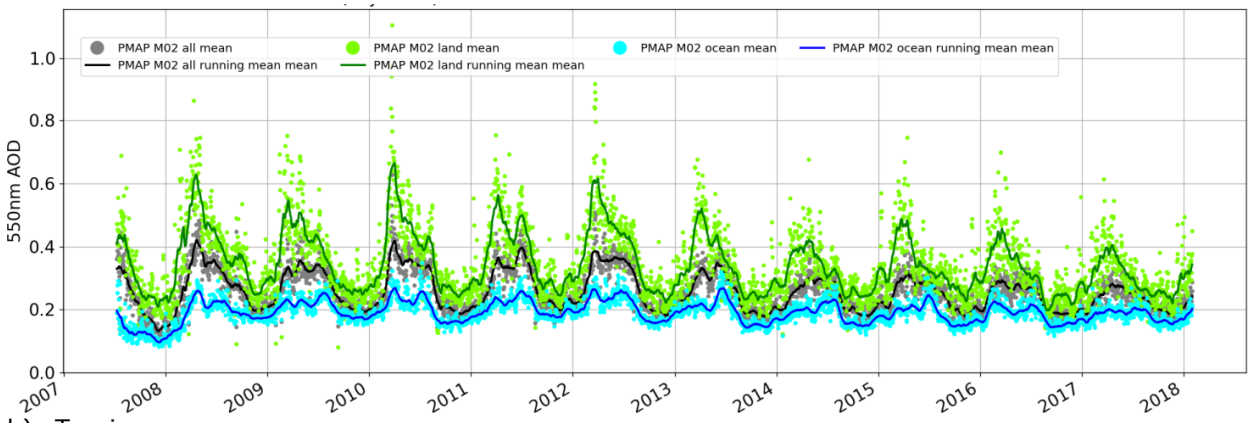

b) Tropics

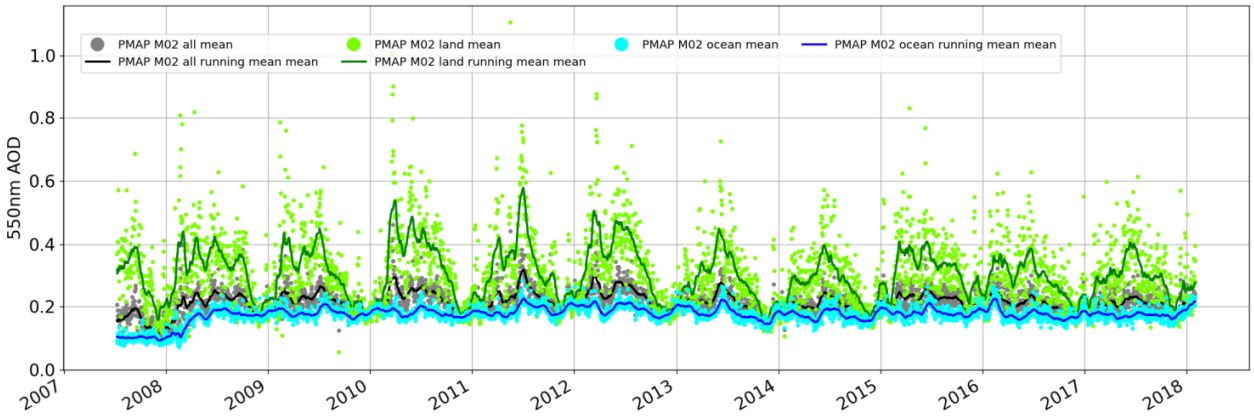

c) Southern hemisphere

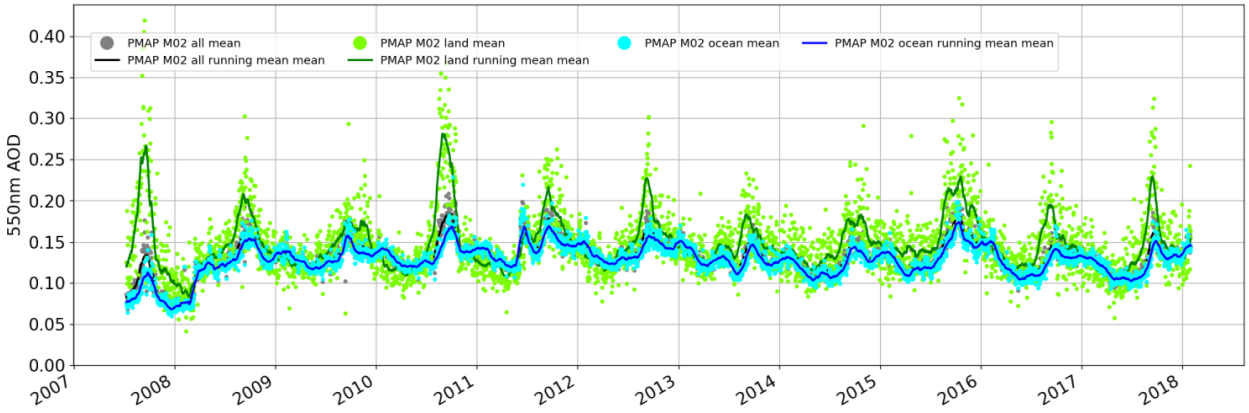

Figure 9: Same as Figure 4 but over three different areas: Northern, Southern hemisphere and tropics.

With the exception of the first increase in 2008, the ocean values over the tropics, a region less affected by seasonal variation, are very stable and show no apparent annual cycle. In the Southern hemisphere, land and ocean values are very similar most of the time, being the consequence of the fact the land surface is much smaller in this hemisphere. Exceptions occur in southern spring time, when biomass burning releases large quantities of aerosols into the atmosphere. Due to the different geographical distribution of land, the AOD signal is strongly regionally dependent.

Figure 10 shows the daily zonal average AOD obtained from the daily data gridded at a 1°x1° resolution over the entire period (2007 to January 2018) as a Hovmoeller plot for Metop-A. The high AOD values over northern continental areas clearly stand out and are in line with the features already detected in the time series analysis. Once again, the analysis shows a stable performance of the Metop-A AOD CDR over the entire period.

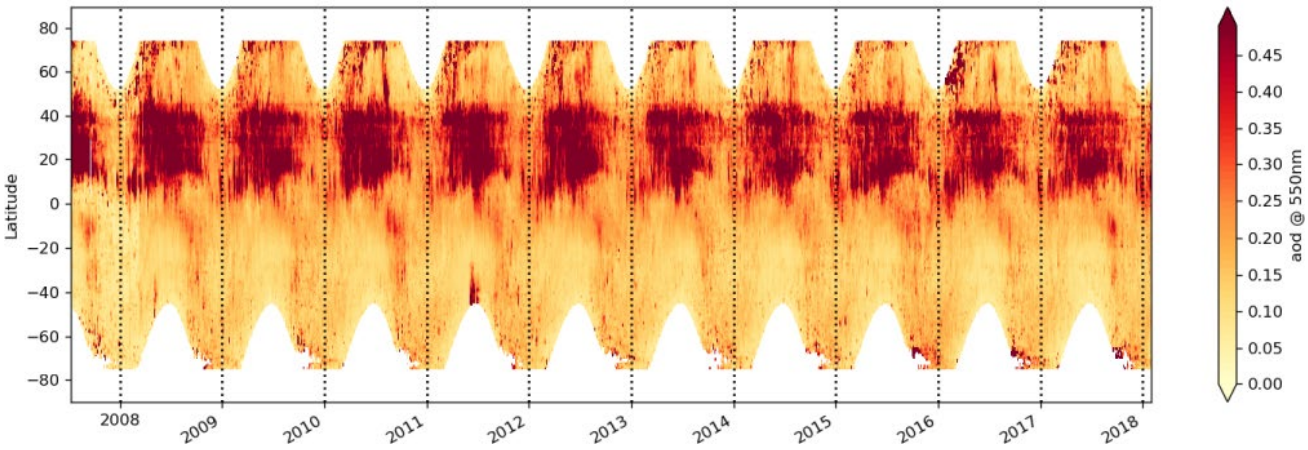

Figure 10: Hovmoeller plot of Metop-A (M02) daily average of the PMAp AOD at 550nm.

The corresponding zonal latitudinal averages for Metop-B is shown in Figure 11. Again, the high values over the northern land mass during spring and summer are clearly visible. In addition, we see high AOD values in spring in the high latitudes (north and south) from end 2015 onwards. These higher values seem to come from increased AOD values over high latitude oceans as shown in Figure 12 (right). The reason for these high values is probably linked with an issue of correctly identifying sea ice and residual polar clouds.

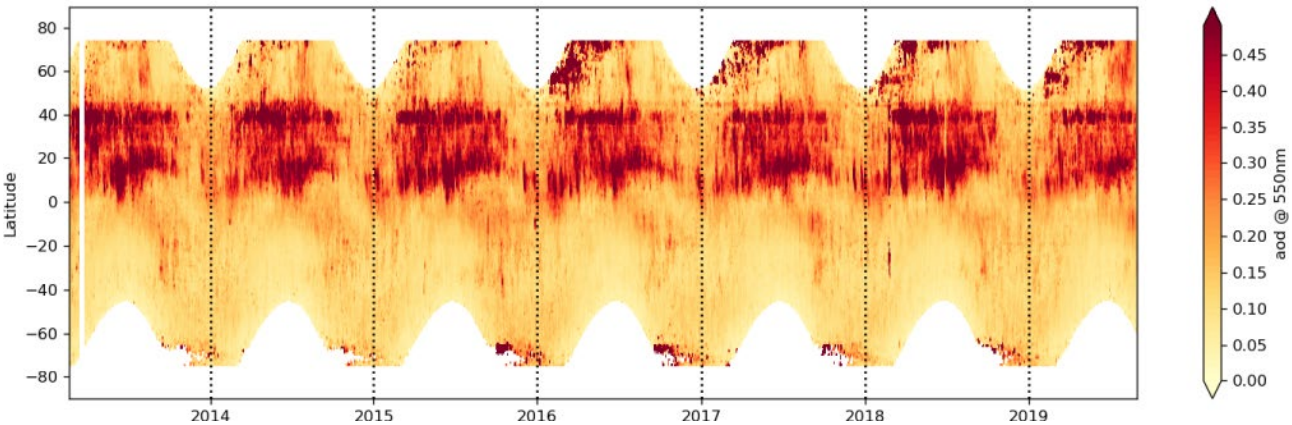

Figure 11: Hovmoeller plot of Metop-B (M01) daily average of the PMAp AOD at 550nm.

The plots in Figure 12 show an example of the monthly AOD geographical distribution over the globe for two months of Metop-A (left) and Metop-B (right) for April in 2014 and 2016. There is as expected a high aerosol loads over Africa and Asia. Especially in 2016, we can also detect high AOD values over the northern Pacific at the coasts of East Asia, which lead to the increase visualised in the zonal averaged plot (Figure 12).

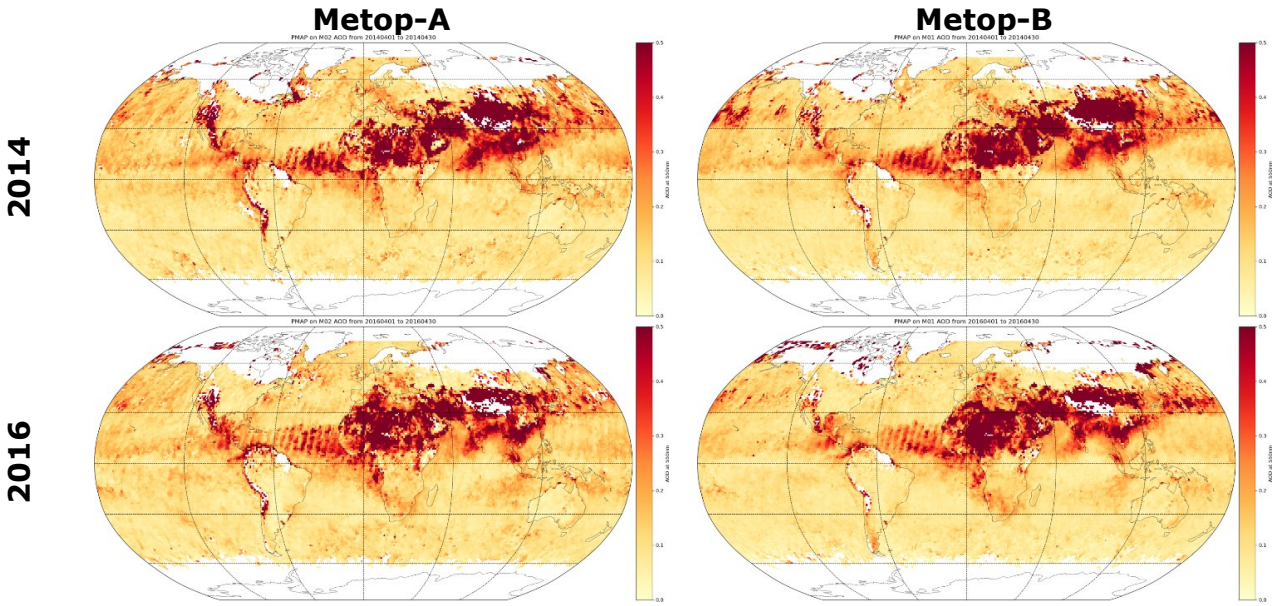

Figure 12: Selected monthly AOD maps for Metop-A (left) and B (right) for April 2014 (top) and 2016 (bottom). High aerosol load due to biomass burning, industry and local emitter over Africa and Asia clearly visible. For Metop-B in 2016 high values over ocean in north East Asia. AOD values are ranging between 0 and 0.5.

5 Comparison to near real time PMAp

The PMAp CDR data homogenisation is clearly visible when comparing with the PMAp NRT data. Those are generated in the operational ground segment at EUMETSAT with evolving versions of the AOD algorithm and changing auxiliary data with unavoidable discontinuities (see section 2.3 of (EUMETSAT, 2021c)). By definition, the archived NRT PMAp AODs are strongly affected by every operational improvement/change over time. The objective here is to evaluate whether the CDR has improved earlier NRT retrievals (prior to version 2.2.4) and generated a more homogeneous time series.

Throughout the periods illustrated in Figure 13 and Figure 14, 2014-2018 for Metop-A and 2014-2021 for Metop–B. In both cases, the retrieval over land only started in 2016. At the time of the end of the CDR (2018 for Metop-A and 2019 for Metop-B), the software version running in NRT in the ground segment was not the same than the one used for the CDR processing, which was only introduced in 2021.

In Figure 13, Metop-A data over ocean is very close together in the CDR and NRT data, but over land there are major differences. Although only less than two years overlap are available, we can clearly see an out-of-sync annual cycle in the NRT data.

In Figure 14, Metop-B data over ocean shows much larger differences, about 0.05 AOD (or up to 50% higher values in the NRT data). Over land we see the similar differences

in the annual variation as for Metop-A. The 1.5 years longer time series shows that this also continued in 2019. The CDR is not reaching 2021, thus a final statement of the agreement between CDR and latest NRT data cannot be made, especially as the auxiliary data input (NWP model data) is not the same.

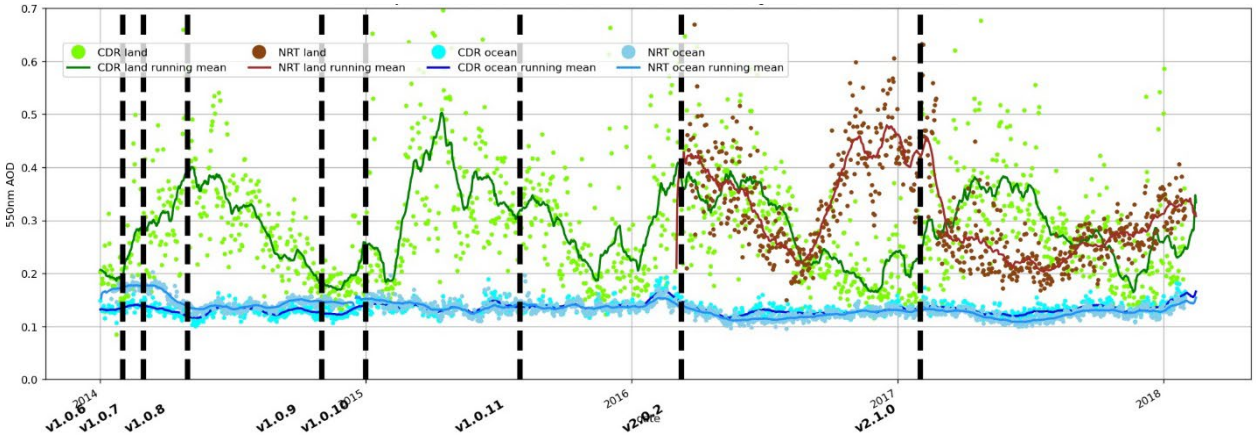

Figure 13: Metop-A (M02) comparison between climate data record (CDR, dark green (land) and dark blue (ocean)) and near real time (NRT, brown (land) and light blue (ocean)). Black dashed vertical lines show the introductions of main NRT algorithm updates. Individual dots are daily AOD means and lines are 30-days running means.

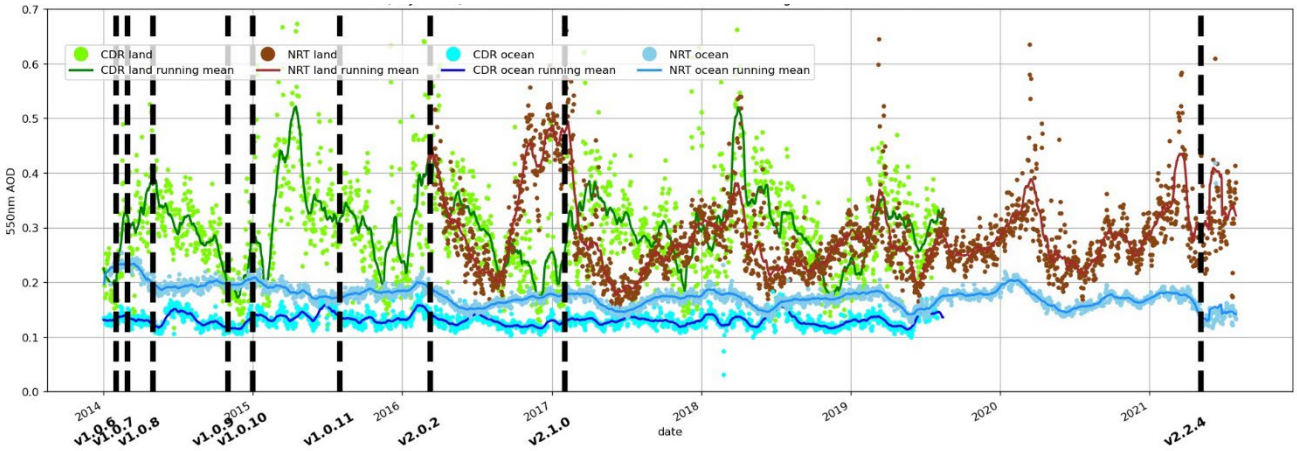

Figure 14: Same as Figure 13 but for Metop-B (M01).

We can see that the generation of the climate data record has extended the available data back in time, before the operational NRT data started. The CDR has also completely homogenised the AOD based on the same single algorithm, which is in addition the best available version of the processor. Whether the CDR has an obviously better quality compared to the NRT products will be shown by the comparisons with independent data in the following sections.

6 Validation based on independent data

6.1 Validation using AERONET measurements

The quantitative validation of the PMAp AOD data is based on the comparison against other corresponding independent data sets to ensure an unbiased validation. In this section, the ground-based reference is AERONET data described in section 3.1. This allows for a thorough comparison of the PMAp output against a well-documented and quality-controlled ground-based network.

AOD retrieved for the validation periods have been compared with the AERONET data set using the EUMETSAT operational PMAp/AERONET monitoring internal tool (EUMETSAT, 2021c).

The validation exercise is carried out using the following method and criteria:

- Collect AERONET measurements within a 30-minute span of a Metop overpass;
- Identify corresponding GOME-2 measurements in a 30 km circle around the station;
- Calculate the average AOD and plot the minimum and maximum value around the station;
- If AERONET measurement at 550 nm wavelength is not available, the AERONET value is extrapolated to 550 nm from the 500nm measurements.

6.2 Validation for a reference period

In this section, the PMAp performance for this CDR is evaluated for a chosen reference period for which the NRT PMAp algorithm version has been evaluated in (EUMETSAT, 2021b) as described in section 2.1.3.

6.2.1 Statistics based on direct comparison

A few examples of comparisons over land for Metop-A and -B are presented for two periods in 2013 and 2015. More than 2000 retrieval cases were available for validation of Metop-A and Metop-B respectively. A significant number of sites show a good agreement between PMAp and AERONET which can be seen in the density scatter plot with the highest population around the 1:1 line in Figure 15.

The performance of the PMAp retrieval is indicated in terms of gain, offset, Pearson correlation coefficient (R) and number of retrievals (N). The gain and offset refer to the slope and offset of the line of best fit in the scatterplot of PMAp and Aeronet AOD. The Pearson correlation coefficient is a measure of linear correlation between PMAp and AERONET AOD. It is the covariance of two variables, divided by the product of their standard deviations.

For the reference period in 2013 R is 0.58 for Metop-A and 0.56 for Metop-B, in 2015, R is 0.57 and 0.64 for Metop-A and -B, respectively. All statistics show improvement compared to the validation of NRT PMAp (EUMETSAT, 2021c), e.g. increase of R from 0.58 to 0.64 for Metop-B and decrease of offset from 0.10 to 0.06 in 2015. This improvement is expected due to the degradation correction used in reprocessed PMAp. Although the highest density of points is around 1:1 line, we also see a dispersion. Our investigations show that most of these pixels are the retrieval cases for dust over bright land surfaces, which is known to be challenging. For this reason, we provide a second

set of statistics, whereby we limit the validation to cloud-free cases over dark/normal land surfaces – called filtered data in Table 7. The statistics indicate a better agreement between PMAp and AERONET for the validation of filtered data, e.g. increase of R from 0.64 to 0.76.

To have a measure of the bias value between PMAp retrievals and AERONET, we use the Symmetric Mean Absolute Percentage error (SMAPE) and analyse its distribution as a function of AOD values. SMAPE is an accuracy measure based on percentage (or relative) errors and is defined as follows:

$$SMAPE = \frac{100\%}{n}\sum_{i=1}^{n}\frac{|x_i - y_i|}{(|x_i| + |y_i|)/2}$$

where *x* is the observation (here PMAp AOD) and *y* is the reference value (here AERONET AOD) and the range of SMAPE is 0-200%. The performance of PMAp over land are overall around 50% for SMAPE, which corresponds to an uncertainty on AOD of about 15%, i.e., higher than the threshold requirements defined by GCOS (10%). But in some of the AOD bins (in bias per AOD distribution), the bias is less than 40%. The bottom panels of Figure 15 and Figure 16 shows SMAPE per bin of AOD. SMAPE values are binned with 0.05 bin-width in the 0 to 0.5 AOD range, for AOD values greater than 0.5 bin width is equal to 0.1. Bars with number of co-located measurements less than three are shown in blue. SMAPE average values are also reported for all available measurements in blue dashed line, for all available measurements from bins with AOD > 0.05 and having more than 3 measurements (red dashed line), and for all available measurements from bins with AOD > 0.2 and having more than 3 measurements (green dashed line).

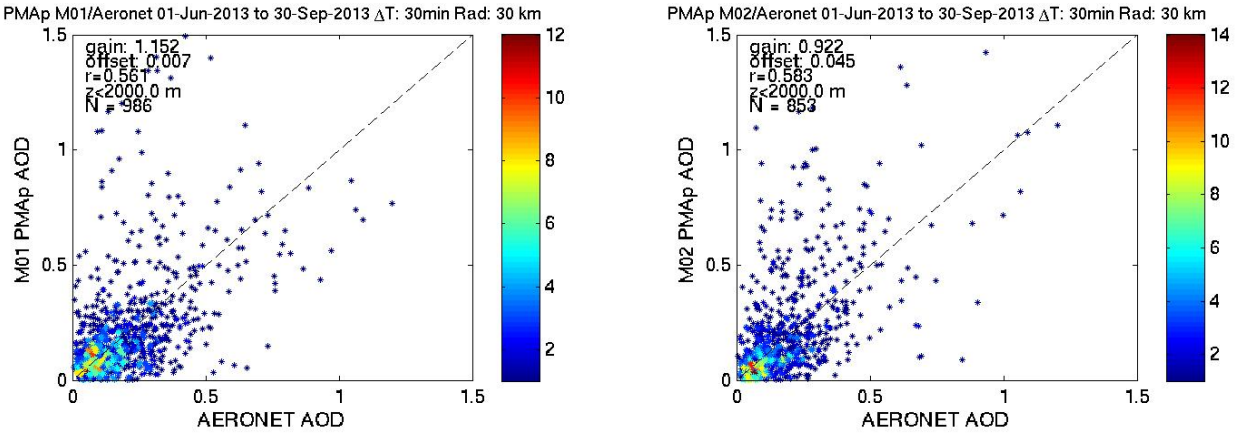

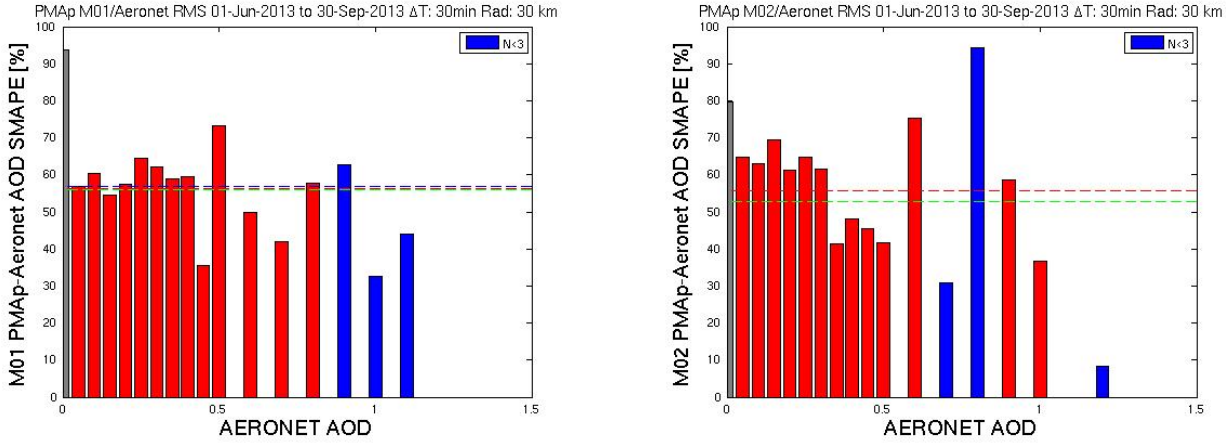

Figure 15: Validation of PMAp over land for June-September 2013. Top panels: scatterplots of PMAp and AERONET AOD, left Metop-B, right: Metop-A; bottom panels: SMAPE per bin of AOD in AERONET.

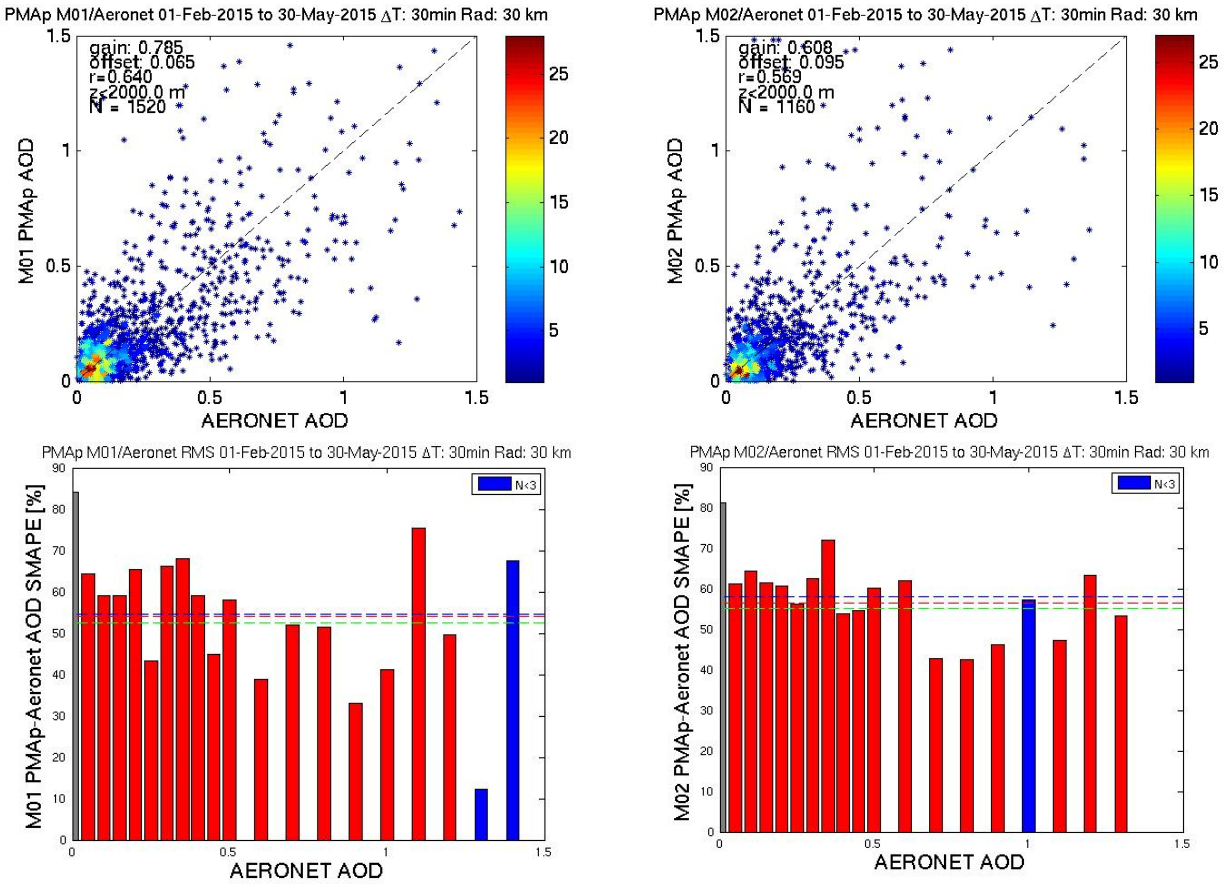

Figure 16: Validation of PMAp over land in February-May 2015, top panels: scatterplots of PMAp and AERONET AOD, left Metop-B, right: Metop-A; bottom panels: standard mean absolute percentage error per bin of AOD in AERONET. Bins for which the number of measurements is < 3 are shown in blue.

For the validation of PMAp over ocean, the AERONET measurements of stations located at small islands have been used, since, most AERONET stations are distributed over land. For this reason, the number of validation cases over ocean is considerably smaller compared to the land. Figure 17 and Figure 18 show validation results over ocean for

Metop-A and -B over ocean for 2013 and 2015 with scatter plots at the top, and SMAPE at the bottom. A good overall agreement is observed between PMAp and AERONET over ocean. In 2015, the correlation coefficient is 0.85 and 0.75 for Metop-A and B, respectively. SMAPE values are mostly smaller compared to PMAp retrieval over land. A summary of validation over ocean is given in Table 6.

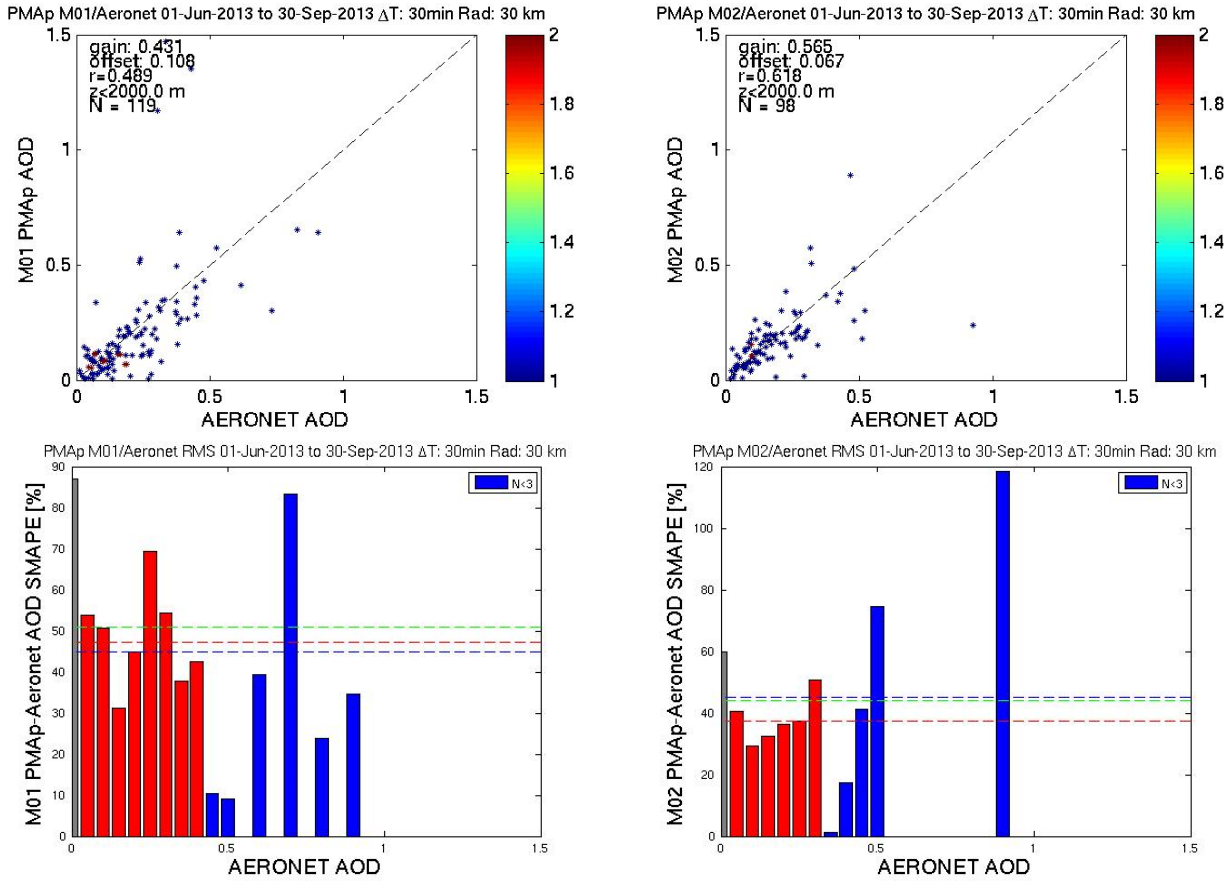

Figure 17: Validation of PMAp over ocean in June-September 2013. Top panels: scatterplots of PMAp and AERONET AOD, left Metop-B, right: Metop-A; bottom panels: SMAPE per bin of AOD in AERONET.

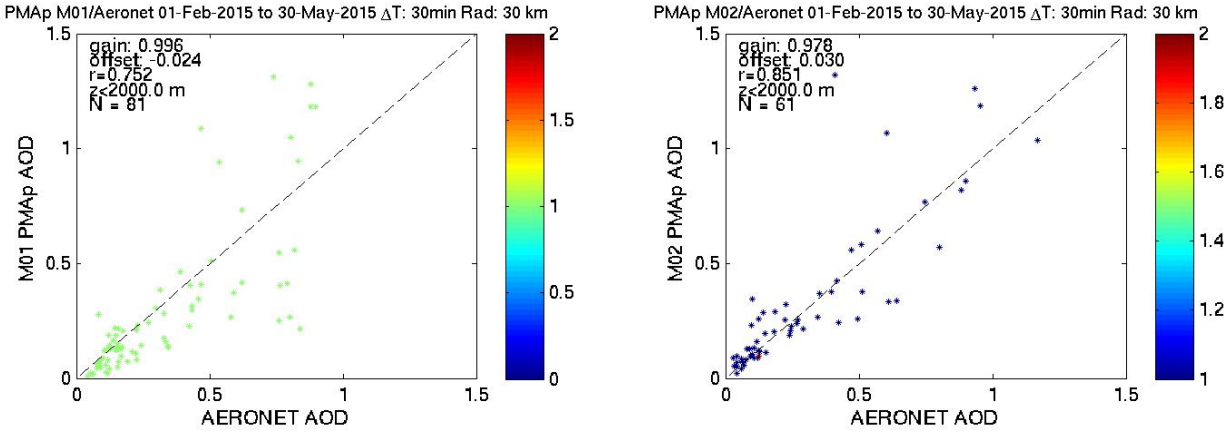

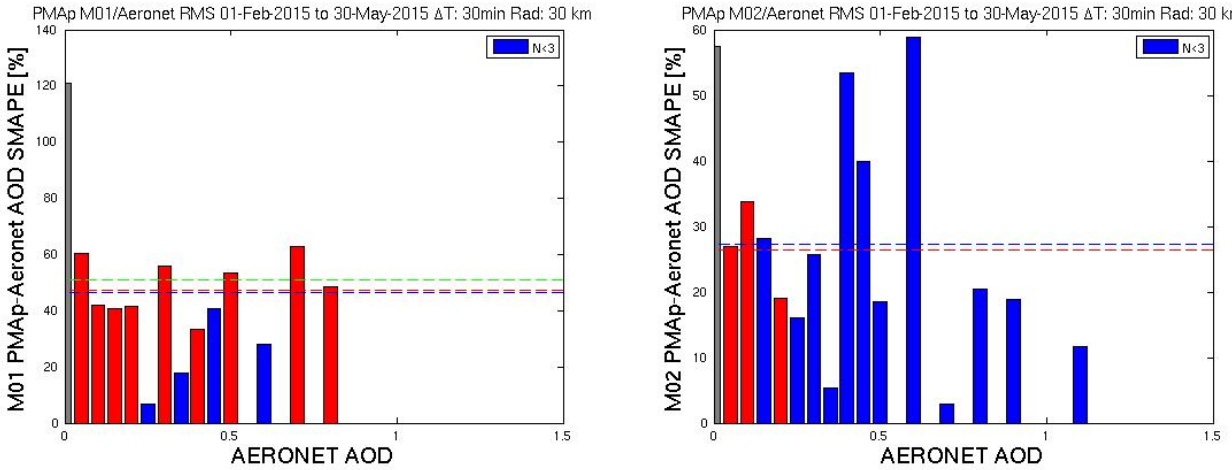

Figure 18: Validation of PMAp over ocean in February-May 2015. Top panels: scatterplots of PMAp and AERONET AOD, left Metop-B, right: Metop-A; bottom panels: SMAPE per bin of AOD in AERONET

In Table 6 and Table 7, a summary of statistics for the validation of PMAp AOD against AERONET AOD over land and ocean is presented. Over land, the statistics are presented for two cases: "all data" for which all retrieved AOD are collocated and "filtered ones" for which only cloud-free and normal/dark land surfaces are included. The increase of correlation and decrease of offset in case of filtered data indicate a trend towards a slight overestimation of AOD when PMAp retrieves in partially cloudy scene or over bright surfaces. Compared to Table 1 providing similar results from the evaluation based on the PMAp NRT AOD, the performance is fully comparable, and even slightly better (for instance for R). The only exception is found for Metop-A in 2013 over ocean but this difference is explained by outliers which mostly impact the calculation of the gain.

Table 6: Summary of validation of PMAp v2.2.3 AOD against AERONET AOD over **ocean**.

	June - Sept 2013		**Feb – May 2015**	
	Metop-A	**Metop-B**	**Metop-A**	**Metop-B**
gain	0.56	0.43	0.97	0.99
offset	0.06	0.10	0.03	-0.02
R	0.61	0.49	0.85	0.75
N	98	119	61	81

Table 7: Summary of validation of PMAp v2.2.3 AOD against AERONET AOD over land.

	June - Sept 2013				**Feb – May 2015**			
	Metop-A		**Metop-B**		**Metop-A**		**Metop-B**	
	All data	**Filtered data**	**All data**	**Filtered data**	**All data**	**Filtered data**	**All data**	**Filtered data**
gain	0.92	1.05	1.15	0.83	0.60	0.50	0.78	0.61
offset	0.04	-0.04	0.00	0.00	0.09	0.07	0.06	0.04
R	0.58	0.70	0.56	0.80	0.57	0.74	0.64	0.76
N	853	150	986	127	1160	356	1520	298

6.2.2 Case study for one AERONET station

Beyond the overall statistics presented in the previous section it is interesting to see if the PMAP CDR can depict single events. This is now analysed for the AERONET station Badajoz in Spain for which the dust forecast from the WMO Sand and Dust Storm Warning Advisory and Assessment System (SDS-WAS) (shown in Figure 19), shows predicted high AOD values.

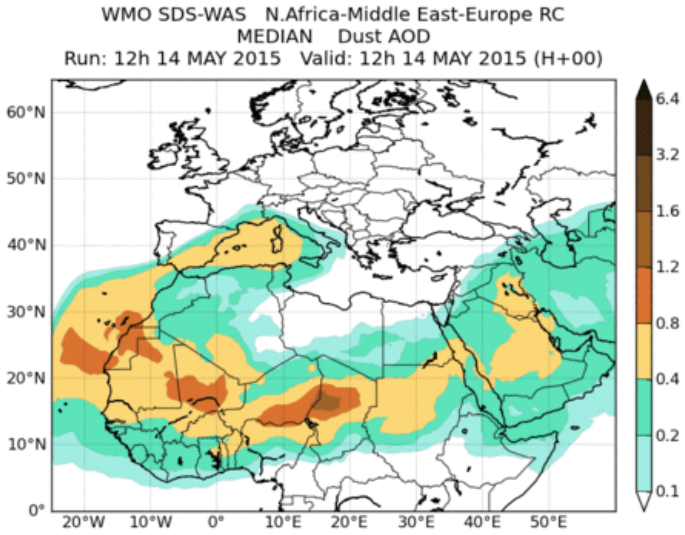

Figure 19: Dust forecast from the WMO Sand and Dust Storm Warning Advisory and Assessment System, showing the high AOD values also detected by the AERONET station an Badajoz and PMAp for mid-May 2015.

6.3 Statistics for longer time periods

In Figure 20, the AOD values from PMAp (red line) and AERONET (blue line) are compared for this AERONET station. The comparison shows a very good agreement, especially for Metop-B over the three month period from March to May 2015. The dust event in the middle of May 2015 is also well depicted in both, the AERONET and the PMAp data. Due to the different orbits and hence collocation times between Metop-A and -B the peak values differ, but timing and intensity between PMAp and AERONET agree very well and confirm the forecast.

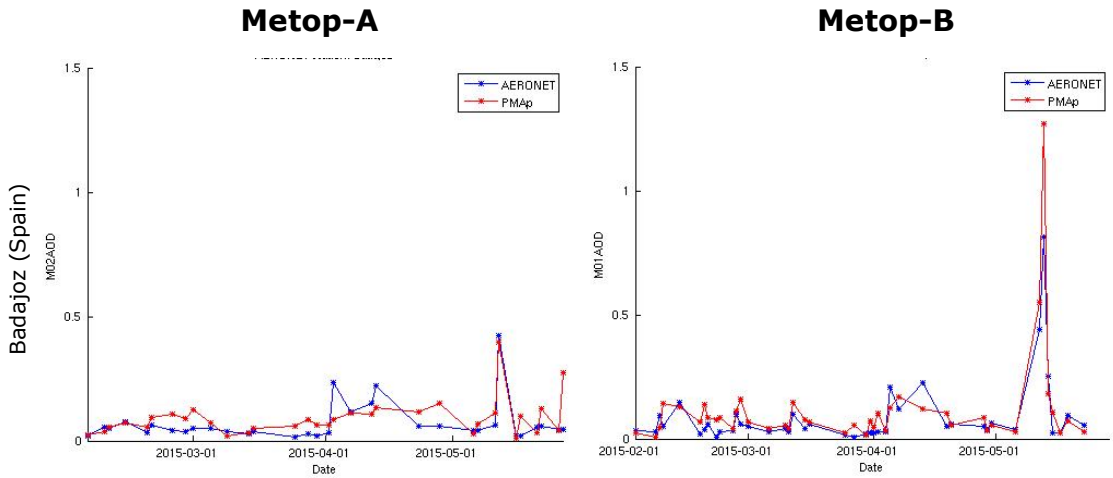

Figure 20: Time series of PMAp AOD (in red) compared to AERONET (in blue) for the site in Badajoz for the reference period February-May 2015. Left is PMAp from Metop-A, right is PMAp from Metop-B.

This case study for one single station shows that we can go from the overall scatter plot statistics to the point comparison of single AERONET stations. In the following sections the short time period selected to have a link between the NRT and CDR validation, is extended to cover the entire period covered by the CDR.

6.4 Statistics for longer time periods

6.4.1 Comparison on annual basis

In this section, statistics for annual data are presented. Figure 21 provides a summary of validation for the years 2008 and 2016 for Metop-A. For Metop-B eleven months of 2017 are shown in Figure 22. The statistics from the scatterplots and SMAPE plots show an overall stable performance of PMAp in different selected years of the CDR comparable to the reference periods shown before. Note that the number of validation cases in 2008 is significantly smaller than that of 2016. This is due to less AERONET stations available in prior years. Our investigations show that half of the AERONET stations used in 2016 did not provide data in 2008.

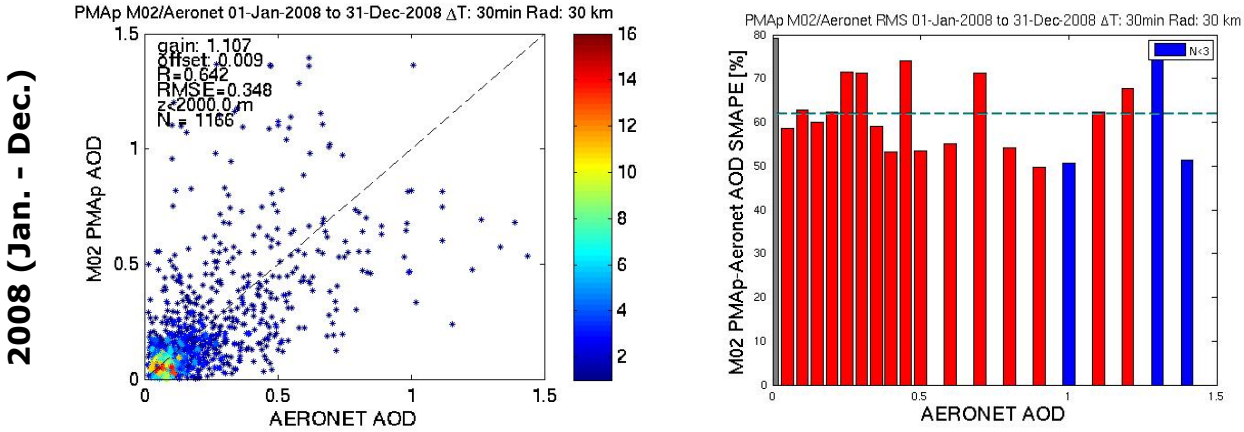

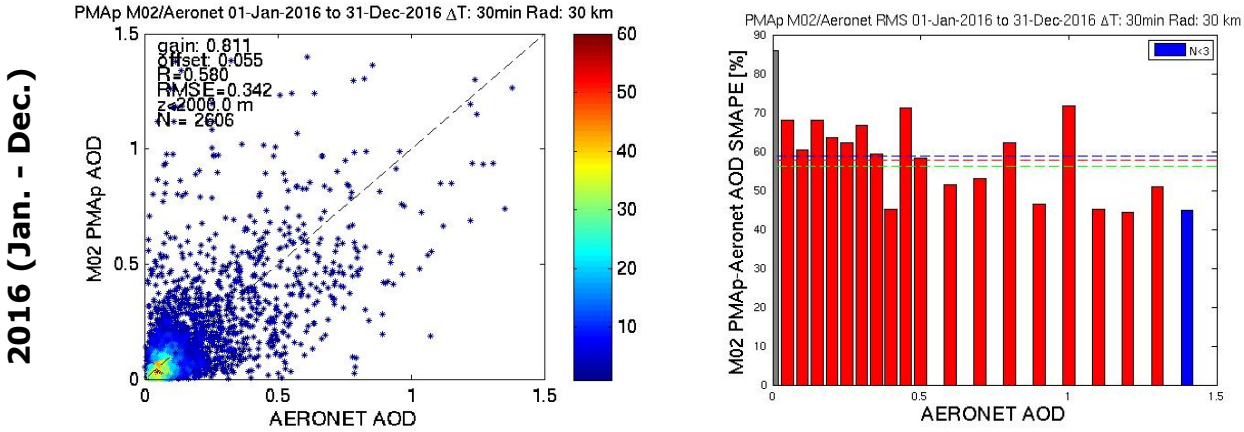

Figure 21: Validation of PMAp-A for years 2008 and 2016 in PMAp CDR, left column: scatterplots and relevant statistics, right column the distribution of SMAPE per AOD bin.

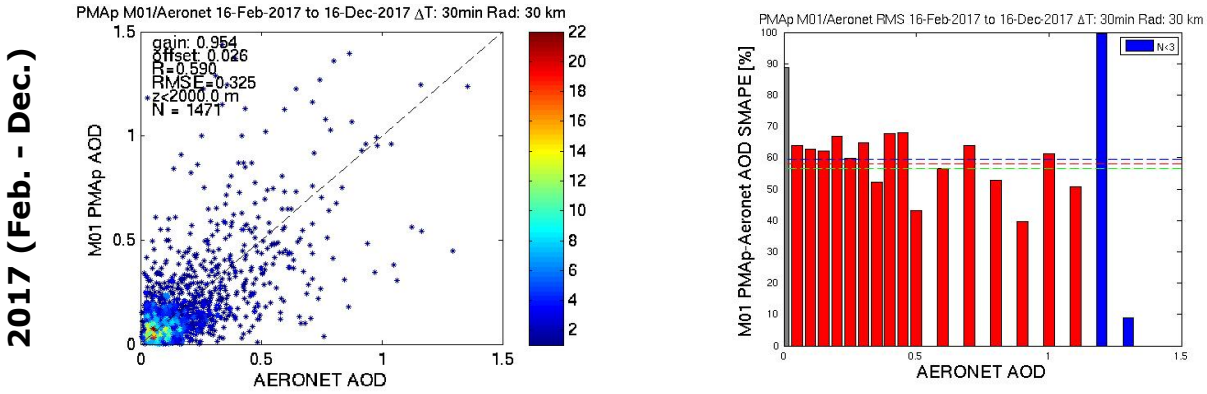

Figure 22: Validation of PMAp-B for year 2017 in PMAp CDR, left column: scatterplots and relevant statistics, right column the distribution of SMAPE per AOD bin.

6.4.2 Extended time series per station

In this section, a few examples of AERONET stations are selected, based on location providing examples for different aerosol regimes, quality and availability for comparison with PMAp. Data for Metop-A is shown in Figure 23 for eight different stations. These are (in decreasing latitudinal order): Hohenpeissenberg, University of Wisconsin, Beijing, Badajoz, Santa Cruz (Tenerife), Tamanrasset, Alta Floresta and La Réunion. These stations represent continental areas, desert stations, high pollution areas, rain forests and ocean. For all stations the trends and cycles agree well between the satellite and ground based measurements. In many cases, the variability and spikes are comparable. However, we see a couple of situations, e.g., Beijing in early 2015 and several occasions for Santa Cruz where PMAp has significantly higher AOD values than the corresponding AERONET station.

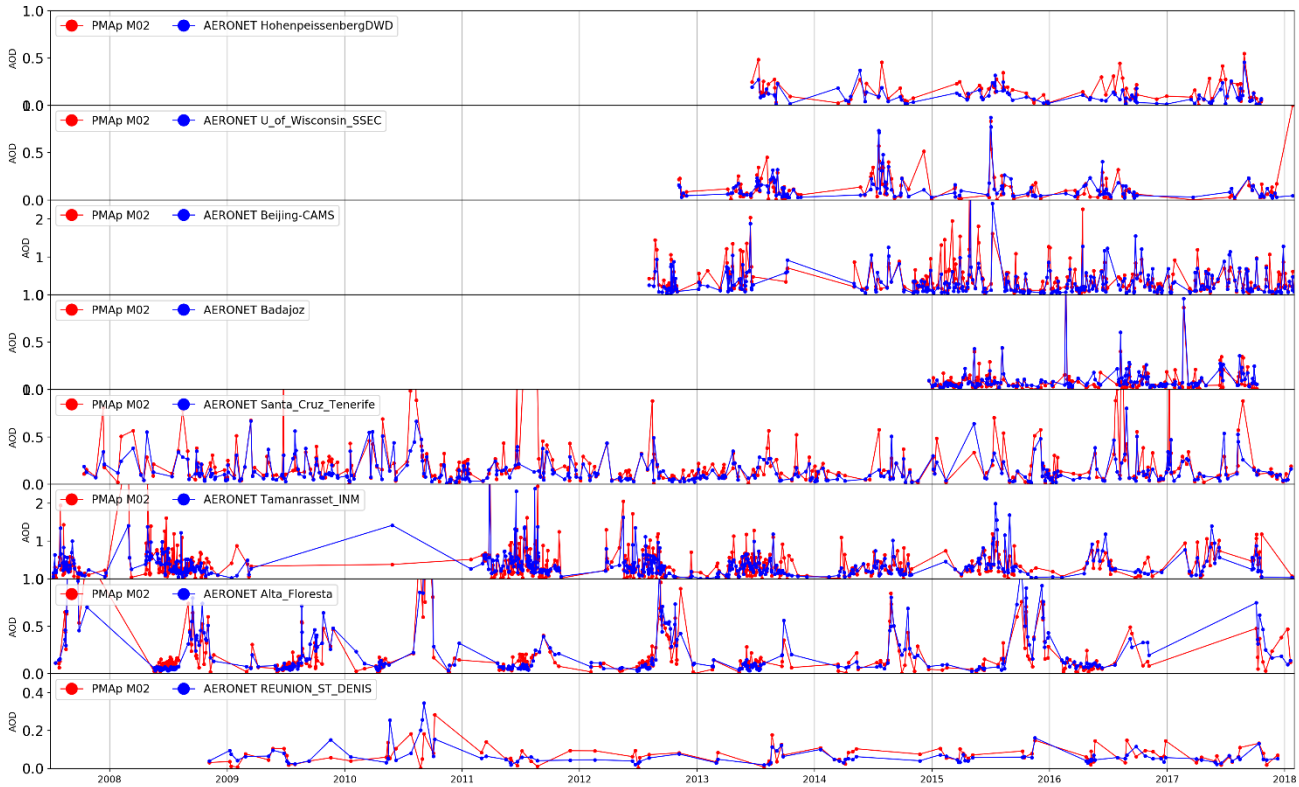

Figure 23: Time series of selected AERONET vs. PMAp stations, ordered by descending latitude for Metop-A from 2007 to 2018.

For Metop-B, we have selected the same stations as for Metop-A, the time series are displayed in Figure 24. The agreement again is very good between PMAp and AERONET measurements. As for Metop-A, we see the differences, especially for Beijing and Santa Cruz.

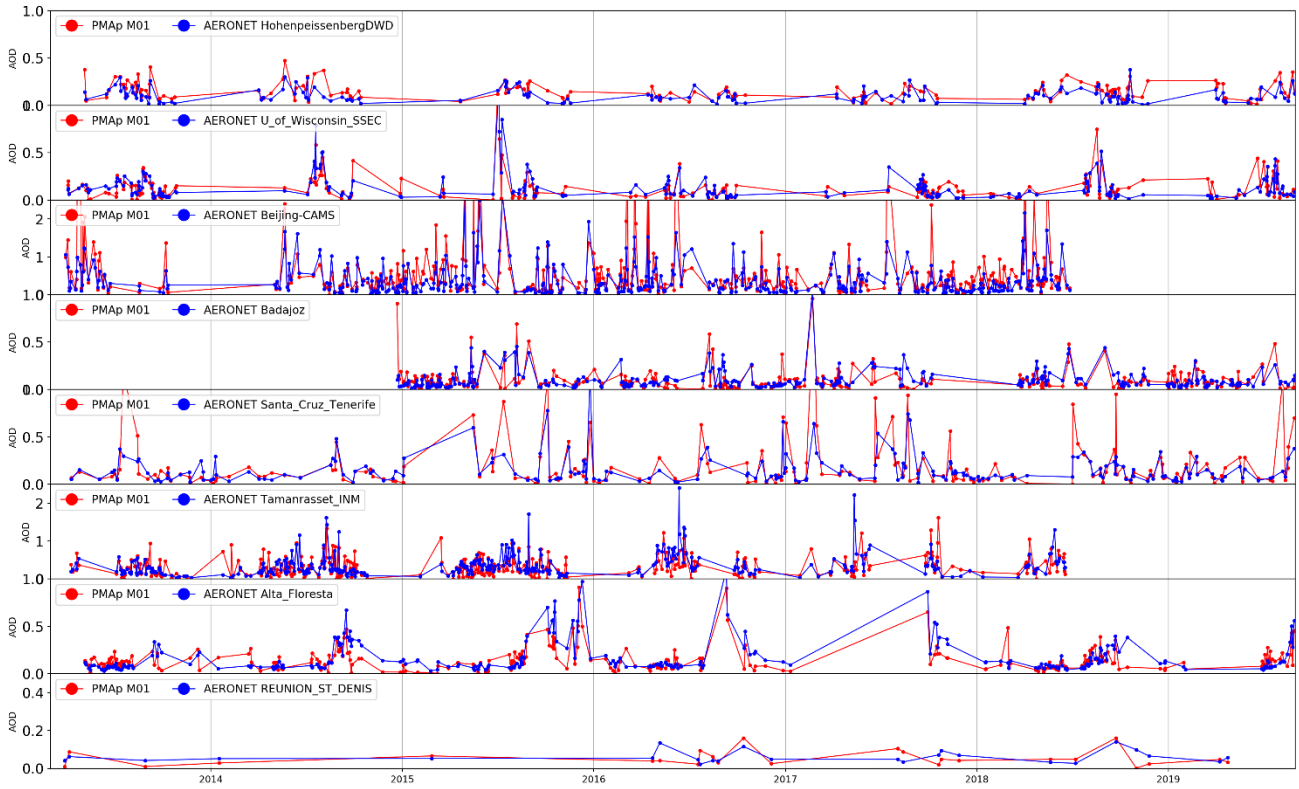

Figure 24: Time series of selected AERONET vs. PMAp stations, ordered by descending latitude for Metop-B from 2013 to 2019.

6.4.3 Global statistics

To gain an understanding of the performance of PMAp at different AERONET stations, some statistics were calculated for an increased number of locations compared to the previous section. The absolute bias and the correlation coefficient are shown for Metop-A and -B in Figure 25 and Figure 26 respectively, both figures covering the entire available data record. The largest differences appear in the subtropics, over desert targets with negative biases exceeding 0.2. In tropical regions, positive biases, also reaching 0.2 AOD difference can be found.

In Figure 27 and Figure 28, the root mean square error (RMSE) and Pearson correlation coefficient per AERONET station are presented for 2009 for Metop-A and some months in 2015 for Metop-B. The RMSE is often ~0.1 or below other stations in Europe at which correlation is mostly larger than 0.5 and close to 0.75. The highest values of the RMSE are in the northern subtropics, especially in Africa and Asia. Very good statistics are present for Europa, North and South America, where darker surfaces and lower aerosol loads are dominant.

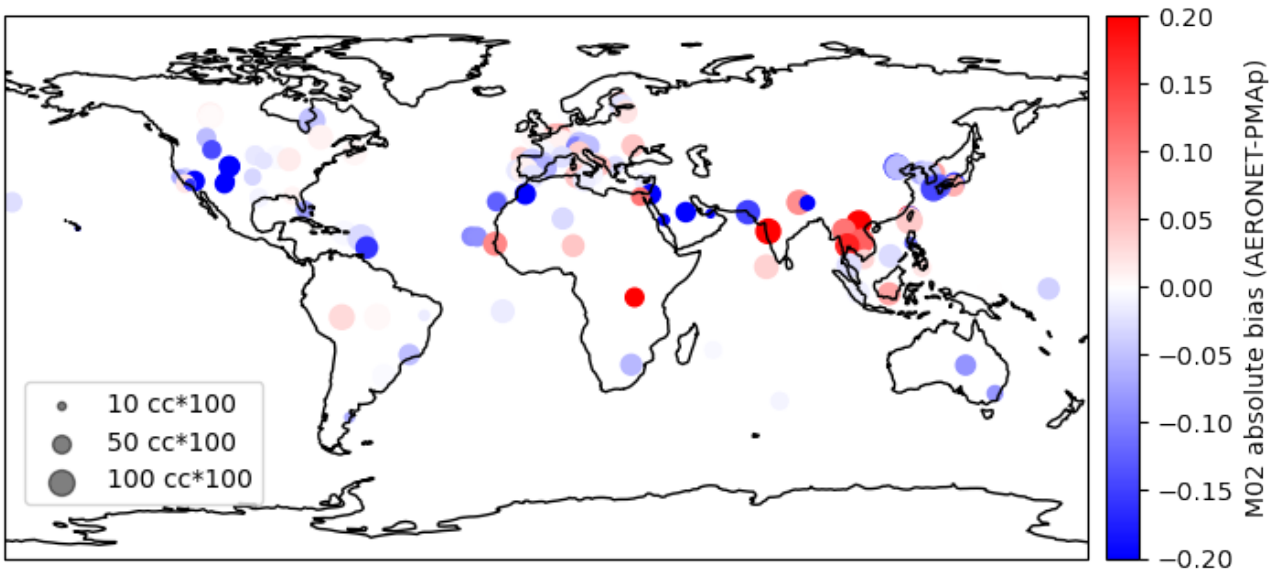

Figure 25: Metop-A (from 2007 to 2018) statistics for the difference AERONET stations minus PMAp. Colour coded show the absolute bias and the dot size show the correlation coefficient (cc). For.

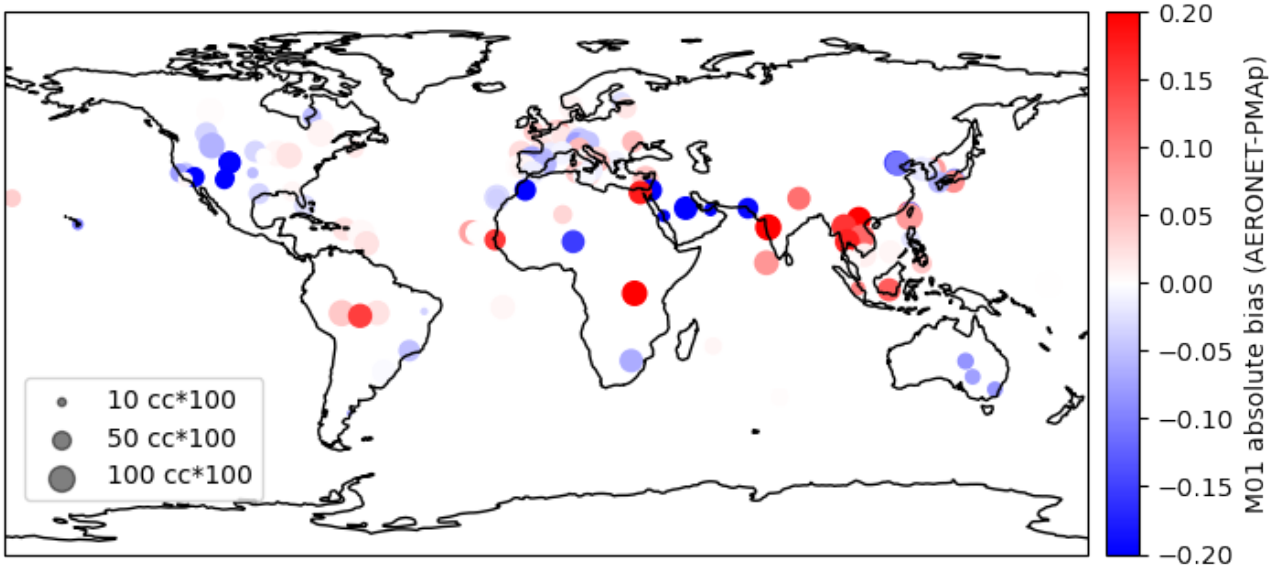

Figure 26: Same as Figure 25 but for Metop-B (M01) from 2013 to 2019.

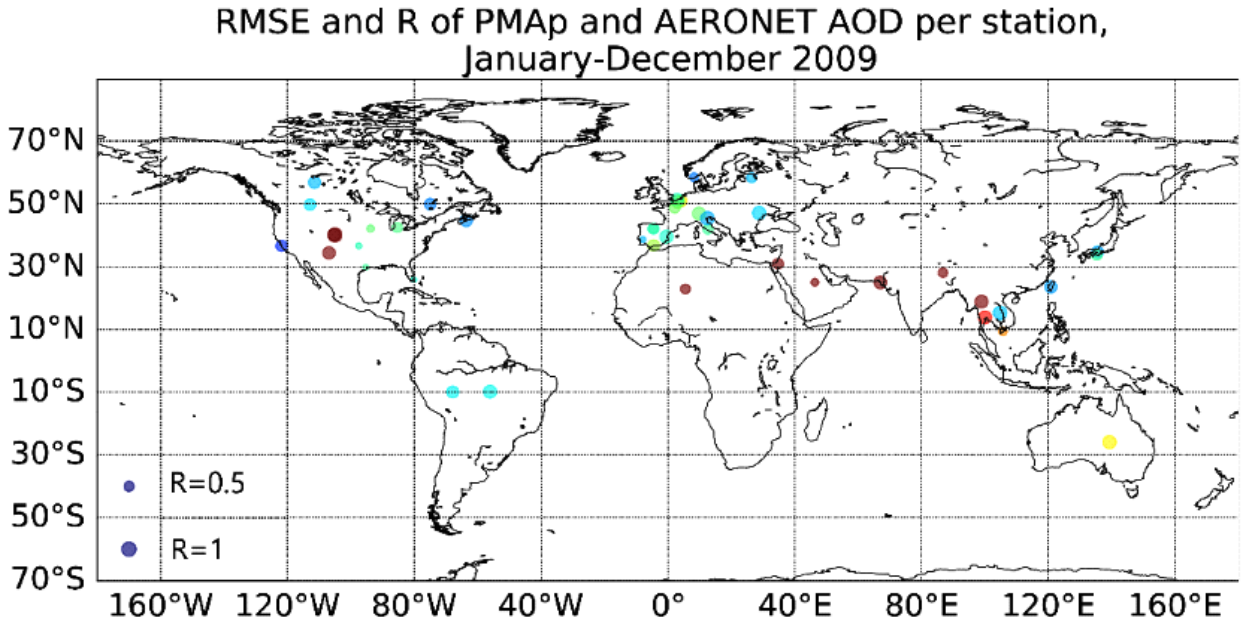

Figure 27: Pearson correlation (R) and RMSE per AERONET station for Metop-A for 2009, indicated by size and colour (scale see Figure 28) respectively (the larger the size, the higher is Pearson correlation).

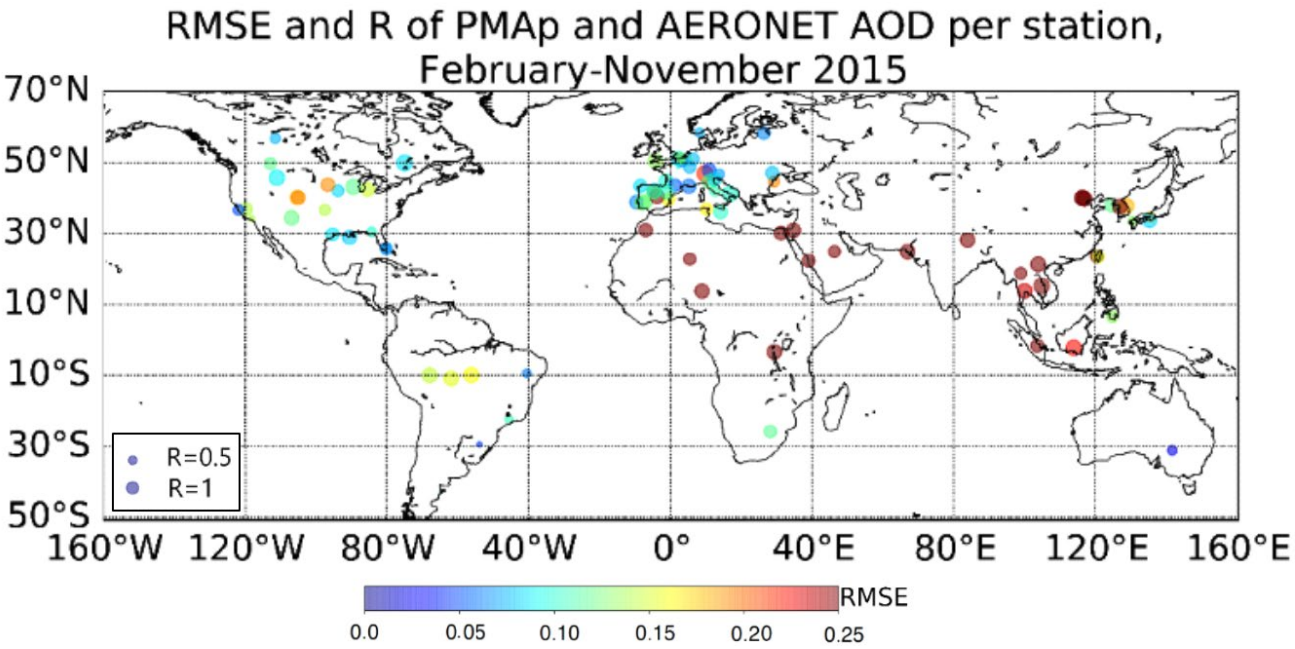

Figure 28: Pearson correlation (R) and RMSE per AERONET station for Metop-B and Feb-Nov 2015, indicated by size and colour respectively (the larger the size, the higher is Pearson correlation).

6.4.4 Space-time analysis for all AERONET stations

Results from the matchups with AERONET measurements can be presented all on one plot, AERONET sites sorted by decreasing latitude from north to south on the Y-axis, and time on the X-axis. The relative difference between PMAp and AERONET AODs is plotted in Figure 29 (Metop-A) and Figure 30 (Metop-B). Collocations can only be obtained when PMAp and AERONET measurements are both available, thus for AERONET stations with low solar elevation during winter gaps in the comparison time series are caused by the

fact that no retrieval can be performed under such conditions, which also causes a sampling bias in the winter hemisphere.

In most cases, the northern mid latitudes show higher AOD values for the AERONET stations, with some exceptions (e.g. University of Lethbridge). Between 40 to 42°N, we see a number of stations with a negative difference, most of these stations are located in the Mediterranean. Further to the south, we have a number of stations where positive and negative values interchange. In the northern sub-tropics, the PMAp measurements are very often higher than the corresponding AERONET values. In the tropics, the AERONET measurements then are again higher in most cases. In the Southern Hemisphere the AERONET stations are only sparse, the few available outside of the tropics show generally lower AODs compared to PMAp measurements.

This analysis shows that there is no clear over- or underestimation of PMAp aerosols compared to AERONET, but rather a diverse picture with some indications of where the retrieval might have deficits as mentioned above, i.e., over bright or heterogeneous surfaces and at high aerosol values. It can also be seen that the systematic deviation for a station is either positive or negative for the whole period and the difference only changes sign for a few stations.

For Metop-B (Figure 30) we have a very similar picture, especially the geographical distribution and evolution over time matches Metop-A very good. Thus another indication that the two Metop satellites deliver data of comparable quality.

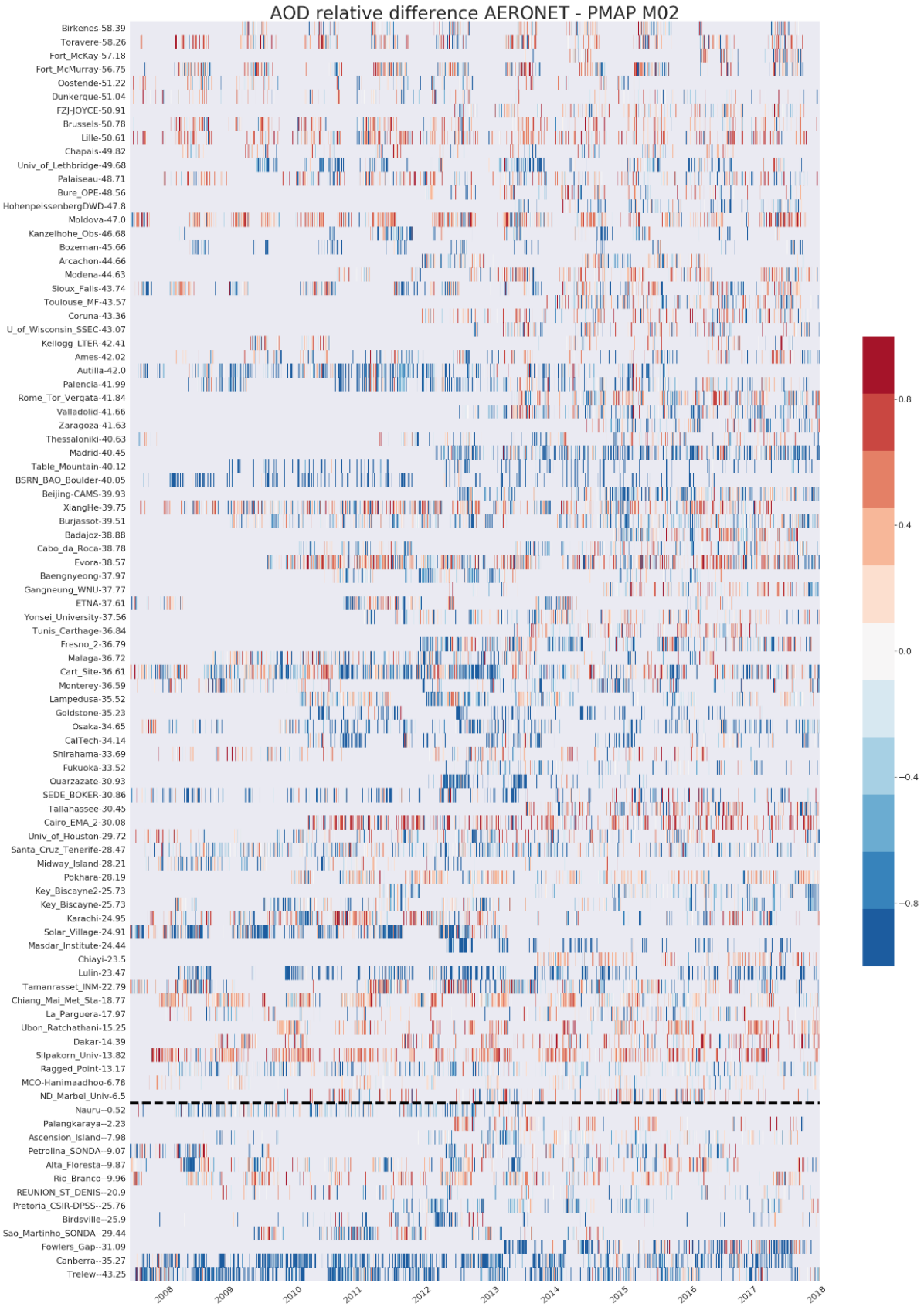

Figure 29: Relative AOD difference: (AREONET – PMAp)/AERONET for Metop-A for the period 2007 to 2018. AERONET stations ordered by descending latitude. Dashed black horizontal line indicates the equator.

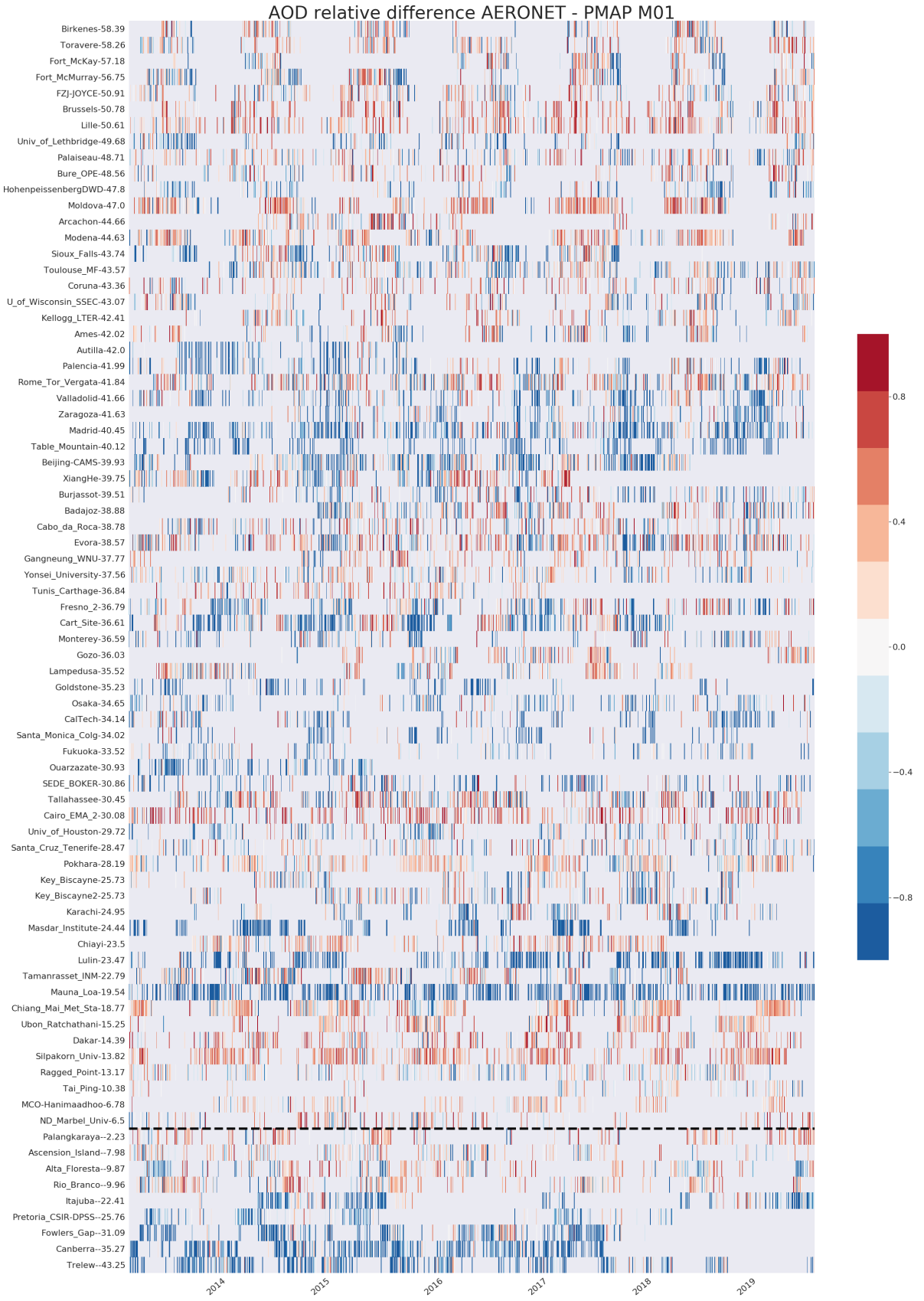

Figure 30: Relative AOD difference: (AREONET – PMAp)/AERONET for Metop -B for the period 2013 to 2019. AERONET stations ordered by descending latitude. Dashed black line indicates the equator.

Overall, the comparison between PMAp and AERONET confirms the good validation results for the latest NRT product as described in the beginning. Results in Section 6.2.1 for a selected period and Section 6.3 extended in time and to more stations have demonstrated this. The PMAp CDR thus has consistent quality over the entire time domain covered.

6.5 Comparison with MODIS AOD

The MODIS collection 6.1 AOD at 550nm is compared with the PMAp CDR AOD. The comparison to MODIS is done on daily and monthly AOD mapped to the same 1° latitude and longitude grid.

The analysis based on daily AOD allows a more direct comparison of retrieval between PMAp and MODIS and reflects the higher temporal resolution, which is closer to the instantaneuos PMAp products generated for this CDR. Due to the fact that this comparison is computationally heave starting from the L2 products it remains limited in terms of temporal coverage.

Even though the monthly AOD values of MODIS and PMAp differ in many ways (instruments, sampling, cloud masks, etc.), a comparison based on the monthly average values reveals important additional features of the AOD behaviour. Time series and spatial analysis allows to study the behaviour of the PMAp CDR AOD in terms of temporal changes, annual cycles and monthly maps showing the geographical distributions in comparison to the MODIS data.

The MODIS products used for this comparison are described in Table 5. For the analysis performed in this section, all PMAp AODs greater than zero were mapped to a regular 1x1° grid comparable to the MODIS grid. Negative AOD monthly means in the MODIS product were removed for the following analysis.

6.5.1 Comparison based on daily data

In this section daily mean AOD from PMAp/Metop-B and MODIS/Terra are compared over land and ocean.

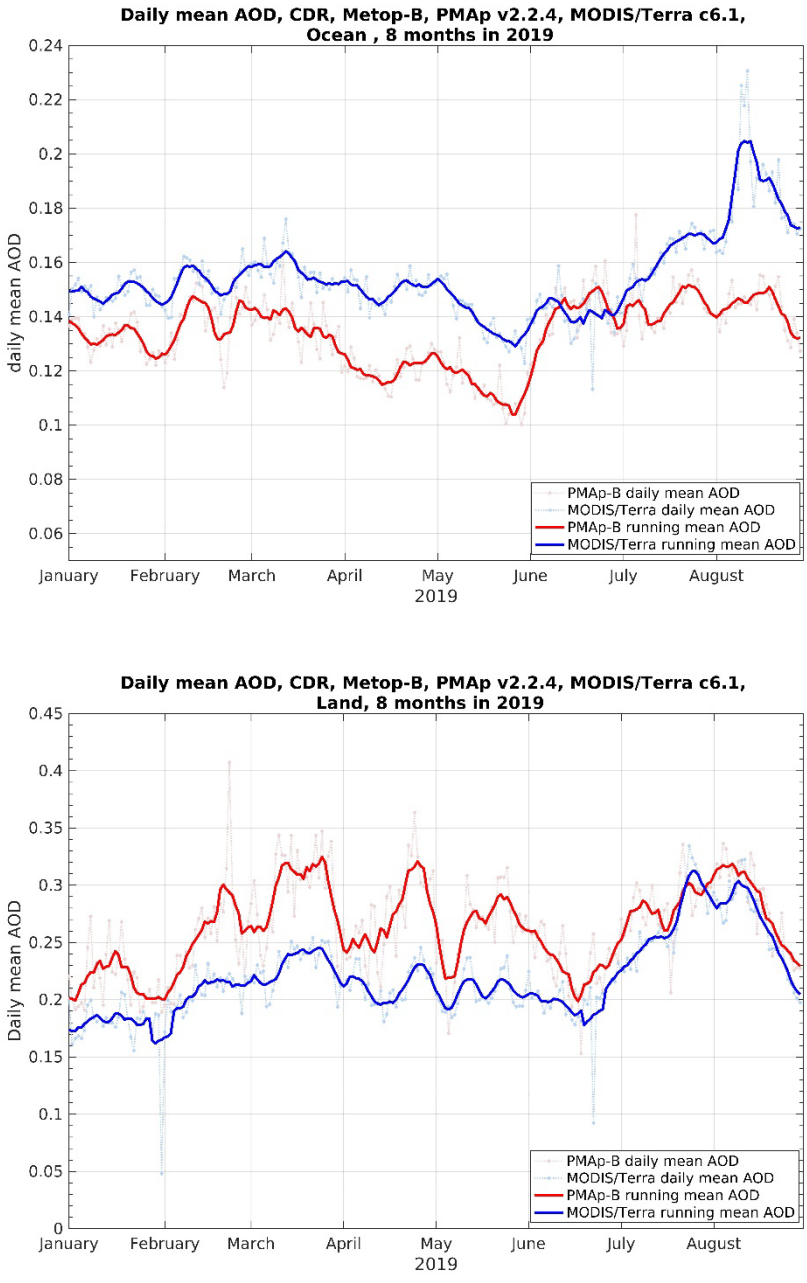

Figure 31: Comparison of daily mean AOD from PMAp CDR and MODIS/Terra. Top panel: over ocean and bottom panel: over land. Both data are gridded with a grid cell size of 1.0°.

Over ocean (top panel in Figure 31) high agreement between PMAp and MODIS/Terra daily mean AOD is observed in particular in January and February during which massive aerosol events are not frequent. It can be seen that PMAp AOD is lower than MODIS, while following the temporal variation. The difference between PMAp and MODIS/Terra

is in the range of 0.01-0.02 for these periods. However, in June and August when heavy aerosol plumes are observed, e.g. dust outbreaks from Sahara and fires in Amazon, the difference between PMAp and MODIS daily mean AOD becomes larger and PMAp shows larger AOD values in June but much smaller values in August compared to MODIS. This can be partly explained by the different aerosol models and schemes used in PMAp and MODIS for the retrieval of dust. However, the difference during June and August are not fully understood and more investigation is needed to confirm the source of these differences.

Over land (bottom panel in Figure 31), there is an overall agreement between PMAp daily mean AOD and MODIS/Terra in terms of temporal variation and AOD peaks. However, PMAp AOD is systematically larger until August when the difference is about 0.02-0.03. More investigation is needed to explain the higher AOD values of PMAp in earlier months of year.

In Figure 32 a comparison of global (land and ocean) daily mean AOD is presented for PMAp and MODIS/Terra. Because the ocean surface is much larger than land surface, typically twice more, the global daily statistics is mostly influenced by the ocean comparison. Consequently, the global agreement between PMAp and MODIS remains close to 0.02 over the full period, because the systematic differences are mostly cancelling.

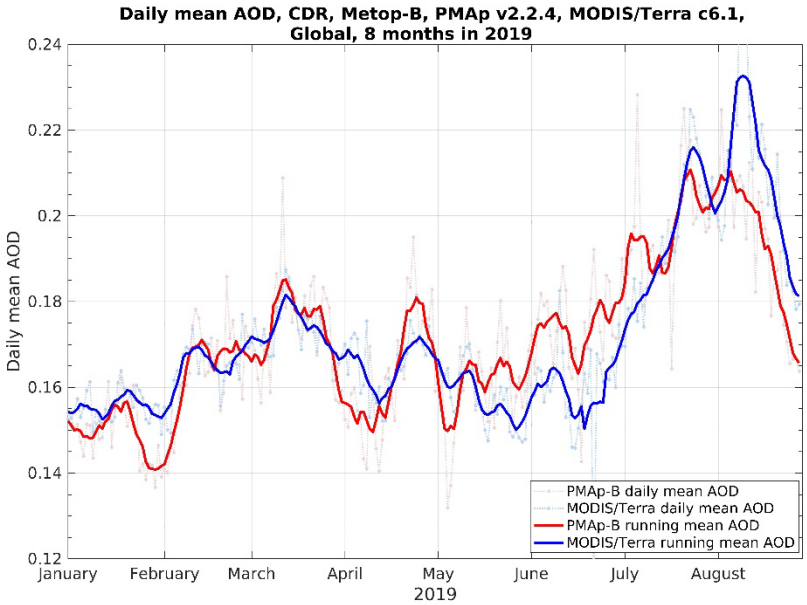

Figure 32: Comparison of global (land and ocean) daily mean AOD from PMAp CDR and MODIS/Terra.

6.5.2 Monthly Metop-A

The first comparison addresses the PMAp AOD values from Metop-A (M02) versus the MODIS/TERRA AOD values based on monthly averages. This comparison allows checking the good correlation in term of spatial and temporal variation of AOD between the two instruments.

In Figure 33, the time series of PMAp and MODIS AODs are shown for the 2007 to 2018 period. The global data (land and ocean, in grey) show a very similar annual cycle, the minimum (around 0.15) in the northern hemisphere autumn and winter is nearly identical. From March to July, we see higher values in both data sets, but higher in PMAp (reaching 0.25 AOD, MODIS 0.22). This is connected with very high AOD values in PMAp over land (above 0.5), while with MODIS the highest values reach 0.28. On the other hand, PMAp is constantly lower over ocean (~0.16) compared to MODIS (~0.19). It is known that the MODIS products is slightly overestimating over ocean by about +0.03 (Levy et al., 2013). In the first couple of months, lower PMAp values over ocean (minimum 0.10) are observed, as already reported on previous sections (early period not fully consistent with the rest of the CDR). In addition, the step change observed mid-2013 due to the swath reduction, which was reported in section 4.1, is also visible in this comparison.

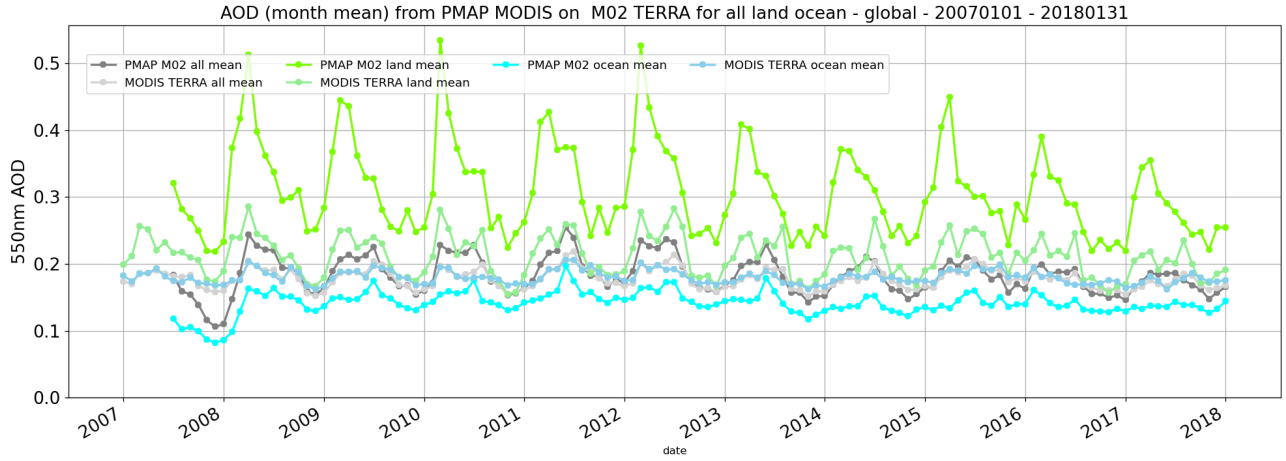

Figure 33: Monthly AOD average over the globe (grey), land (green) and ocean (blue) for PMAp/Metop-A (dark colours) and MODIS/TERRA (light colours).

In Figure 34 to Figure 37 monthly maps of AOD from PMAp/M02 (top), MODIS/TERRA (middle) and the difference (bottom) is shown for the centre month of each season for the year 2009. Plots for the other years can be found in the Annex in Figure 42.

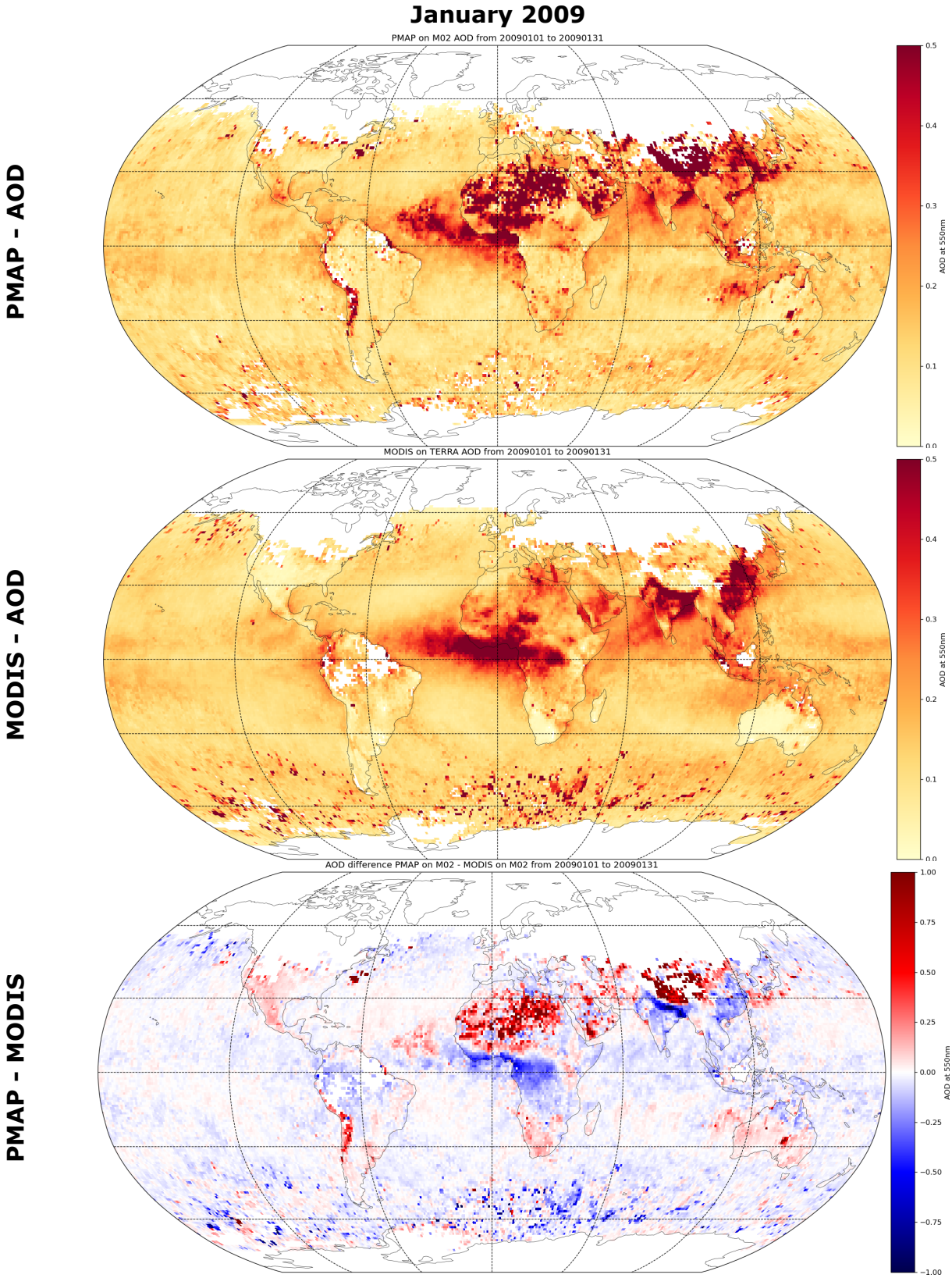

Figure 34: Monthly average of Metop-A (M02) PMAP AOD at 550 nm (top), MODIS (TERRA) (middle) and the difference PMAp minus MODIS (bottom) for January 2009. The scale for AOD is ranging from 0 to 0.5 and the difference scale is ranging from -1 to +1. The plots for the other years can be found in the Appendix in Figure 40.

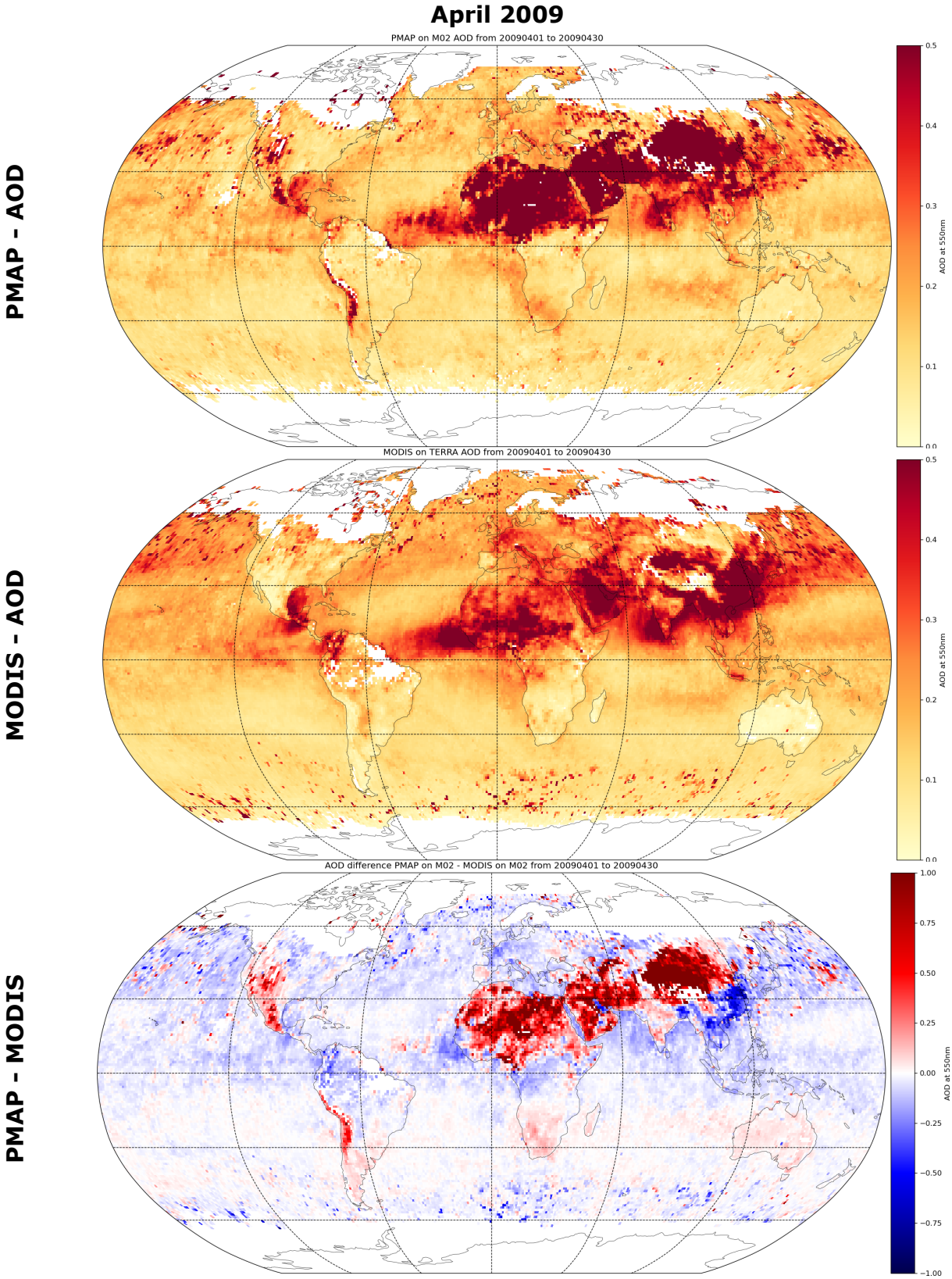

Figure 35: Monthly average of Metop-A (M02) PMAP AOD at 550 nm (top), MODIS (TERRA) (middle) and the difference PMAp minus MODIS (bottom) for April 2009. The scale for AOD is ranging from 0 to 0.5 and the difference scale is ranging from -1 to +1. The plots for the other years can be found in the Appendix in Figure 42.

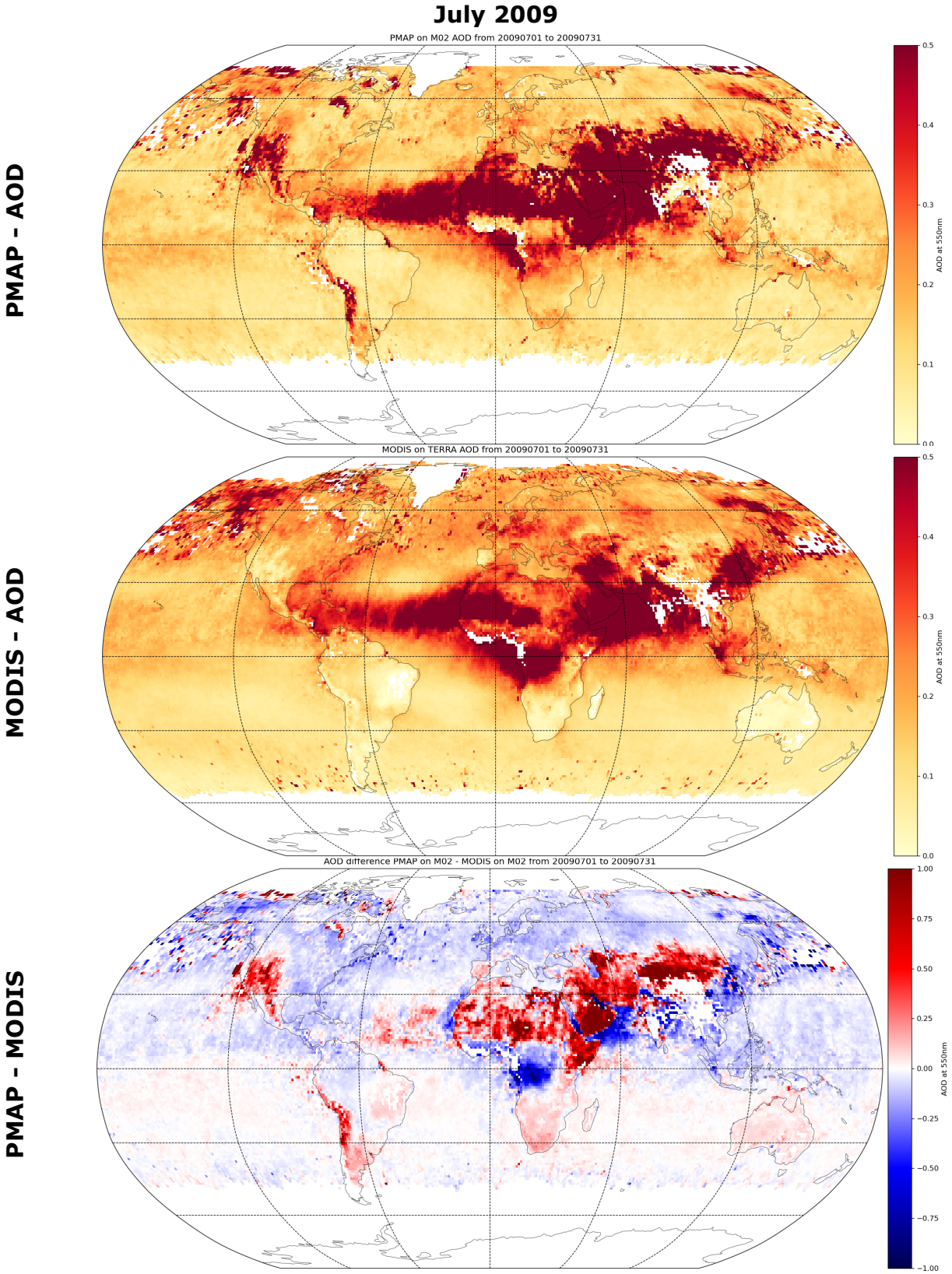

Figure 36: Monthly average of Metop-A (M02) PMAP AOD at 550 nm (top), MODIS (TERRA) (middle) and the difference PMAp minus MODIS (bottom) for July 2009. The scale for AOD is ranging from 0 to 0.5 and the difference scale is ranging from -1 to +1. The plots for the other years can be found in the Appendix in Figure 42.

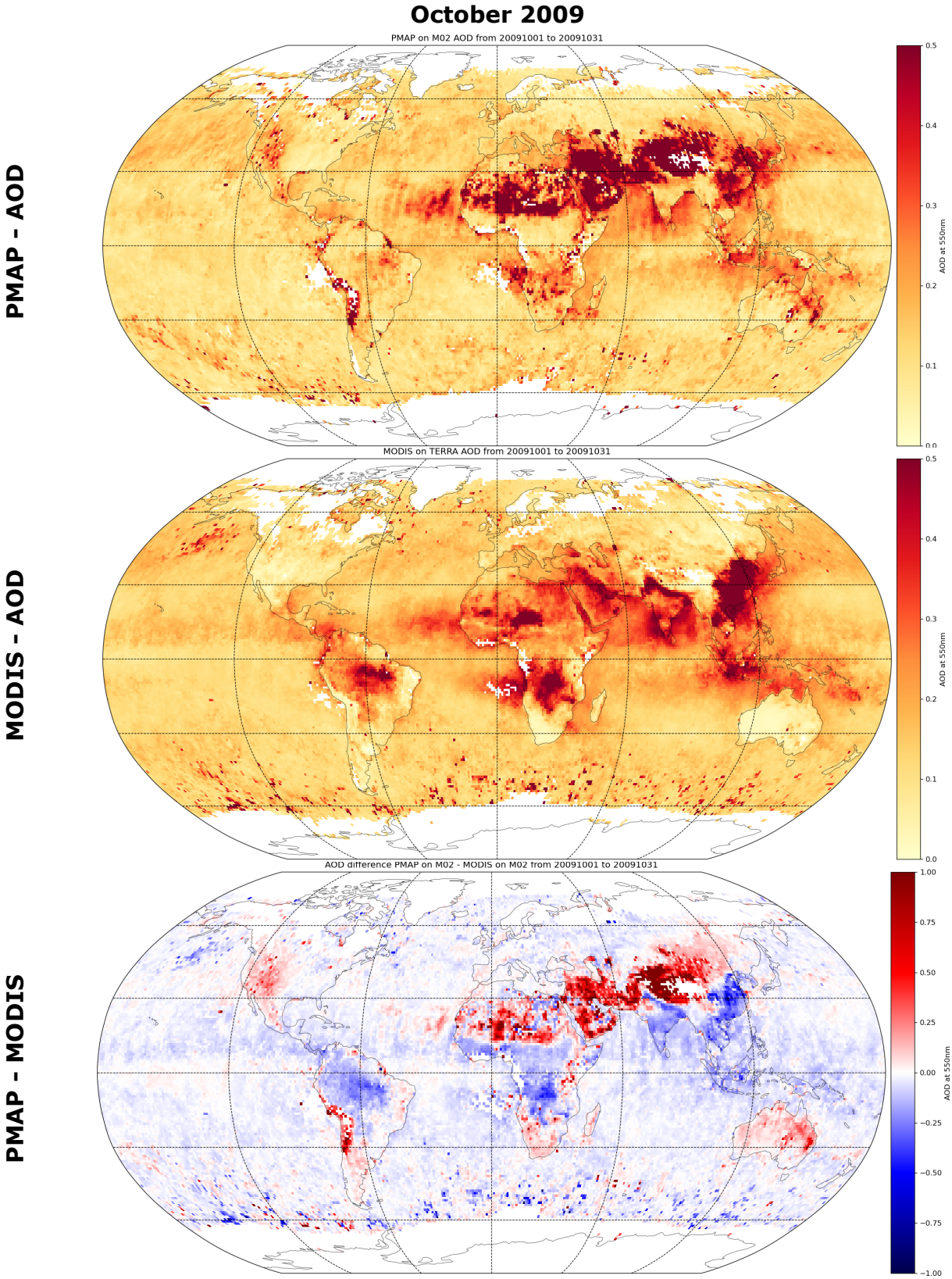

Figure 37: Monthly average of Metop-A (M02) PMAP AOD at 550 nm (top), MODIS (TERRA) (middle) and the difference PMAp minus MODIS (bottom) for October 2009. The scale for AOD is ranging from 0 to 0.5 and the difference scale is ranging from -1 to +1. The plots for the other years can be found in the Appendix in Figure 42.

The geographical distribution of AOD is similar for PMAp/Metop-A and MODIS/TERRA. The major sources of aerosol are easily identified from every continent: North/South Africa (dust and biomass burning respectively), Asia, Australia, North/South America (mostly biomass burning). The differences are more difficult to interpret, the sampling from PMAp and MODIS being different. Nevertheless, PMAp shows higher values over deserts (e.g. Africa, Arabia, China). At the opposite, MODIS shows higher values over the tropical Africa, South East Asia and the Amazon rainforest, regions more associated to biomass burnings.

Due to the higher AOD values over land these continental regions show up more prominent. Nevertheless, it is important to notice the very good land/sea transition on PMAp compared to MODIS which shows some artefacts (e.g. Australia, South America & Africa). As already observed in the time series, some differences are visible over oceanic regions as well. During April and July the southern hemispheric oceans show very little differences, in the Northern Hemisphere and for most other months MODIS shows slightly higher values. Again, MODIS is known to show a small positive bias over ocean (Levy et al., 2013).

6.5.3 Monthly Metop-B

This section addresses at the comparison between PMAp/Metop-B and MODIS/TERRA AOD. In Figure 38, the monthly averaged AOD values from PMAp and MODIS are shown from the beginning of Metop-B in 2013 to the end of the CDR in 2019.

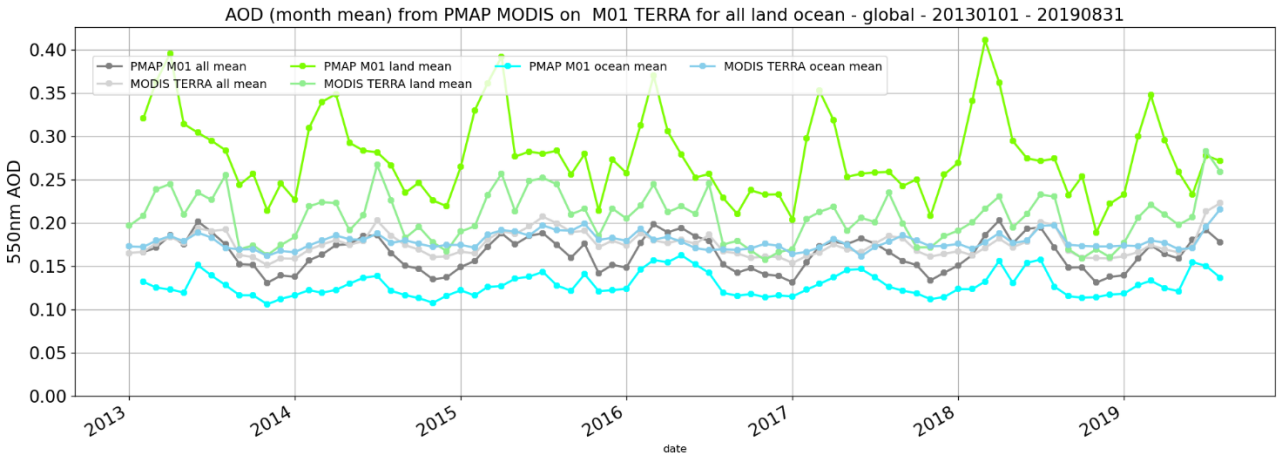

Figure 38: monthly AOD average over the globe (grey), land (green) and ocean (blue) for PMAp/Metop-B (dark colours) and MODIS/TERRA (light colours).

The global data is displayed in grey colours, AOD over land in green and over ocean in blue. Time series for PMAp and MODIS global AOD appear similar both exhibiting a distinct annual cycle, with peaks in the March to June period and lowest values in October and November. In the global average, the PMAp and MODIS values are very close. When data are split into land and ocean values, differences appear. Over ocean, PMAp is slightly lower than MODIS, approximately 0.05 in AOD, with values between 0.10 and 0.15 for PMAp and 0.15 and 0.20 for MODIS. As already mentioned, MODIS is known to show a positive bias over ocean (about 0.03 according to (Levy et al., 2013)). Larger differences appear over land where PMAp is significantly higher than MODIS. Peak values of PMAp reach up to 0.4 while MODIS hardly reaches values above 0.25 AOD. The land values peak mainly in March and drop to a minimum towards the end of the year. The annual

pattern remains similar for PMAp and MODIS. It is known that PMAp provides higher AOD than MODIS over bright surfaces (see above), but this difference on the monthly average is also be due, at least partly, to a difference in term of statistics (e.g. if high AOD are not retrieved on MODIS, this would create artificially a lower monthly AOD).

The time series from Figure 38 gives an overview of the global behaviour. To get an idea how the aerosols are distributed geographically and how PMAp compares in this domain with MODIS monthly AOD maps are shown from Figure 43 to Figure 46 in the Appendix. Same conclusions as Metop-A can be derived (see previous section).

7 Known limitations

The following limitations for the PMAp AOD CDR can be derived from this validation report:

- AOD from Metop-A before the 11th of March 2008 are not fully consistent with the rest of the time series because of the changes in the GOME-2 band definition on that date. The performance documented in this report are valid after March 2008. It is therefore suggested to use the data only from April 2008 onwards.
- AOD (usually representing dust in the atmosphere) retrieved over bright surfaces needs to be used with caution, with limited absolute performance of the AOD retrieval. However, intense aerosol episodes (e.g. dust events) are well captured, for spatial patterns and temporal evolution.
- Unrealistic high values of AOD are observed in polar spring for very high latitudes, these are probably the consequence of miss-identification of sea ice and/or residual polar clouds.
- High AOD values are also present in some cases for Metop-A in the wide swath configuration prior to August 2013. These values need to be treated with caution.
- The Metop-A series ends in January 2018 due to the first loss of solar visibility of GOME-2. The degradation correction for GOME-2 is not yet adapted to cover this and the following periods.

Note that validation and evaluation addressed only the AOD product. Other variables present in PMAp may be used but there is no guarantee for high quality.

8 Summary and conclusions

The climate data record of aerosol optical depth, generated using version 2.2.3 of the PMAp aerosol retrieval software for the Metop-A and -B archive from 2007 to 2019, has been evaluated for the AOD parameter. We can conclude that the AOD CDR is of good quality compared to reference data records and is homogeneous and consistent in time. Finally, it provides a major improvement compared to the near real time archived/produced PMAp data, due to an extension backwards in time and a consistent use of one algorithm and input data throughout the entire period.

The performance of the aerosol optical depth parameter has been evaluated for the entire CDR based on matchups with AERONET stations. It was found to be in agreement and even slightly better than the performance previously described for the PMAp NRT operational algorithm (version 2.2.4) in a dedicated validation report. Correlation values between 0.6 and 0.85 are reached for land and ocean stations. The validation also shows

the limitation of the PMAp retrieval performance over complex surface types, e.g. bright surfaces and highly variable topography.

The temporal consistency of the AOD from the CDR has been evaluated through various time series of different types: at the level of input data based on the Level-1 radiometry, and at the level of output based on comparison with ground-based data from AERONET, space-based data from MODIS as well as sensor internal and sensor cross comparisons. As expected from using a consistent Level-1 along the time series, the performance of AOD from PMAp remains also consistent with time. The comparison of Metop-A and -B shows a very good agreement over land and ocean, especially after 2014. For data before 2013 values are slightly higher for Metop-A (by 0.01 AOD over ocean and up to 0.1 over land).

The comparison with MODIS data shows systematic positive differences in daily and monthly data comparisons over land of up to ~0.2 AOD (~50%) at monthly scale, especially for bright surfaces or dust events. Over the ocean, the MODIS data is systematically higher than the PMAp data at daily and monthly scales and the observed difference seems to be compatible with the too high AOD documented for MODIS over ocean. The transition from ocean to land is more realistic in PMAp compared to MODIS, especially for southern hemisphere continents.

The same limitations as for the current NRT processor have been observed and confirmed (especially in the case of retrieval of dust or over bright surface). In addition, a non-consistency has been observed for Metop-A before March 2008. Consequently, the performance of the NRT processor can be considered representative for the period after March 2008 of the reprocessing which is an important asset for the CDR users.

As demonstrated in this validation report, the goal to produce a long record of AOD based on PMAp with a consistent performance has been achieved. We can conclude that the AOD CDR is of good quality compared to reference data records, is homogeneous, and consistent in space and time. Finally, it provides a major improvement compared to the near real time produced PMAp data, due to an extension backwards in time and a consistent use of algorithm and input data.

Appendix A PMAp daily AOD for the CDR time series

a) Northern hemisphere

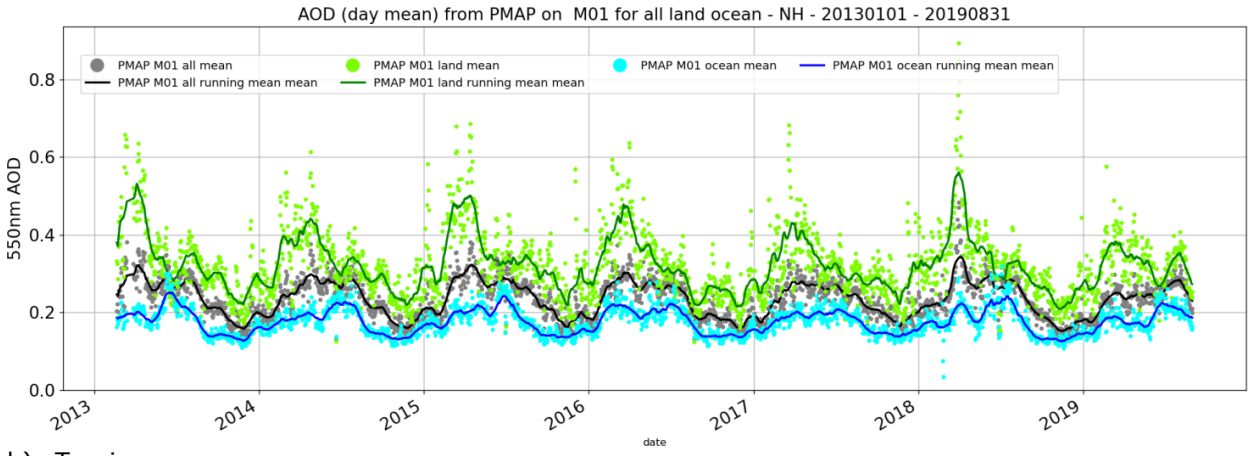

b) Tropics

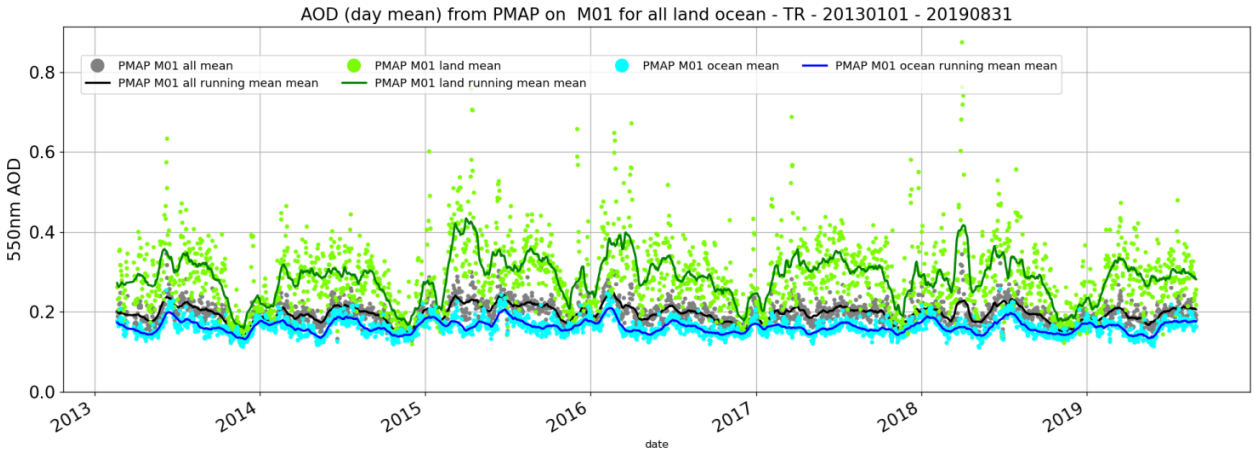

c) Southern hemisphere

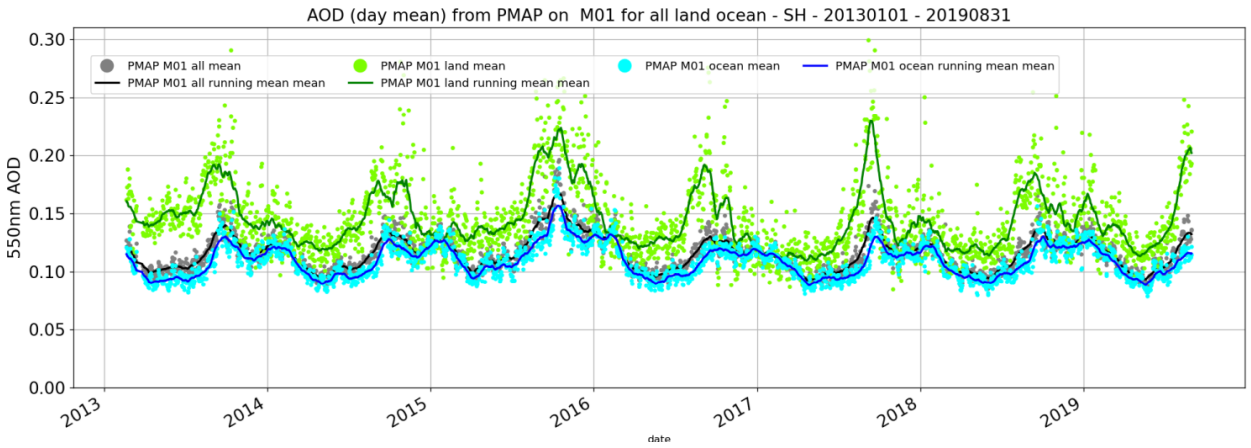

Figure 39: Same as Figure 7 (daily Metop-B AOD) but over three different areas: Northern, Southern Hemisphere and tropics.

Appendix B Yearly statistics per AERONET station

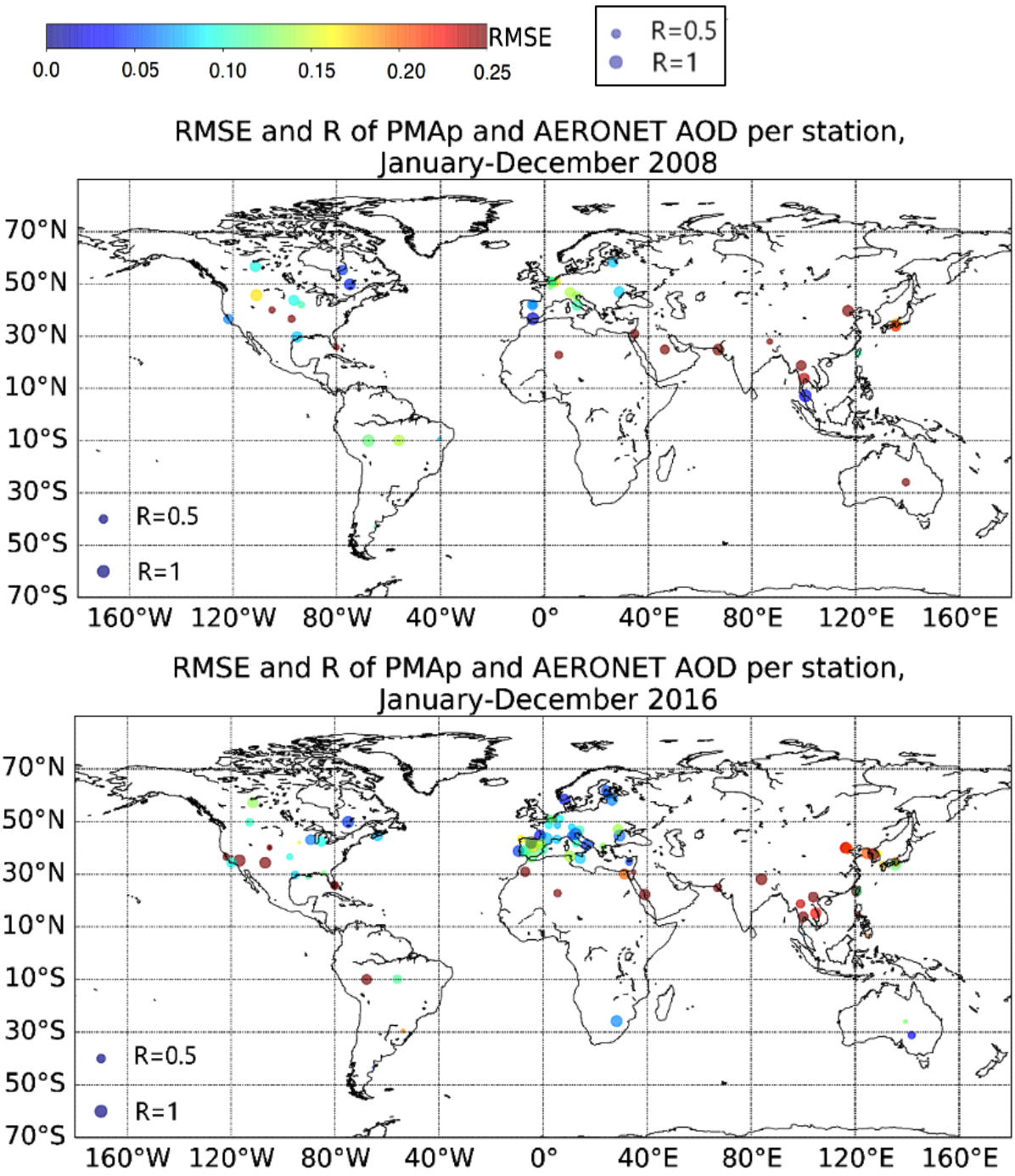

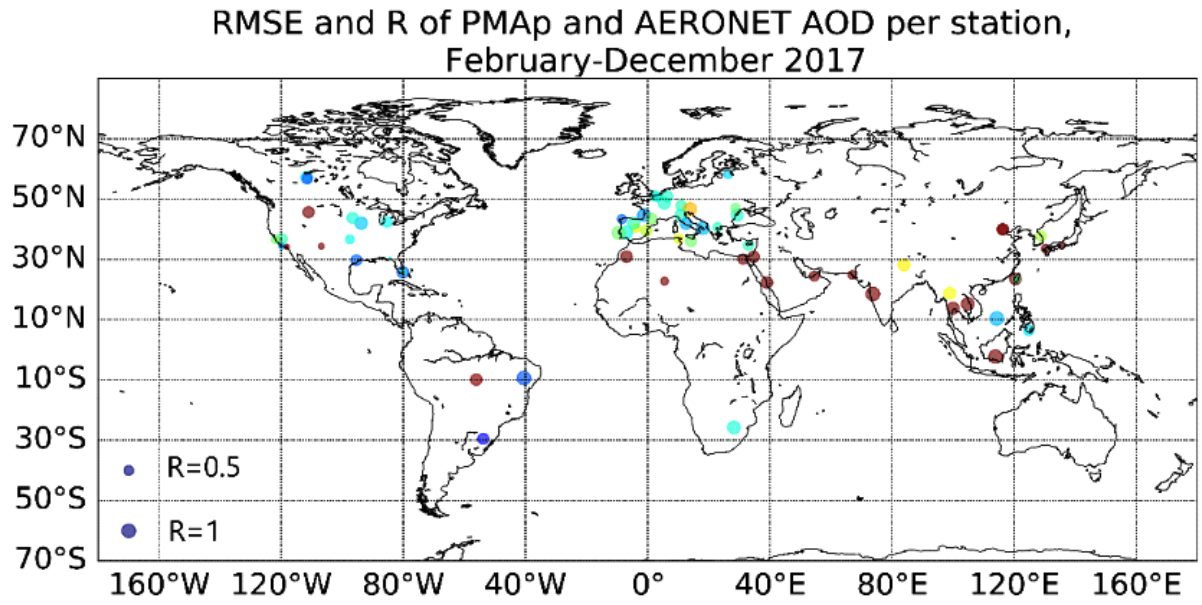

Figure 40: Pearson correlation (R) and RMSE per AERONET station for Metop-A, indicated by size and colour respectively (the larger the size, the higher is Pearson correlation).

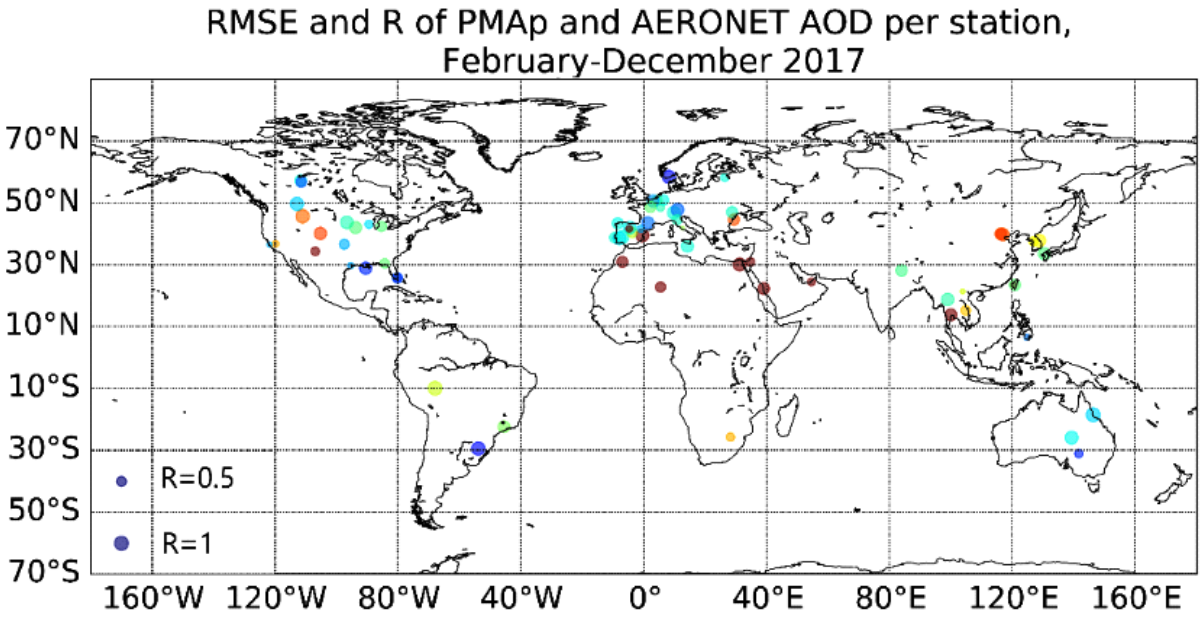

Figure 41: Pearson correlation (R) and RMSE per AERONET station for Metop-B, indicated by size and colour respectively (the larger the size, the higher is Pearson correlation).

Appendix C Comparison with MODIS – monthly average for Metop-A

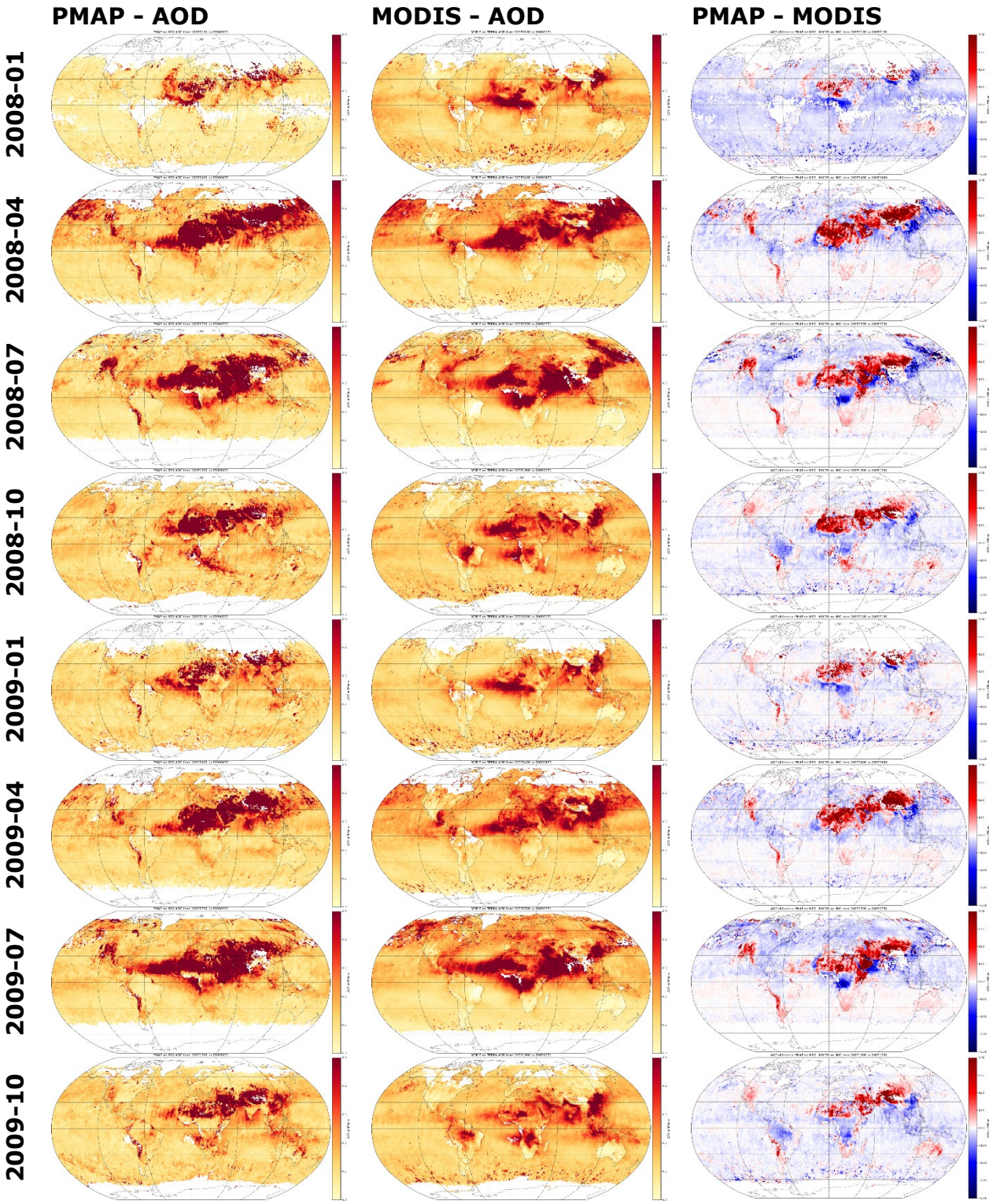

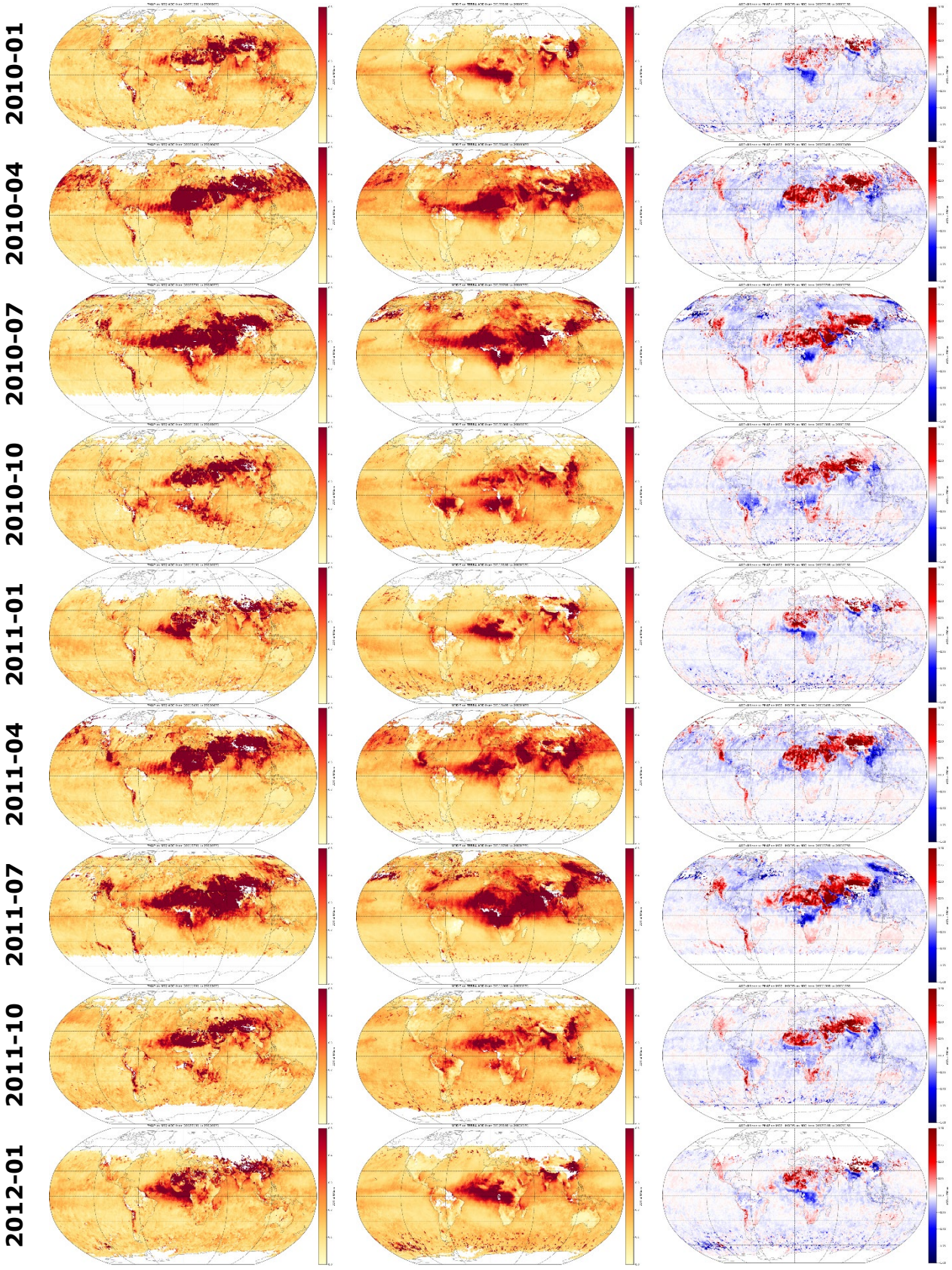
2010-01
2010-04
2010-07
2010-10
2011-01
2011-04
2011-07
2011-10
2012-01

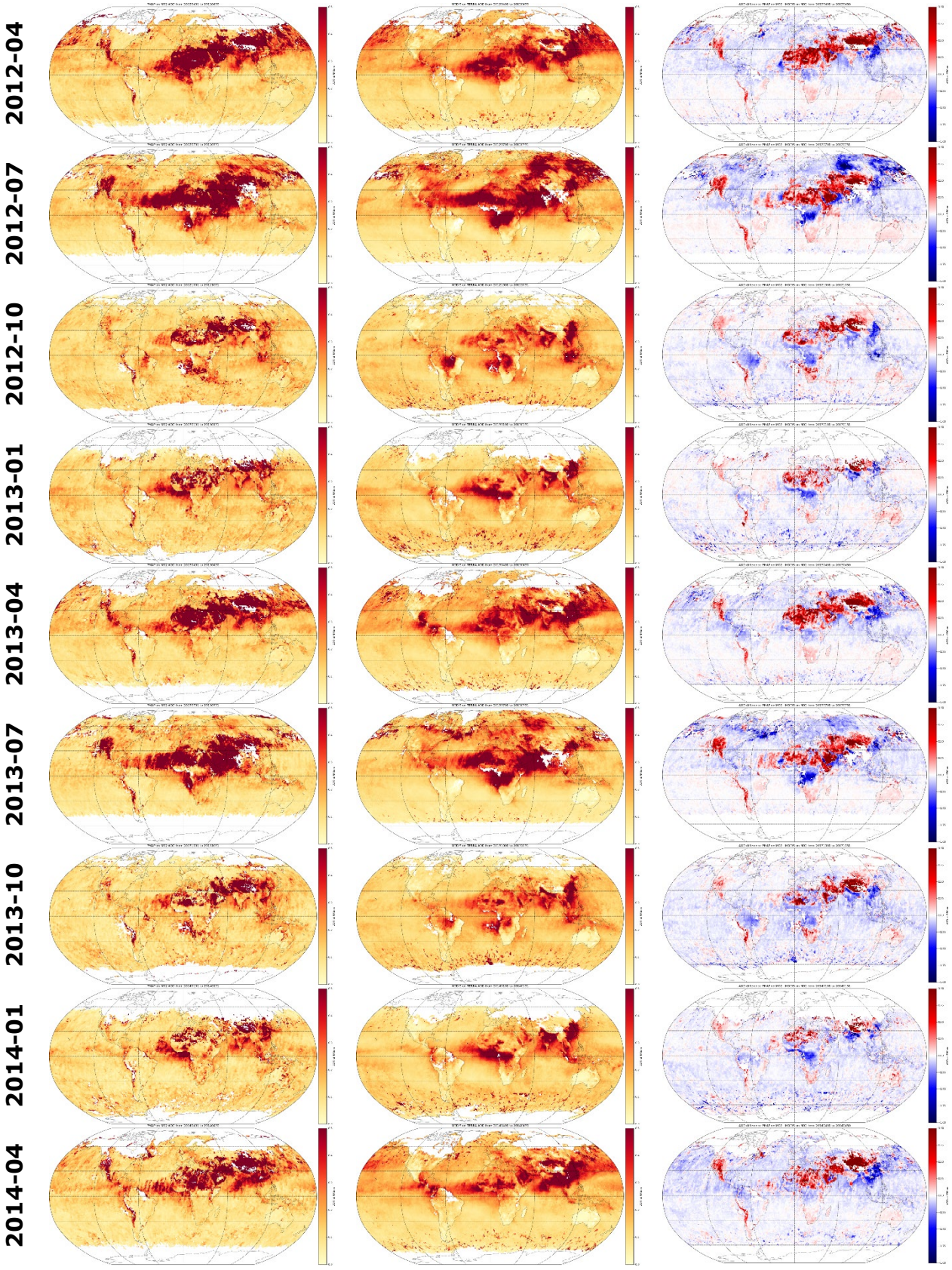
2012-04
2012-07
2012-10
2013-01
2013-04
2013-07
2013-10
2014-01
2014-04

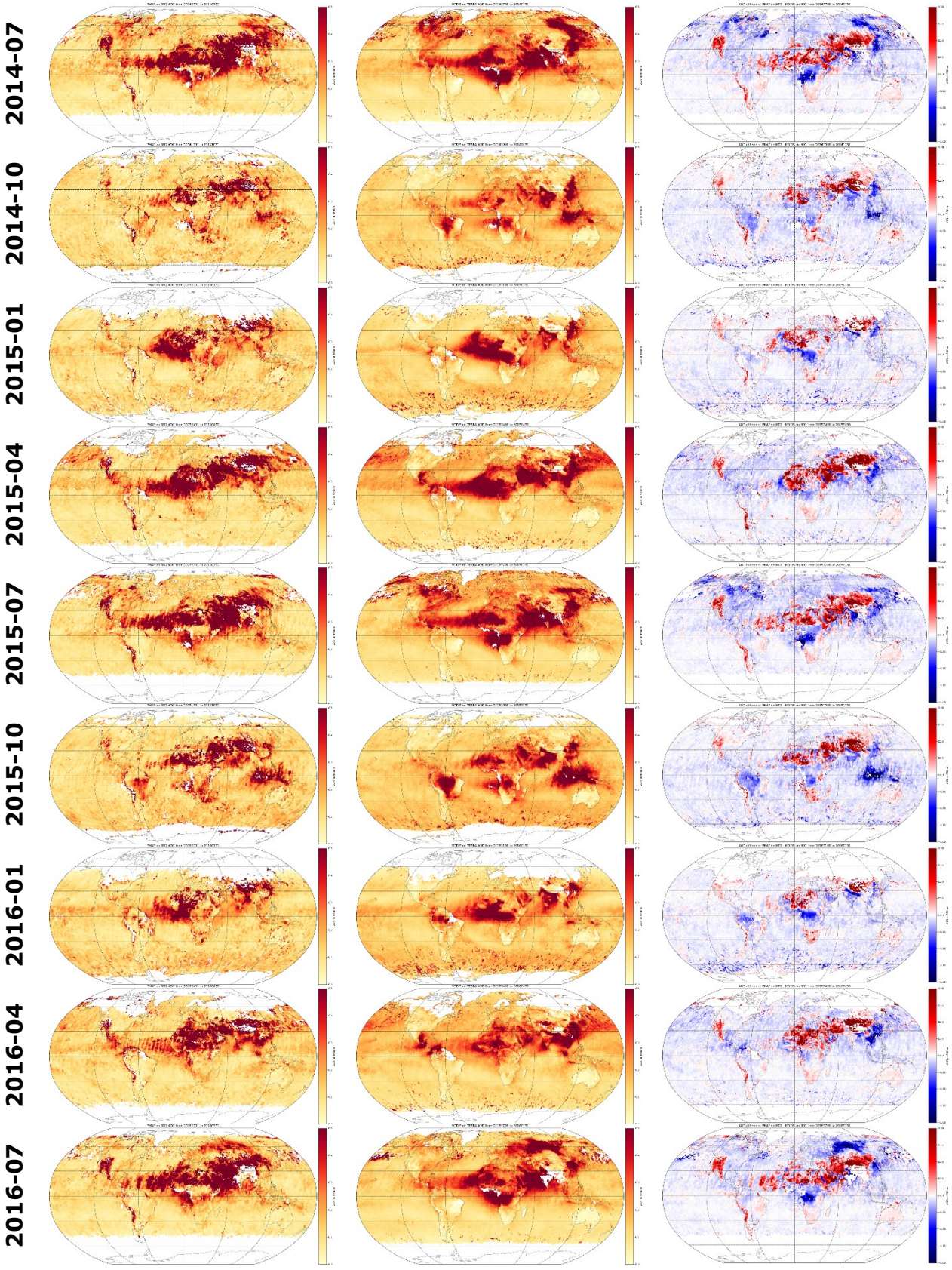
2014-07
2014-10
2015-01
2015-04
2015-07
2015-10
2016-01
2016-04
2016-07

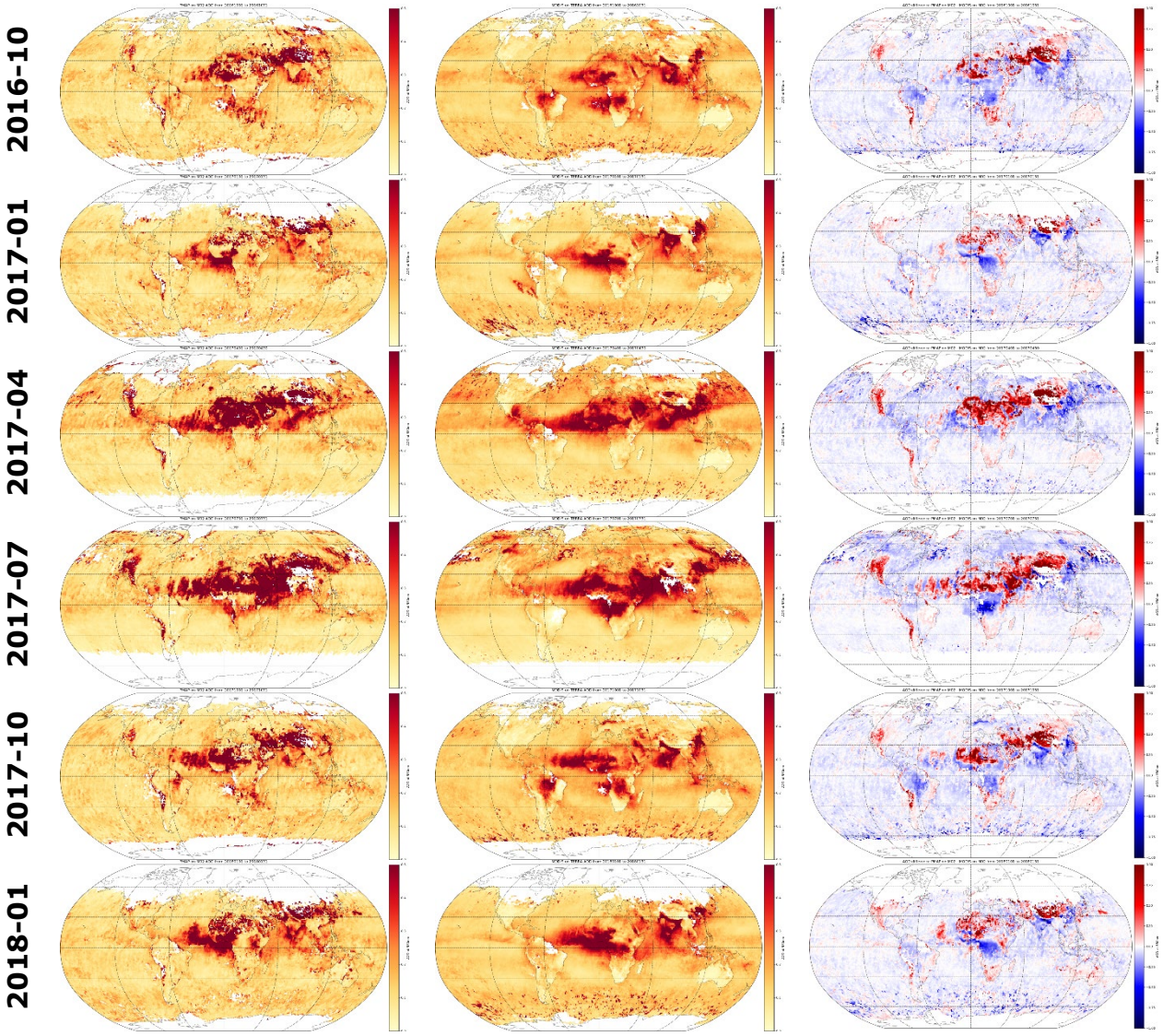

Figure 42: Monthly average of Metop-A (M02) PMAP AOD at 550 nm (left), MODIS (TERRA) (centre) and the difference PMAp minus MODIS (right). The scale for AOD is ranging from 0 to 0.5 and the difference scale is ranging from -1 to +1.

Appendix D Comparison with MODIS – monthly average for Metop-B

Enlarged maps for one year, to better illustrate the regional behaviour in Figure 41 to Figure 44

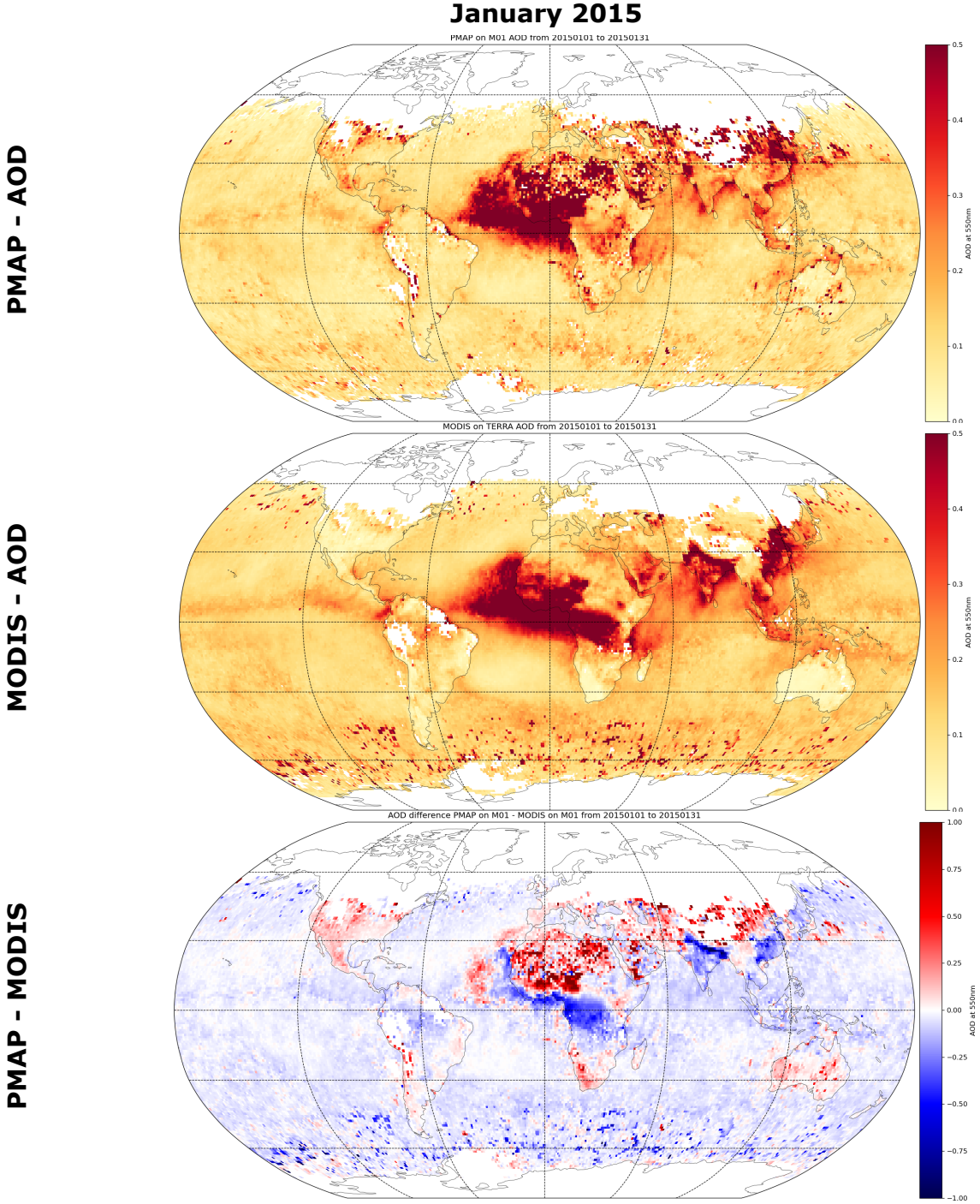

Figure 43: Monthly average of Metop-B (M01) PMAP AOD at 550 nm (top), MODIS (TERRA) (middle) and the difference PMAp minus MODIS (bottom) for January 2015. The scale for AOD is ranging from 0 to 0.5 and the difference scale is ranging from -1 to +1. The plots for the other years can be found in the Appendix in Figure 45.

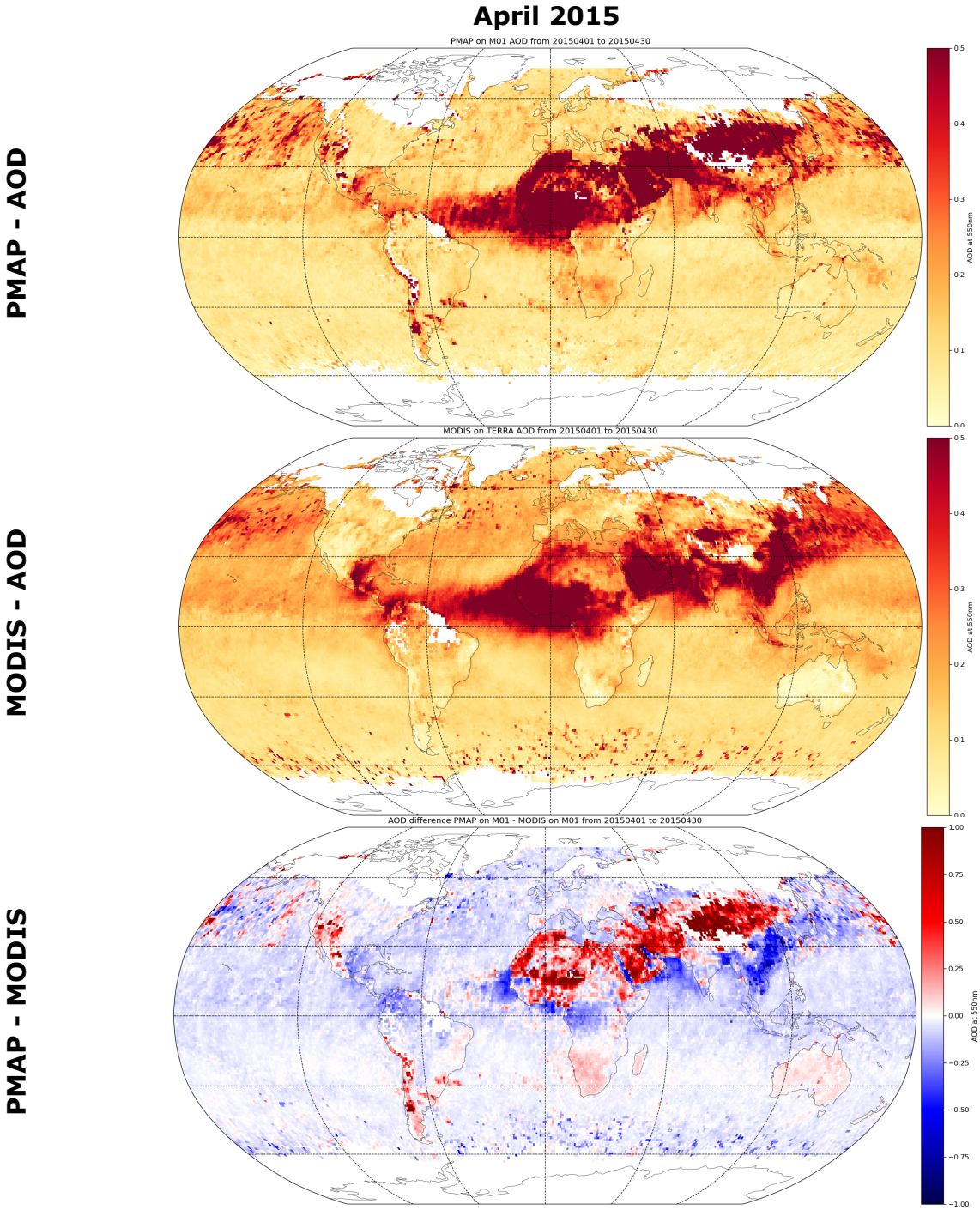

Figure 44: Monthly average of Metop-B (M01) PMAP AOD at 550 nm (top), MODIS (TERRA) (middle) and the difference PMAp minus MODIS (bottom) for January 2015. The scale for AOD is ranging from 0 to 0.5 and the difference scale is ranging from -1 to +1. The plots for the other years can be found in the Appendix in Figure 45.

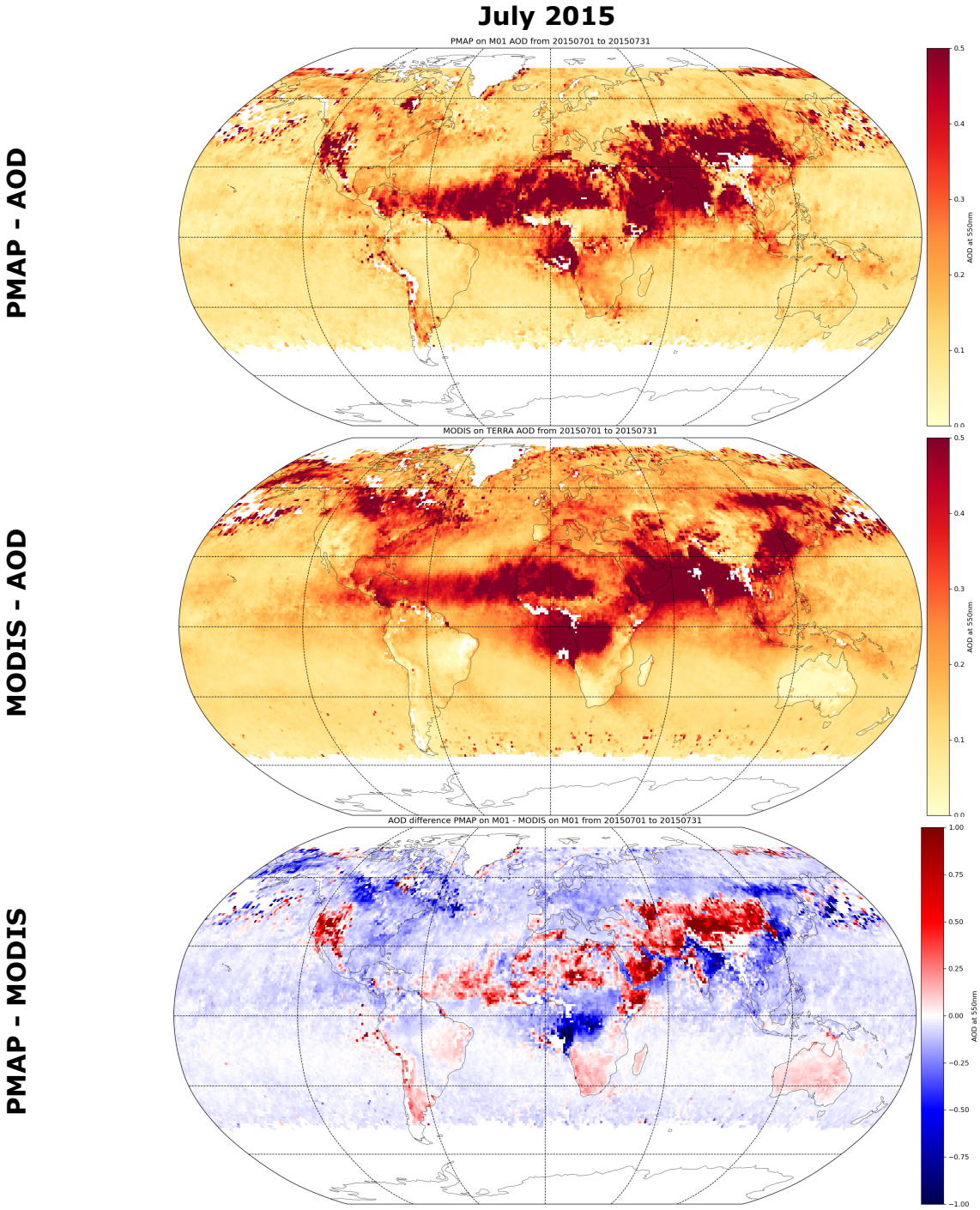

Figure 45: Monthly average of Metop-B (M01) PMAP AOD at 550 nm (top), MODIS (TERRA) (middle) and the difference PMAp minus MODIS (bottom) for January 2015. The scale for AOD is ranging from 0 to 0.5 and the difference scale is ranging from -1 to +1. The plots for the other years can be found in the Appendix in Figure 45.

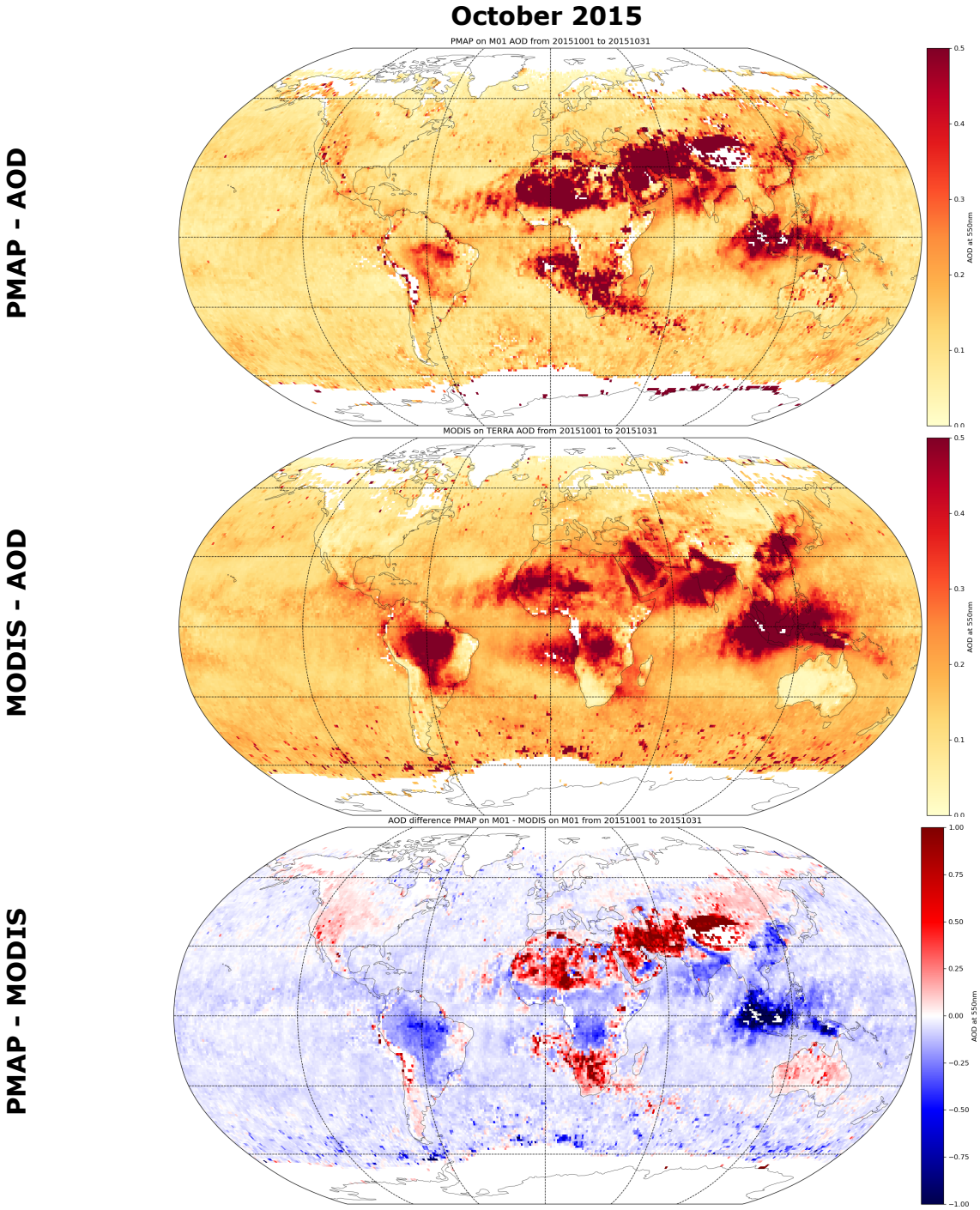

Figure 46: Monthly average of Metop-B (M01) PMAP AOD at 550 nm (top), MODIS (TERRA) (middle) and the difference PMAp minus MODIS (bottom) for January 2015. The scale for AOD is ranging from 0 to 0.5 and the difference scale is ranging from -1 to +1. The plots for the other years can be found in the Appendix in Figure 45.

Smaller maps for all years of Metop-B.

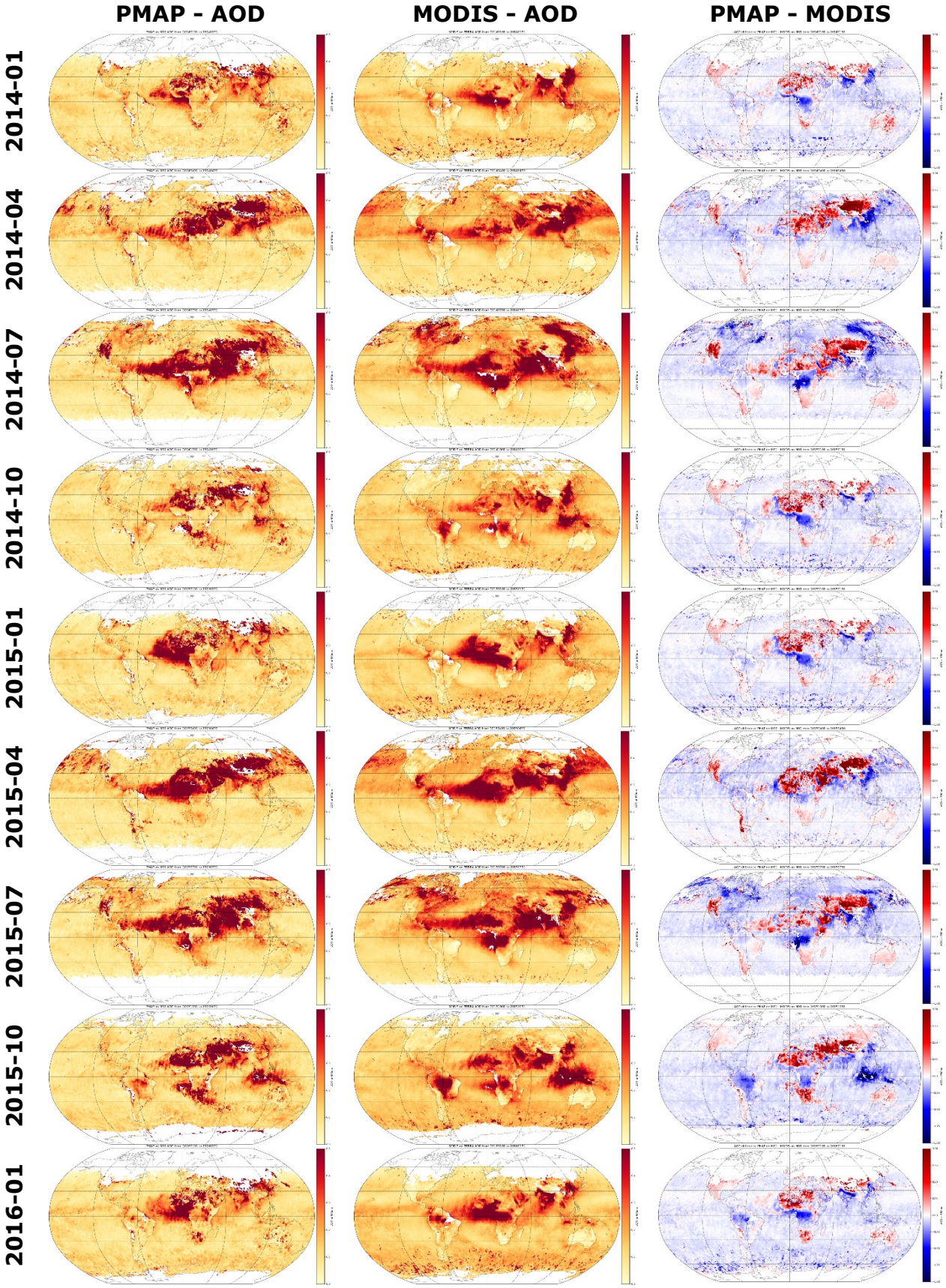

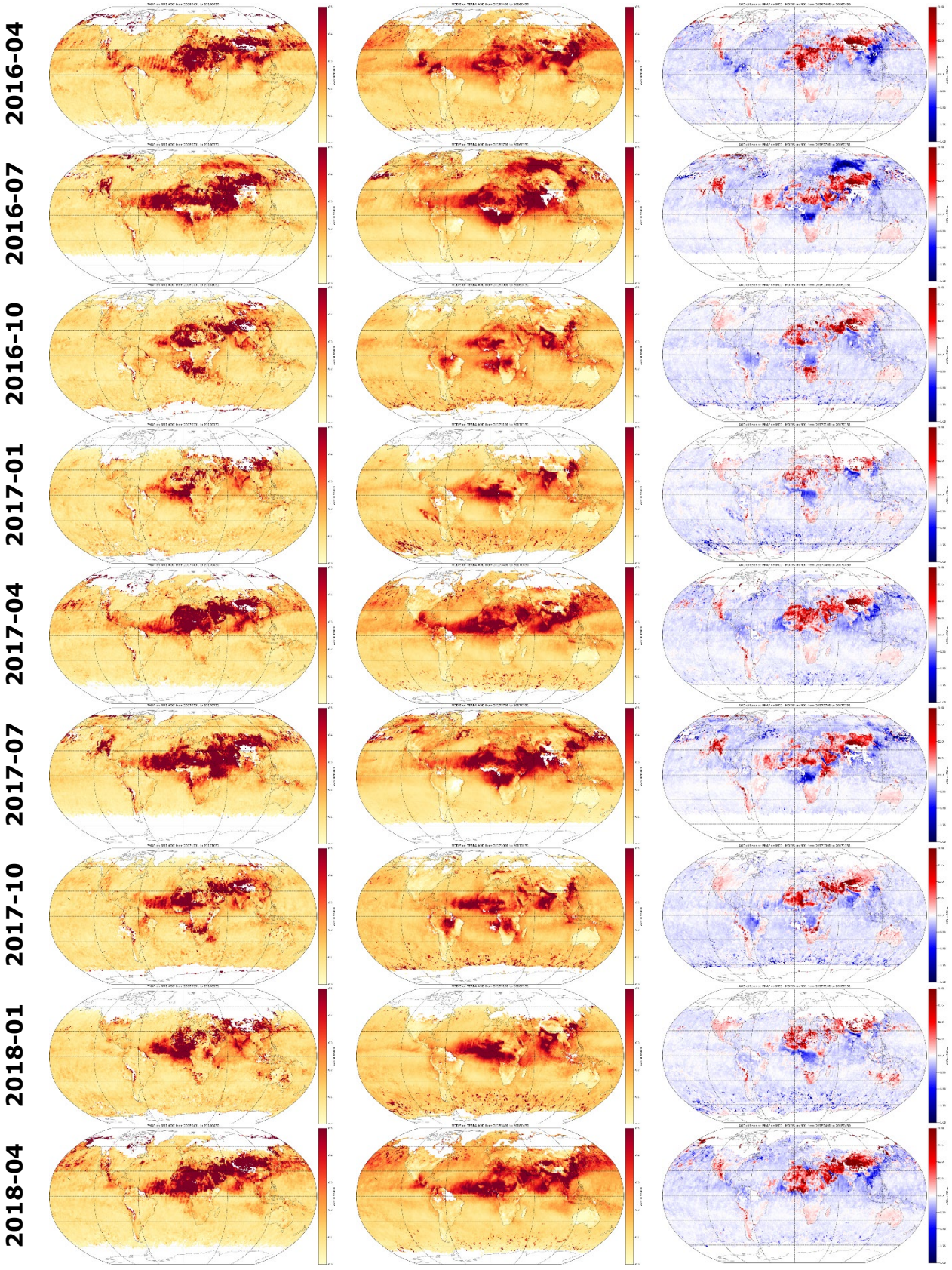
2016-04
2016-07
2016-10
2017-01
2017-04
2017-07
2017-10
2018-01
2018-04

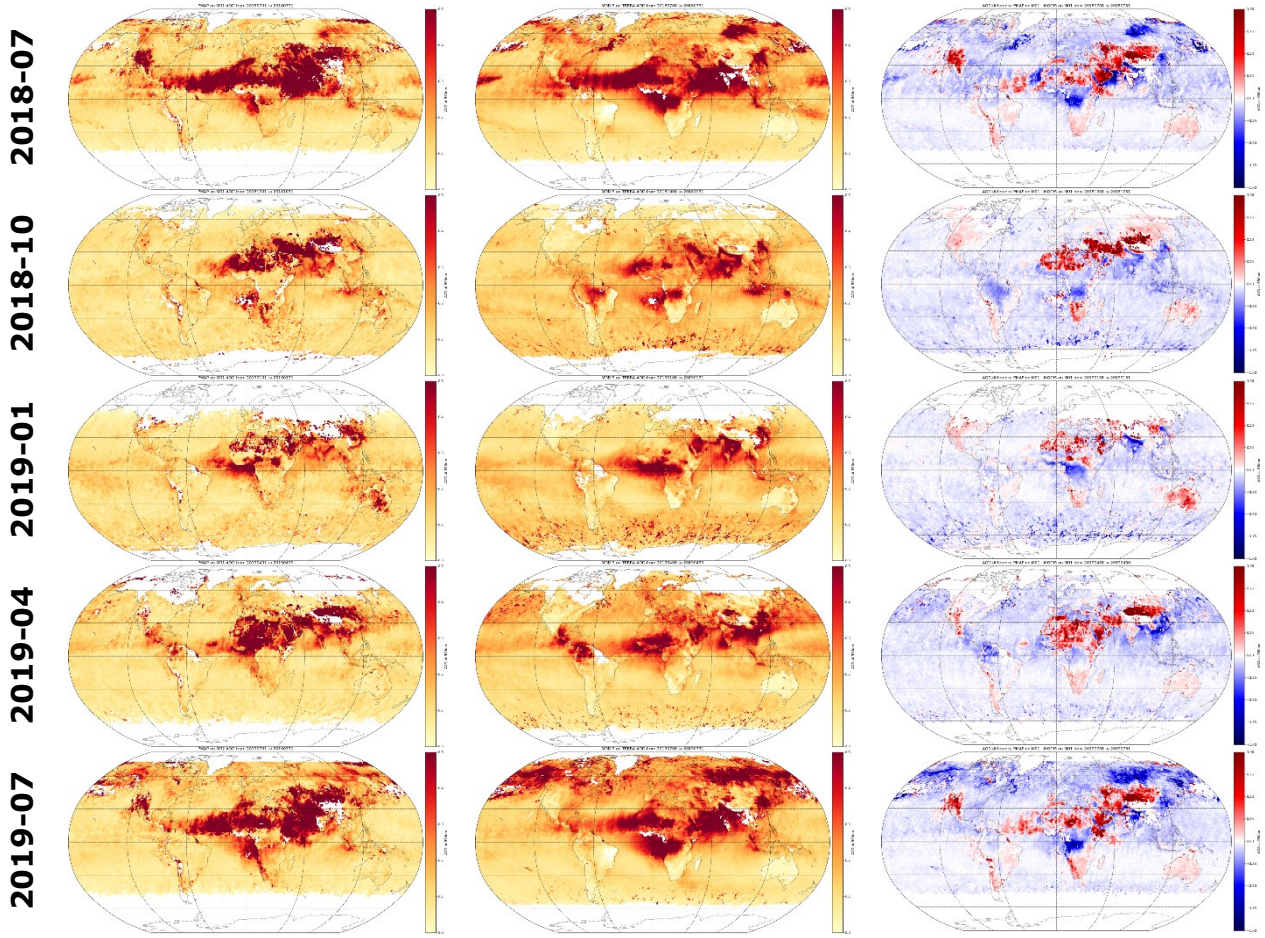

Figure 47: Monthly average of Metop-B (M01) PMAp AOD at 550 nm (left), MODIS (TERRA) (centre) and the difference PMAp minus MODIS (right). The scale for AOD is ranging from 0 to 0.5 and the difference scale is ranging from -1 to +1.

ECMWF Shinfield Park Reading RG2 9AX UK